TAMPEREEN TEKNILLINEN YLIOPISTO
TAMPERE UNIVERSITY OF TECHNOLOGY

Heli Koivuluoto

# Microstructural Characteristics and Corrosion Properties of Cold-Sprayed Coatings

Julkaisu 882 • Publication 882

Tampere 2010

Tampereen teknillinen yliopisto. Julkaisu 882
Tampere University of Technology. Publication 882

Heli Koivuluoto

# Microstructural Characteristics and Corrosion Properties of Cold-Sprayed Coatings

Thesis for the degree of Doctor of Technology to be presented with due permission for public examination and criticism in Konetalo Building, Auditorium K1702, at Tampere University of Technology, on the 4th of June 2010, at 12 noon.

Tampereen teknillinen yliopisto - Tampere University of Technology
Tampere 2010

ISBN 978-952-15-2353-3 (printed)
ISBN 978-952-15-2373-1 (PDF)
ISSN 1459-2045

**PREFACE**

The work presented in this dissertation was carried out at the Department of Materials Science, Tampere University of Technology during the years 2005-2009. This work was supervised by Prof. Petri Vuoristo to whom I would like to address my deepest gratitude and thank for all his guidance and for giving me the opportunity to prepare this dissertation under his supervision.

In addition, I would like to thank all of the co-authors: Lic.Tech. Juha Lagerbom for his guidance at the beginning of this work, M.Sc. Jonne Näkki for corrosion tests which were performed at KETEK and M.Sc. Mari Honkanen for TEM evaluations. Mr. Werner Krömmer of Linde AG Gas for spraying the high-pressure cold-sprayed coatings and Mr. Mikko Kylmälahti for spraying the low-pressure cold-sprayed coatings are also gratefully acknowledged. Furthermore, I would like to express many thanks to Dr. Minnamari Vippola for her guidance, help and fruitful discussions during this work period. The research assistants, who have assisted me during this work, are also acknowledged. I would also like to express thanks to the members, past and present, of the Surface Engineering Group and to all the staff of the Department of Materials Science for the nice working atmosphere.

I am much obliged for the financial support by the Academy of Finland (2009-2010), the Graduate School on New Materials and Processes (2009), and the KINE-MATEK (2005-2008) project funded by the Finnish Funding Agency for Technology and Innovation (TEKES), the European Regional Development Fund (ERDF), Metso Paper Oy, Outotec Research Oy, Kemira Oy, Oy AGA Ab, TTT Technology Oy, Fincoat Oy, Oseir Oy, and KMT Group Oy. The Jenny and Antti Wihuri Foundation, the Finnish Foundation for Technology Promotion (TES), Walther Alhström Foundation and the City of Tampere are also gratefully acknowledged for their financial supports.

My parents, Merja and Matti, are also gratefully thanked for their supports and encouragements. Finally, my beloved husband Petteri is most deeply thanked for his endless patience, support and encouragement during this hard work.

Tampere, May 2010

Heli Koivuluoto

**ABSTRACT**

Cold spraying is a thermal spray process which enables production of metallic and metallic-ceramic coatings with dense (very low porosity level) and pure (low oxygen content) structures. Several coating properties such as corrosion resistance and electrical conductivity rely on these properties. Cold spraying consists of two processes: high-pressure cold spraying (HPCS) and low-pressure cold spraying (LPCS) divided by the pressure level used in the processes (40 bar versus 10 bar). Generally, cold spraying is based on higher particle velocities and lower process temperatures than in other thermal spray processes. The coating is formed in a solid state when powder particles impact on a sprayed surface with high kinetic energy, deform and adhere to the substrate or to other particles. Therefore, a high level of plastic deformation and adiabatic shear instability are required for a tight bonding between powder particles and for the formation of dense microstructures. Moreover, in cold spraying, many factors, e.g., powder characteristics and compositions, spraying parameters, and post-treatments affect the formation and properties of the coating.

This work focuses on the characterization of the microstructural properties (microstructure, grain structure, particle deformation, and fracture behavior), corrosion resistance (denseness, impermeability, and corrosion properties), and mechanical properties (hardness and bond strength) of the cold-sprayed metallic and metallic-ceramic coatings. Furthermore, the aim of this work is to find relationship between microscopic details and macroscopic properties and affecting factors for these in order to produce fully dense coatings using cold spray processes. The coating materials are pure metals: Cu, Ta, and Ni, metal alloys: Ni-20Cr, Ni-20Cu, and Ni-30Cu, and metallic-ceramic composites: Cu+$Al_2O_3$, Ni-20Cr+$Al_2O_3$, and Ni-20Cr+WC-10Co-4Cr. Structural details are characterized using electron microscopy techniques (SEM, FESEM, and TEM) whereas denseness and corrosion properties are evaluated with corrosion tests (open-cell potential measurements, salt spray tests, and polarization measurements).

Typically, cold-sprayed coatings appeared to be dense without porosity or other defects in their structures according to visual examinations. However, corrosion tests revealed through-porosity in the coating structures, indicating an existence of weak points inside the coatings. Therefore, denseness and impermeability play an important role in the corrosion resistance of the coatings. Good corrosion resistance is based on the formation of a protective oxide layer in case of passivating metals and metal alloys. Fully dense coating structures are required for the capability of the cold-sprayed coatings to act as real corrosion barrier coatings and to perform well in all corrosion tests. Three ways to eliminate or decrease the number of weak points and defects in the coating structures were found. Firstly, the denseness improvement was done with an optimal combination of powder and spraying parameters (HPCS Cu, Ta, and Ni coatings). These combinations are strongly material-dependent. HPCS Ta coatings also have similar corrosion properties with corresponding bulk material, indicating excellent corrosion protection. Secondly, the denseness of metallic coating can be increased by adding ceramic particles into the metallic powder as a powder mixture. These hard particles keep the nozzle clean; activate the sprayed surface; and reinforce the coating by hammering the structure. The significant denseness improvement was observed with HPCS Ni-20Cr+$Al_2O_3$, HPCS Ni-20Cr+WC-10Co-4Cr and LPCS Cu+$Al_2O_3$ coatings. In addition to these, thirdly, the denseness improvement of HPCS Ni-20Cu coatings was done with heat treatments due to the void reduction and recrystallization.

**TABLE OF CONTENTS**

## LIST OF ORIGINAL PUBLICATIONS

This thesis is based on the original experimental work presented in detail in the following 7 publications, which are referred in the text with corresponding Roman numerals I-VII.

**I** Heli Koivuluoto, Juha Lagerbom, and Petri Vuoristo, Microstructural Studies of Cold Sprayed Copper, Nickel, and Nickel-30%Copper Coatings, *Journal of Thermal Spray Technology*, 16 (4) 2007, p. 488-497

**II** Heli Koivuluoto, Juha Lagerbom, Mikko Kylmälahti, and Petri Vuoristo, Microstructure and Mechanical Properties of Low-Pressure Cold-Sprayed (LPCS) Coatings, *Journal of Thermal Spray Technology*, 17 (5-6) 2008, p. 721-727

**III** Heli Koivuluoto and Petri Vuoristo, Effect of Ceramic Particles on Properties of Cold-Sprayed Ni-20Cr+$Al_2O_3$ Coatings, *Journal of Thermal Spray Technology*, 18 (4) 2009, p. 555-562

**IV** Heli Koivuluoto, Jonne Näkki, and Petri Vuoristo, Corrosion Properties of Cold-Sprayed Tantalum Coatings*, Journal of Thermal Spray Technology*, 18 (1) 2009, p. 75-82

**V** Heli Koivuluoto, Mari Honkanen, and Petri Vuoristo, Cold-sprayed copper and tantalum coatings – Detailed FESEM and TEM analysis, *Surface & Coatings Technology*, 204 (15) 2010, p. 2353-2361

**VI** Heli Koivuluoto and Petri Vuoristo, Structural Analysis of Cold-Sprayed Nickel-Based Metallic and Metallic-Ceramic Coatings, *Journal of Thermal Spray Technology*, in press, DOI:10.1007/s11666-010-9481-4

**VII** Heli Koivuluoto and Petri Vuoristo, Effect of Powder Type and Composition on Structure and Mechanical Properties of Cu+$Al_2O_3$ Coatings Prepared by using Low-Pressure Cold Spray Process, *Journal of Thermal Spray Technology*, in press, DOI: 10.1007/s11666-010-9491-2

## AUTHOR'S CONTRIBUTION

Heli Koivuluoto (née Mäkinen) is the main researcher and writer of all the publications. She planned and organized all experiments, performed most of the tests and characterizations, analyzed the results, and prepared the manuscripts. In the publications I and II, Lic.Tech. Juha Lagerbom gave advises and comments on the manuscripts. In the publication IV, M.Sc. Jonne Näkki carried out the polarization measurements and in the publication V, M.Sc. Mari Honkanen performed the TEM studies. In addition, all of the manuscripts were commented by Prof. Petri Vuoristo who also was the supervisor in the research.

**PUBLICATIONS ON THE RESEARCH AREA BUT NO INCLUDED IN THE THESIS**

**VIII** Heli Koivuluoto, Jonne Näkki, and Petri Vuoristo, Structure and Corrosion Behavior of Cold-Sprayed Tantalum Coatings, *Thermal Spray 2009: Expanding Thermal Spray Performance to New Markets and Applications,* B. Marple, M. Hyland, Y.-C. Lau, C.-J. Li, R. Lima, G. Montavon (Eds.), ASM International, May 4-7, 2009 (Las Vegas, Nevada, USA), p. 314-319

**IX** Heli Koivuluoto, Minna Kotilainen, and Petri Vuoristo, Overview of Structure and Properties of High-Pressure and Low-Pressure Cold-Sprayed Coatings, *Welding and Cutting*, (2) 2009, p. 98-104

**X** Heli Koivuluoto, Minna Kulmala, and Petri Vuoristo, Structural Properties of High-Pressure Cold-Sprayed and Low-Pressure Cold-Sprayed Coatings*, Surface Modification Technologies XXII*, T. Sudarshan, P Nylen (Eds.), September 22-24, 2008, (Trollhättan, Sweden), p. 65-72

**XI** Heli Mäkinen, Juha Lagerbom, and Petri Vuoristo, Adhesion of cold sprayed coatings: effect of powder, substrate, and heat treatment, *Thermal Spray 2007: Global Coating Solutions*, B. Marple, M. Hyland, Y.-C. Lau, C.-J. Li, R. Lima, G. Montavon (Eds.), ASM International, May 14-16, 2007 (Beijing, China), p. 31-36

**XII** Heli Mäkinen, Juha Lagerbom, and Petri Vuoristo, Mechanical properties and corrosion resistance of cold sprayed coatings, *Thermal Spray 2006: Building on 100 Years of Success*, B. Marple, M. Hyland, Y.-C. Lau, R. Lima, J. Voyer (Eds.), ASM International, May 15-18, 2006 (Seattle, USA), 6 p

## LIST OF SYMBOLS AND ABBREVIATIONS

*Greek symbols*

| | |
|---|---|
| ρ | Density |
| $\sigma_u$ | Yield strength |
| $\sigma_{TS}$ | Tensile strength |

*Latin symbols*

| | |
|---|---|
| Ø | Diameter |
| $c_p$ | Specific heat |
| $E_0$ | Resting potential |
| $E_{corr}$ | Corrosion potential |
| $E_p$ or $E_{pp}$ | Passivation potential |
| $F_1$ | Mechanical calibration factor (for cold spray 1.2) |
| $F_2$ | Thermal calibration factor (for cold spray 0.3) |
| $i_c$ | Critical passivation current density |
| $i_{corr}$ | Corrosion current density |
| $i_p$ or $i_{pp}$ | Passivation current density |
| $RT$ | Room temperature, 22ºC |
| $T_i$ | Impact temperature |
| $T_m$ | Melting point |
| $T_{particle}$ | Particle temperature |
| $T_{particle,\ initial}$ | Initial particle temperature |
| $T_R$ | Reference temperature (293 K) |
| $v_{cr}$ or $v_{crit}$ | Critical velocity needed for coating formation, Eq. 1 |
| $v_{crit}^{th,mech}$ | Critical velocity in advanced Eq. 2 |
| $v_{erosion}$ | Erosion velocity |

*Materials abbreviations*

| | |
|---|---|
| Al | Aluminum |
| Al+$Al_2O_3$ | Aluminum+aluminum oxide (composite) |
| $Al_2Cu$, $Al_4Cu_9$ | Aluminum-copper intermetallic alloy |
| $Al_2O_3$ | Aluminum oxide (alumina) |
| $Al_2O_3$-$Ti_2O$ | Aluminum oxide-titanium dioxide (composite) |
| Al-$MnO_2$ | Aluminum-manganese dioxide (composite) |
| Al-Si | Aluminum-silicon (alloy) |
| Al+SiC | Aluminum+silicon carbide (composite) |
| Al-Zn-Ti | Aluminum-zinc-titanium (composite) |
| Ag | Silver |
| Ar | Argon |
| Ar-3$H_2$ | Argon-3%hydrogen |
| BCC | Body-centered cubic lattice structure |
| CoNiCrAlY | Cobalt-nickel-chromium-aluminum-yttrium (alloy) |
| Cu | Copper |
| Cu+$Al_2O_3$ | Copper+aluminum oxide (composite) |
| CuAl | Copper-aluminum (alloy) |
| Cu-Al | Copper-aluminum (composite) |
| $Cu_2O$ | Copper oxide, patina |
| Cu-Sn | Copper-tin (bronze) |
| Cu-W-Zn | Copper-tungsten-zinc (composite) |
| Cu-Zn | Copper-zinc (brass) |
| FCC | Faced-centered cubic lattice structure |
| Fe | Iron |
| Fe52 | Carbon steel |

| | |
|---|---|
| $H_2SO_4$ | Sulfuric acid |
| HCl | Hydrochloride acid |
| He | Helium |
| HF | Hydrogen fluoride |
| MCrAlY | M-chromium-aluminum-yttrium, M=metal (alloy) |
| $N_2$ | Nitrogen |
| NaCl | Sodium chloride |
| Nb | Niobium |
| Ni | Nickel |
| Ni+TiC | Nickel-titanium carbide (composite) |
| NiAl | Nickel-aluminum (alloy) |
| $NiAl_3$, $Ni_3Al$ | Nickel aluminide (intermetallic alloy) |
| Ni-Cu | Nickel-copper (alloy) |
| Ni-30Cu | Monel 400 alloy |
| Ni-Cr | Nickel-chromium (alloy) |
| NiO | Nickel oxide |
| Si | Silicon |
| SiC | Silicon carbide |
| SiO | Silicon oxide |
| Ta | Tantalum |
| Ta-$MnO_2$ | Tantalum-manganese dioxide (composite) |
| $Ta_2O_5$ | Tantalum pentoxide |
| Ti | Titanium |
| TiMo | Titanium-molybdenum (alloy) |
| $TiO_2$ | Titanium dioxide |
| W | Tungsten |
| WC-Co | Tungsten carbide-cobalt (hardmetal, alloy) |
| WC-Co-Cr | Tungsten carbide-cobalt-chromium (hardmetal, alloy) |
| $WO_3$ | Tungsten trioxide |
| $Y_2O_3$ | Yttrium oxide |
| Zn | Zinc |
| Zn-Al | Zinc-aluminum (composite) |
| Zn/Al/$Al_2O_3$ | Zinc-aluminum-aluminum oxide (composite) |
| Zr | Zirconium |

*Methods and other abbreviations*

| | |
|---|---|
| Ag/AgCl | Silver/silver chloride reference electrode |
| APS | Atmospheric plasma spraying |
| ARC | Electrical arc spraying |
| ASM | American Society for Material |
| ASTM B117 | Standard for salt spray test |
| ASTM G59 | Standard for anodic polarization measurements |
| BSE | Backscattered electrons |
| CS | Cold spraying |
| CGT | Cold Gas Technology |
| DE | Deposition efficiency |
| EBSD | Electron backscattering diffraction |
| EDS | Energy dispersive X-ray spectrometer |
| EN 582 | Standard for tensile pull test |
| FLAME | Flame spraying |
| FESEM | Field-emission gun-scanning electron microscopy |
| HPCS | High-pressure cold spraying |
| $HV_{0.2}$ | Vickers hardness, weight of load 200 g |
| $HV_{0.3}$ | Vickers hardness, weight of load 300 g |
| HVOF | High-velocity-oxygen-fuel spraying |
| ITAM SB RAS | Institute of Theoretical and Applied Mechanics of the Siberian Branch of the Russian Academy of Sciences |

| | |
|---|---|
| LALPCS | Laser-assisted low-pressure cold spraying |
| LPCS | Low-pressure cold spraying |
| Nd:YAG | Neodymium-doped yttrium-aluminum-garnet laser |
| OCPS | Obninsk Center for Powder Spraying |
| PIC | Optimal impact conditions |
| SCE | Saturated calomel electrode |
| SE | Secondary electrons |
| SEM | Scanning electron microscopy |
| TEM | Transmission electron microscopy |
| VPS | Vacuum plasma spraying |
| WS | Window of sprayability |

## 1 INTRODUCTION

Coating technology is growing because of its important role in improving, e.g., corrosion resistance, conductivity, and other properties of material in order to decrease costs and increase service life and safety. Thermal spray processes, including flame, arc, plasma, high-velocity oxygen fuel (HVOF) and cold spraying, are the techniques to produce coatings from powder or wire feedstock by spraying molten, semi-molten or solid particles on the substrate and forming the coating. Acceleration of particles can be done by several ways based on energy used: electrical (arc and plasma spraying), chemical (flame and HVOF spraying), or kinetic (cold spraying) energy [1]. Cold spraying is a relatively new spraying method, which has many advantages over other forms of thermal spraying. The advantages are high deposition efficiency, low residual stresses, minimal heat input to substrate, phase and compositional stability, and little need for masking [2]. Furthermore, cold spraying is a cost-effective and environmentally-friendly alternative to e.g., soldering, electroplating, and painting [3].

Cold spraying was developed in the former Soviet Union in the 1980´s at the Institute of Theoretical and Applied Mechanics of the Siberian Branch of the Russian Academy of Sciences, ITAM SB RAS, (Novosibirsk, Russia) [2,4]. The latest thermal spray technique is based on the use of significantly lower process temperatures with high particle velocities than those present in other thermal spray techniques [2,5,6]. Figure 1 shows a diagram of gas temperatures and particle velocities in different thermal spray processes. During the past decades, the trend has turned from the use of thermal energy to the use of increasing amounts of kinetic energy. This opens new advantages, e.g., pure and dense coating formation due to the low or zero-level oxidation during the cold spray process. In addition, heat input is significantly low, not changing the substrate properties, and avoiding oxidation during spraying [3,7]. The other advantages are that phase transformations caused by melting and porosity formation caused by solidification in the other methods can be eliminated by the use of cold spray process [8]. Temperature of the gas is well below the melting point of the sprayed material and thus, particles are not melted in the gas flow [9]. Furthermore, residual stresses are compressive (peening effect of impinging solid particles [3]), offering chances to spray dissimilar materials [3,4].

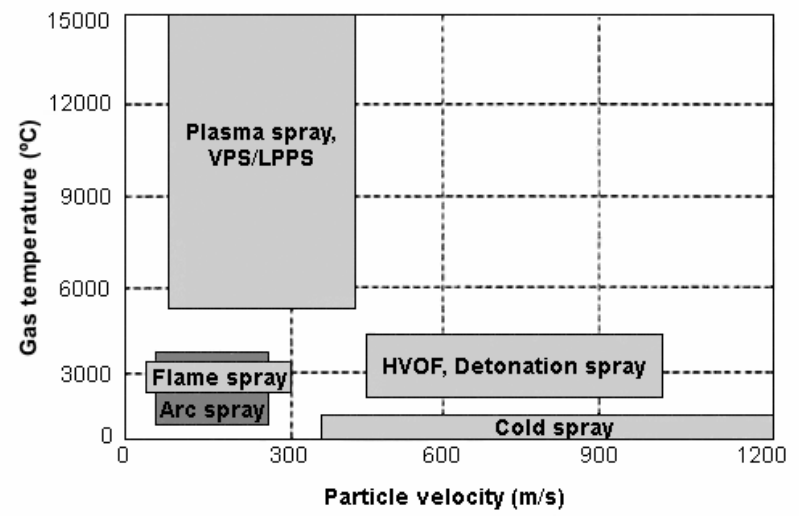


**Figure 1.** Gas temperatures versus particle velocities in the thermal spray processes. VPS is a vacuum plasma spray and LPPS is a low-pressure plasma spray process [1].

Due to the fact that cold spraying is a solid-state method, oxide inclusions, and void formation can be avoided [9]. Typical defects of this kind in other thermally-sprayed coatings are presented in Fig. 2. The schematic presentation is shown in Fig. 2a and typical cross-sectional structure in Fig. 2b.

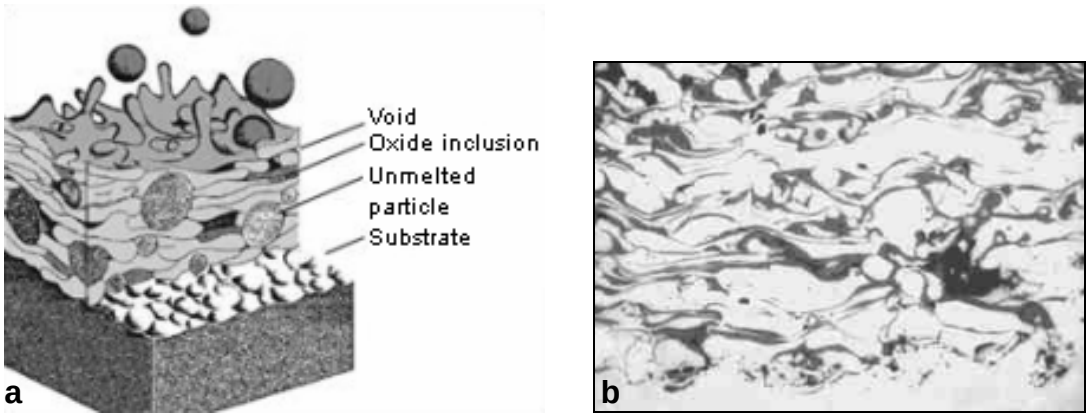


**Figure 2.** Thermally-sprayed coatings: a) typical defects in the coating structure and b) typical lamellar microstructure with oxide inclusions and pores [10].

Typically, almost all materials can be sprayed using the thermal spray methods. The flame and electric arc spray methods are often used to prepare coatings for less demanding applications. Porosity levels and oxygen contents are higher than in the other processes. Plasma spraying is usually used for manufacturing ceramic coatings [1] and HVOF is used as a method to produce metallic and cermet (hardmetal) coatings [8,11]. Material selection is larger in other thermal spray processes than in cold spraying, including metals, metal alloys, ceramics, cermets, composites, and plastics [1]. In turn, cold spraying is a method to produce metallic and composite coatings and there are limitations of coating materials; ceramic and non-ductile materials cannot be sprayed alone, they will need a ductile component in the composite coating. Thus, this is one requirement for the sprayed material in the cold spraying; the capability to be deformed plastically, i.e., the ductility of the powder is needed. [1,2,4] However, embedded ceramic particles as surface treatments produced by using cold spraying are reported [12-15]. Nevertheless, a relatively wide range of coating materials, e.g., pure metals Al, Cu, Zn, Ni, Ti, Ta, Ag, Ni, Fe, metal alloys, Ni-Cr, Ni-Cu, Ni-Al, Cu-Al, Cu-Sn, Cu-Zn, MCrAlY, CoNiCrAlY [16], stainless steel, and composites, Al-$Al_2O_3$, Al-Zn-Ti, Cu-W-Zn, Al+SiC, Cu+$Al_2O_3$, Ni+TiC can be used in cold spray process [1,4,17]. In addition, substrates can be metals, metal alloys, polymers, ceramics, and composites [4].

Comparison between deposition rates and deposition efficiencies of thermal spray methods is presented in Fig. 3 whereas porosity levels and oxygen contents in different thermally-sprayed coatings are shown in Table 1. In cold spraying, the deposition rate is equal or lower than in the other methods. However, the deposition efficiency can be significantly higher in the cold spray process than in the others. It is reported to be as high as 97 % (Cu coating) [18]. In addition, porosity and oxygen contents are lower in cold-sprayed coatings. Generally speaking, porosity and oxygen content decrease with increasing particle velocity (compare Fig. 1 and Table 1).

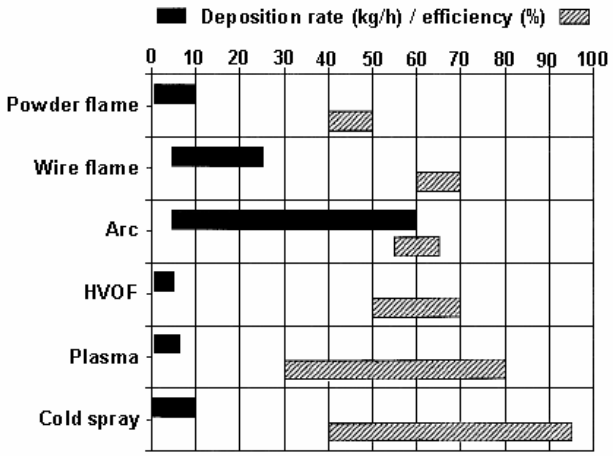


**Figure 3.** Deposition rates and efficiencies: comparison between different thermal spray methods. After Champagne [1].

**Table 1.** Porosity and oxygen contents of coatings in different thermal spray methods [1,11,19,20].

| Method | Porosity (%) | Oxygen content (%) |
|---|---|---|
| **COLD SPRAY** | 0.1 [19] | same as in the powder [1] |
| **HVOF** | 1 [11] | 0.2 [20] |
| **FLAME** | 10-20 [11] | 4-6 [20] |
| **ARC** | 10-20 [11] | 0.5-3 [20] |
| **PLASMA** | 1-7 [11] | 0.5-1 [20] |

Normalized costs in different thermal spray processes according to Champagne [1] are summarized in Fig. 4. Capital costs are shown in Fig. 4a. In flame spray and arc spray processes, capital costs are relatively low. On the other hand, in HVOF process, capital costs are higher and they are the highest in the low-pressure or vacuum plasma process. In cold spray process (high-pressure cold spray system), the main capital costs are come from powder feeder and gas heater [1]. Although capital costs in cold spraying are higher than those of in the other methods (expect low-pressure/vacuum plasma spraying), running costs are at the same level as in the powder flame spraying and in addition, lower than in HVOF and plasma spraying. Typically, methods using wires have lower running costs due to cheaper feedstock materials (wire versus powder). Generally speaking, powders incur the main costs. Moreover, gas costs are the highest in the cold spray process and will be even higher if He is used as a process gas. The normalized running costs are illustrated in Fig. 4b.

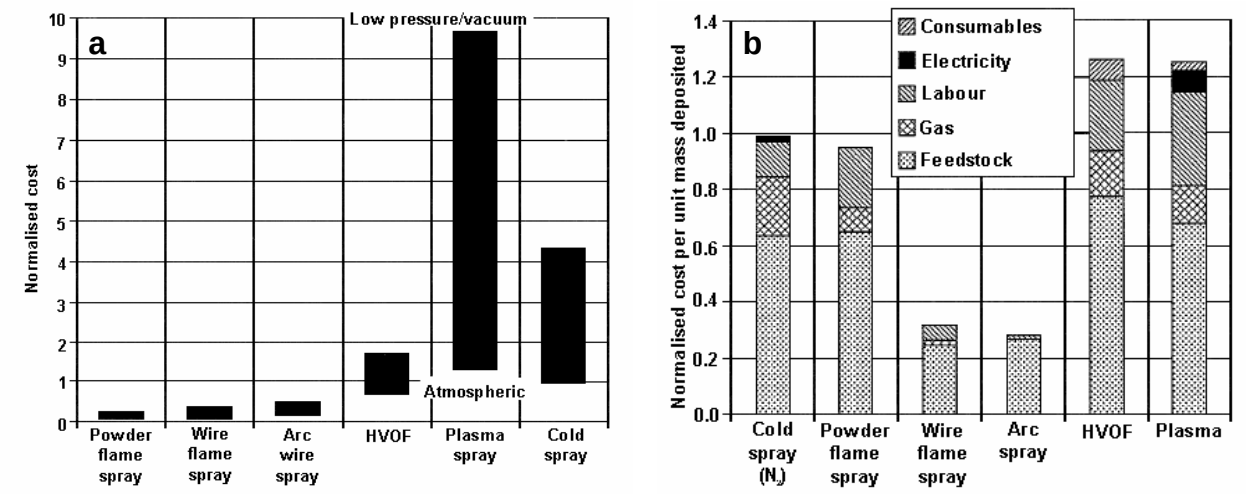


**Figure 4.** Comparison of normalized costs in different thermal spray processes: a) relative capital costs of copper spraying based on proprietary feedstock and gas cost information and b) comparison of running costs based on the average values of deposition rates and efficiencies for copper. After Champagne [1].

Cold spray process was firstly patented (1994) by Alkhimov et al. [21,22]. In addition, various cold spray related innovations are patented by several authors. Patents include cold spray devices, nozzle design, coating materials, applications etc. Cold spraying, high-pressure cold spraying, low-pressure cold spraying, cold gas dynamic spraying, kinetic metallization, dynamic metallization, and kinetic spraying are all based on the same basic idea of the process.

## 2 COLD SPRAYING

In a cold spray process, powder particles impact on the surface with high kinetic energy (high velocity), deform, adhere to the substrate or other particles, and thus, depositing the coating [2,4,9,23,24]. A gas ($N_2$, He or air) is accelerated to supersonic velocity by a converging-diverging de Laval type nozzle. Powder particles are fed into the gas flow and they are accelerated and sprayed on the substrate. [9] This occurs by drag effect [6]. Formation of a cold-sprayed coating depends on the velocity of powder particles. Each material has a specific critical velocity $v_{cr}$. Above $v_{cr}$ the particles adhere to the substrate, causing plastic deformation and formation of the coating whereas at velocities lower than $v_{cr}$ only erosion and particle rebounding occur without coating building up [1,9,23-26].

In cold spraying, several parameters such as a particle size, particle temperature, substrate material and the properties of the coating material have a remarkable influence on the coating formation and the deposition efficiency [4,5,9]. In addition, good bonding between the cold-sprayed powder particles requires heavy plastic deformation during the particle impacts [1,5,6,23]. For successful bonding, deposition conditions, where oxide layers on the particle surfaces are removed during impact, should be created [5]. The powder particles impinge on the substrate in solid form, well below the powder melting temperature [23]. Furthermore, compressed layer takes form near to the impact surface and leads to the formation of shock waves (bow shock) near to the sprayed surface [27]. The shock layer decreases particle velocity and increases particle temperature [2,28,29]. Particles should go through the shock layer and hence, high kinetic energy is needed. At the same time, thermal softening and adiabatic shear instability play a very important role in the bonding between particles and substrate in the cold spray process [24,30,31].

Additionally, coating quality relies on spraying conditions. Reportedly, the preheating temperature of the process gas has an influence on the particle velocity and the coating quality [1,2,9]. Preheating of the gas increases viscosity of the gas which in turn, increases gas velocity and thus, also particle velocity [32]. Furthermore, higher velocity leads to stronger deformation and therefore, coating structure becomes denser and mechanical properties are improved [33,34]. Higher process temperature together with higher pressure promotes denser coating structure precisely due to the thermal softening and local shear instability [31]. Moreover, in the particle interfaces, the temperature is increased due to the adiabatic localization (and thermal softening) [30]. As a materials processing method, cold spraying is kept very similar to an explosive welding [35,36].

Cold spraying is an effective method of depositing dense coatings with very low porosity and pure coatings with low oxygen content [37]. This is regarded as an advantage to several important material properties, such as electrical conductivity and corrosion resistance [9]. Because the sprayed material undergoes neither phase transformations nor melting during the spray process (solid state process), cold spraying enables, in principle, the production of highly dense metallic coatings [1,9,37]. Oxygen contents are reported to be at the same level in the coating compared with the level in the as-received powder [1,7,23].

The basic idea of particle collision in the cold spray process is presented in Fig. 5. Two particles impact on the substrate overlapping with each other. The impacting particles highly deform, forming ring-type material jets around the particle impact zone. The latter particle also enhances the deformation of the first particle due to the overlapping. In the final state, particles are highly deformed with flattened shapes, having material jets formed in the particle interfaces. [31,38]

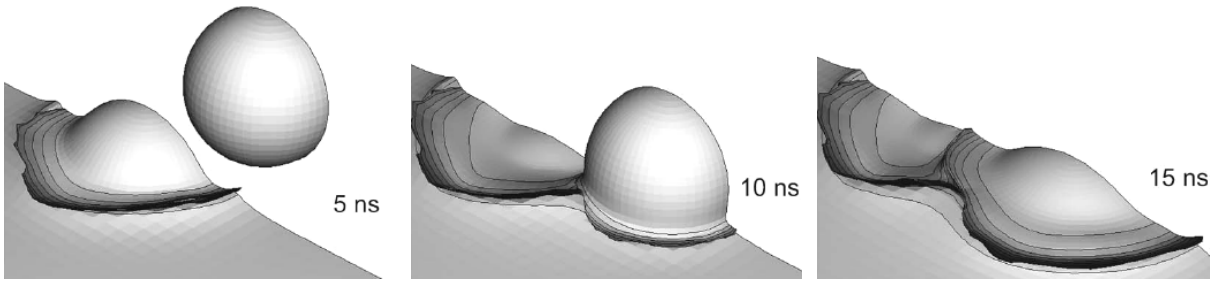


**Figure 5.** Simulated situation of particle impacts after impact times of 5, 10, and 15 ns from the first particle [31,38].

High gas velocities generate high particle velocities [1,2,6]. For that purpose, the gas is preheated in order to increase the velocity of the particles but also to increase the temperature [1,2,9]. High velocities also result in a high impact deformation at the interfaces of both substrate and coating and between particles [9,39,40]. Furthermore, the gas and particle temperatures significantly affect the quality of the cold-sprayed coatings by improving it with higher temperatures. High temperature leads to high velocity and, thus, to strong impacts. [7,32,41,42] Moreover, because deposition efficiency (DE) depends on the temperature of the gas, DE is reportedly improved at high gas temperatures [39,40,43-45]. Furthermore, substrate pretreatments are reported to have an effect on DE. It can be slightly increased with increasing roughness of grit-blasted substrate. On the other hand, for instance increased traverse speed (100 mm/s versus 20 mm/s) decreases DE of Cu and Ti coatings [44].

## 2.1 High-pressure cold spraying

Cold spraying is divided into two different processes by the pressure level used; high-pressure cold spray (HPCS) and low-pressure cold spray (LPCS) processes. The HPCS process enables the use of pressure as high as 40 bar and preheating temperature of max. 800ºC (Kinetiks 4000). Typically, pure metal and metal alloys are used as powder materials in the HPCS process. Furthermore, the selection of powder materials is larger with the HPCS process compared to the LPCS process. Typically, metals and metal alloys, e.g., Cu, Al, Ta, Ni, Cu-Sn, NiCr, and Ni-Al are used as a powder material. Figure 6 shows schematic presentation of the HPCS process. Basically, in the HPCS process, high pressurized gas ($N_2$, He or mixture of these gases) is heated and it flows to the nozzle where powder is fed with carrier gas. Then, the gas-powder flow is fed through the nozzle in which high velocity is generated. After that, particle-gas flow exits the nozzle with high speed and impacts on the sprayed surface. The HPCS process is controlled with a control unit.

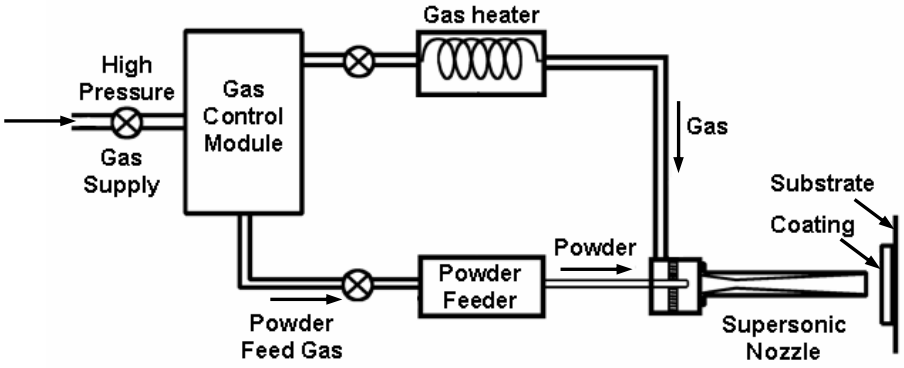


**Figure 6.** Schematic presentation of cold spray process [46].

In cold spraying, converging-diverging nozzle is used to produce supersonic gas flow in which particles achieve supersonic velocity. Supersonic velocity is created in the nozzle throat, in the diverging part of the nozzle. Powder is fed with carrier gas in axial direction and then, mixed

with the main gas forming a particle-gas flow before the nozzle. De Laval type converge/diverge nozzle is the most commonly used. Schematic presentation of one cold spray gun with de Laval nozzle is shown in Fig. 7. The colors indicate temperatures in different regions of the gun, from warmer (red) input to colder (blue) output.

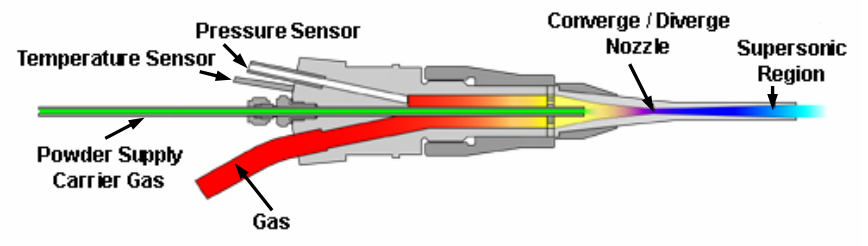


**Figure 7.** Schematic presentation of cold spray gun. Colors indicate temperatures, in the red areas, temperature is the highest and in the blue areas, temperature is the lowest [47].

## 2.2 Low-pressure cold spraying

In the LPCS process, preheating temperatures of the process gas are between room temperature (RT) and 650ºC, and pressures between 5 and 9 bar. Usually, compressed air is used as process gas to spray powder mixtures [48]. Typically, LPCS process is a method to spray metallic powders (e.g., Cu, Al, Ni, Zn) with an addition of ceramic powder ($Al_2O_3$, SiC) as powder mixtures. The main functions of the ceramic powder addition are to activate the sprayed surface and to keep the nozzle of the gun clean. In addition to these, ceramic particles affect the coating by mechanical hammering of the substrate/sprayed layers or by the so-called shot peening via particle impacts [49,50]. The ceramic particle addition in the powder mixtures has also a compacting effect during the impacts, indicating improved coating properties and deposition efficiency of metallic coatings [51-53]. The hard phase can also be used for reinforcing and strengthening the metallic matrix in the LPCS process [54].

The main difference between the spray guns used in the HPCS and LPCS processes is that in the LPCS process, powder is fed to the gas flow perpendicularly (radial injection) to the diverging part of the nozzle as presented in Fig. 8. In addition to that, Papyrin et al. [55] have presented the possibility to inject two powders, e.g., Cu+Al, and Cu+SiC, separately to the nozzle (two powder feeders at the same time) and form composite coatings. Additionally, another difference between the LPCS and HPCS processes is that heating of gas is done only in the spraying gun in the LPCS process whereas in the HPCS process, gas is preheated in the separate heating unit and in addition to that, in the spraying gun. Although powder feed rates are lower in the LPCS process, particle concentration in gas flow can be higher than in the HPCS process [6].

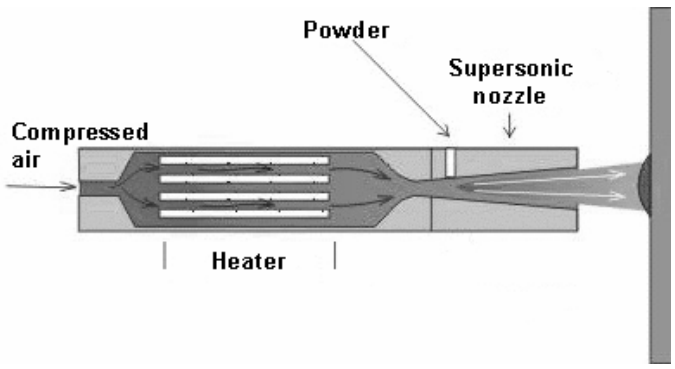


**Figure 8.** Schematic presentation of spraying gun in LPCS process. Powder is fed radially to diverging part of the converging-diverging type nozzle [49,56].

As a summary, typical spraying parameters used in these two cold spray processes are presented in Table 2. The main differences relate to process gas, pressure level and electrical power used. In addition to these, the HPCS system is a more efficient process with higher gas flow and powder feed rates.

**Table 2.** Typical spraying parameters used in cold spray processes.

| Spraying parameter | HPCS | LPCS |
|---|---|---|
| Process gas | N2, He, mixture | Compressed air |
| Pressure (bar) | 7-40 | 6-10 |
| Preheating temperature (ºC) | 20-550-800 | 20-650 |
| Gas flow rate ($m^3$/min) | 0.85-2.5 ($N_2$), max. 4.2 (He) | 0.3-0.4 |
| Powder feed rate (kg/h) | 4.5-13.5 | 0.3-3 |
| Spraying distance (mm) | 10-50 | 5-15 |
| Electrical power (kW) | 17-47 | 3.3 |
| Particle size (µm) | 5-50 | 5-30 |

These two cold spray processes, the HPCS and LPCS processes, have their own advantages and as methods, they support each other. Generally, cold spray processes offer several advantages, e.g., high deposition efficiency, high deposition rate, high denseness, minimal thermal input to the substrate, compressive residual stresses, no oxidation, and no phase changes. On the other hand, some limitations in the number of cold sprayable materials (i.e., mainly ductile metals and alloys are prosessable by cold spraying), low ductility of the coatings in their as-sprayed state and that cold spraying, as also other thermal spray processes, is a line-of-sight process, can be regarded as disadvantages of the cold spray processes [1]. The main advantages of the stationary HPCS process are a significantly larger material selection and higher quality of the coatings whereas the investment costs of the LPCS equipment are lower than those of the HPCS process. In addition, on-site spraying is possible by using the portable LPCS equipment. Furthermore, both cold spray processes have specific powder characteristics of their own together with optimal spraying parameters to produce high quality coatings. Coating properties are presented in the following Chapters.

## 3 COLD-SPRAYED COATINGS

Basics of coating formation by cold spraying and more about specific details in cold spraying as the method to produce metallic coatings are presented here. In addition, coating properties, corrosion resistance of the coatings in general, and potential applications are identified.

### 3.1 Coating formation

As it is generally known, powder particles need certain critical velocity ($v_{crit}$) for successful coating formation in cold spraying. If particle velocity is below the material-dependent critical velocity, then particles rebound and do not form the coating [24]. However, activation (cleaning) of the sprayed surface occurs [6,23,57]. If the particle velocity is above the critical velocity, then particles adhere to the surface and build-up the coating [24]. Particles are stuck to the surface by plastic deformation or they just penetrate (or are embedded) into the sprayed surface [57].

Formation of the cold-sprayed coating is presented in Fig. 9. First particles cause the build-up the coating (adhered particles) and substrate cratering (rebounded particles) [23,58]. Formation of the cold-sprayed coating is based on two steps: build-up of the first layer (particle-substrate interactions) and deposit of the coating (particle-particle interactions). In the first step, adhesion strength between coating and substrate is defined whereas step 2 defines the cohesive strength of the coating [58]. At the first stage, particle-substrate interactions occur and are affected by substrate and coating materials as well as surface preparation. After that, new incoming particles adhere to the previous particles, deform and realign; now the coating is built-up. At the second stage, particles interact with each other and form the coating structure. [57] During the spraying, metallic bonding and void reduction occur and after that, coating structure is densified and work-hardened [23].

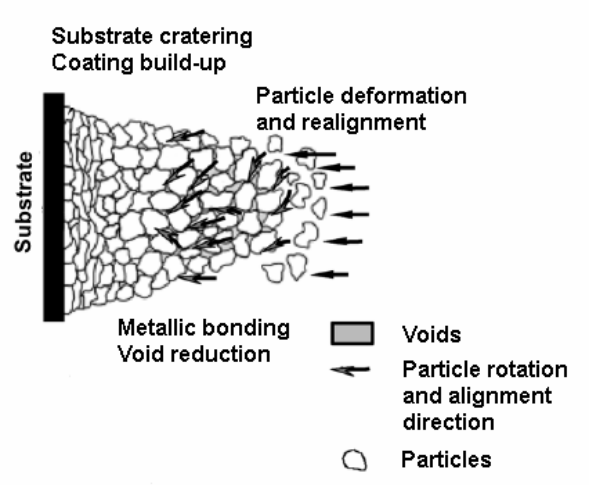


**Figure 9.** Schematic presentation of coating formation in cold spray process. Firstly, substrate cratering occurs together with first coating layer build-up. Secondly, at the same time, particles deform and realign together with resulting void reduction and metallic bonding between particles [23].

Typically, in the LPCS process, powder mixtures and powder blends are used as feedstock materials. Figure 10a presents the formation of the structure from powder mixture and the arrangement of particles of different-type powder materials during impacts. In addition, Fig. 10b shows schematic presentation of the mixture coating with particle alignments in the flow and in the structure [6,49]. Acceleration of particles in the high-velocity air flow is caused by drag forces [6]. According to Maev et al. [6] particles deform highly and inter-particle sliding occurs during particle interactions.

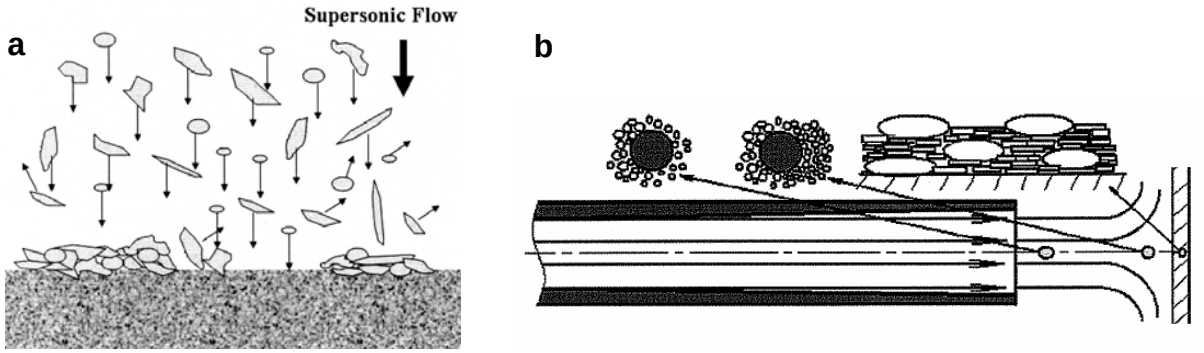


**Figure 10.** Schematic presentation of mixture coating formation in cold spray process: a) particle impacts [49] and b) particle alignment in the flow and in the coating structure [6].

The coating is formed by several particle collisions and thus, structure formation depends on the neighboring particles [23]. During powder particle impacts, high contact pressure forms on the particle-substrate interface. Pressure level generation during impact time is presented in Fig. 11. Obviously, the highest pressure point is formed at the connecting point of the particle and substrate impact [59].

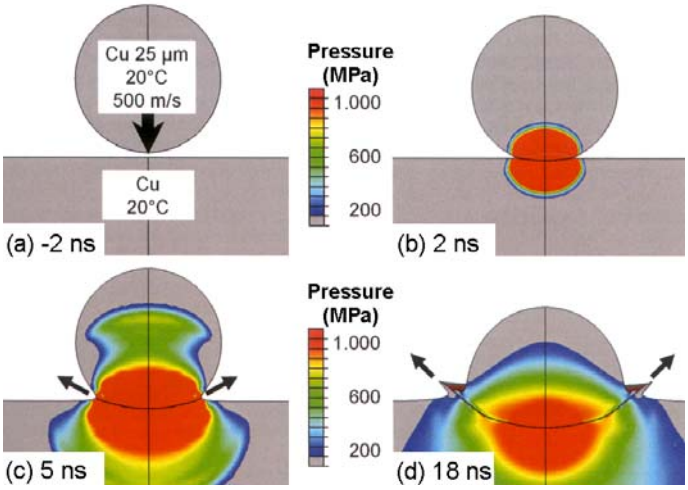


**Figure 11.** Impact of cold-sprayed Cu particle (25 µm) on Cu substrate a) before impact, b) after 2 ns, c) after 5 ns, and d) after 18 ns. Colors indicate pressure distribution during impact. Simulated condition, after Schmidt [59].

As previously known, the powder particle deforms plastically in the particle impact. A high strain level is achieved and is mostly concentrated on the particle-substrate or particle-particle interfaces on the impact surface. The strain distributions after 0.01 µs and 0.05 µs are presented in Figs. 12a and 12b, respectively. Jetting is caused by high straining [59] and thus, the highest strains are detected in the jetting regions [26]. In addition to the high pressure level and high strain, the temperature is increased on the impact surface during the particle impacts [9,59] and concentrated primarily on the jetting area. During impact time, the temperature rapidly decreases [59]. This is presented in Figs. 12c and 12d. In the adhesion and sticking of the particles, kinetic energy transforms into heat and strain energy [7,23]. The temperature and strain are inhomogeneously distributed, indicating localized deformation. Furthermore, the particle deformation is strong at the localized contact interfaces [25].

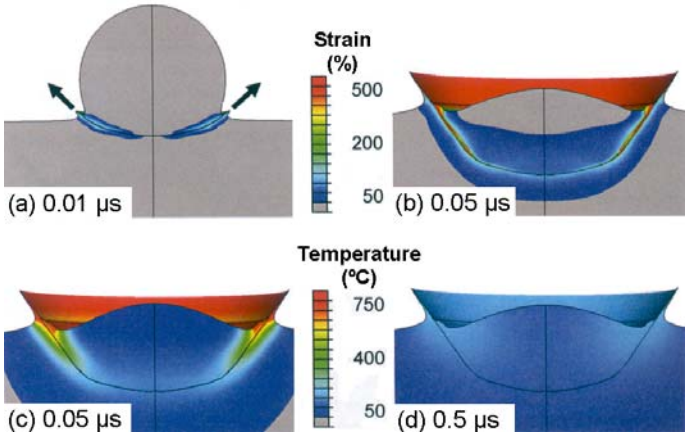


**Figure 12.** Impact of cold-sprayed Cu particle on Cu substrate. Strain distribution a) after 0.01 µs, formation of material jets started and b) formation state after 0.05 µs. Temperature distribution c) after 0.05 µs and d) after 0.5 µs. Colors indicate either strain or temperature distributions after impact. Simulated condition, after Schmidt et al. [40] and Schmidt [59].

### 3.1.1 Velocities

Numerous studies concern modeling and simulation of the cold spray processes, particle velocities, and related phenomena are analyzed elsewhere, e.g., in [6,24,31,60]. In this particular study, critical velocities are not modeled, calculated or measured. Instead of that, this study focused on characterization of the already formed coating structures. However, because of the importance of the particle velocity in order to form the coating, particle velocities and critical velocity are described here.

#### 3.1.1.1 Critical velocity

As mentioned before, in the cold spray process, critical velocity of powder particles is required for the formation and build-up of the coating. Reportedly, critical velocity depends on the sprayed material. Furthermore, critical velocity is influenced by powder quality, particle size (not included in the equations), and particle impact temperature [24,31]. In addition, critical velocity depends on kinetic energy, material strength and heat generation [40]. Schmidt et al. [24] after Assadi et al. [31] have described simple expression for the critical velocity using the following equation (Eq. 1).

$$v_{crit} = 667 - 0.014\rho + 0.08(T_m - T_R) + 10^{-7}\sigma_u - 0.4(T_i - T_R) \quad \text{(Eq. 1)}$$

| | | | |
|---|---|---|---|
| ρ | Density | $T_m$ | Melting point |
| $\sigma_u$ | Yield strength | $T_i$ | Impact temperature |
| | | $T_R$ | Reference temperature (293 K) |

This equation is useful for materials similar to copper [24]. Densities of the particles affect the velocity; heavier particles have a lower critical velocity [31]. In addition to that, particle size can affect the velocity [24,61]. The effect of particle size on the particle impact velocity and critical impact velocity is presented in Fig. 13. Furthermore, particle velocity is said to be a function of its size [24] and thus, powder has a range of particle velocities [62].

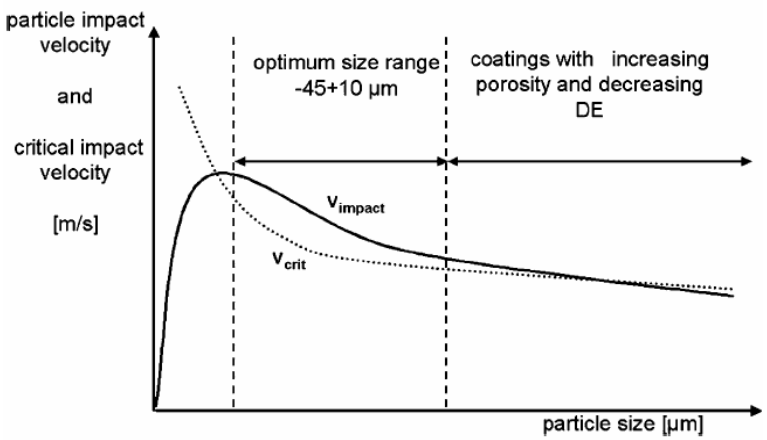


**Figure 13.** Schematic presentation of particle impact velocity and critical impact velocity as a function of particle size. After Schmidt et al. [24].

On the other hand, if the particle size distribution of the powder is wide, critical velocity is defined for the largest particles [24] due to the fact that smaller particles have higher velocity [24,60]. Critical velocities are mostly modeled values and in the evaluations, 90 % of plastic strain energy is assumed to be dissipated into heat [24]. One explanation for the heat transfer is the wave propagation [31]. In addition, Schmidt et al. [24] have presented an advanced equation for the critical velocity, $v_{crit}^{th,mech}$ which also takes specific heat, tensile strength, and mechanical and thermal calibration factors into account, Eq. 2. Calculated critical velocities for 25 µm particles for several metal materials calculated with Eq. 2, are shown in Fig. 14.

$$v_{crit}^{th,mech} = \sqrt{\frac{F_1 * 4 * \sigma_{TS} * (1 - \frac{T_i - T_R}{T_m - T_R})}{\rho} + F_2 * c_p * (T_m - T_i)} \qquad \text{(Eq. 2)}$$

| | | | |
|---|---|---|---|
| $\rho$ | Density | $T_m$ | Melting point |
| $\sigma_{TS}$ | Tensile strength | $T_i$ | Impact temperature |
| $c_p$ | Specific heat | $T_R$ | Reference temperature (293 K) |
| $F_1$ | Mechanical calibration factor (for cold spray 1.2) | | |
| $F_2$ | Thermal calibration factor (for cold spray 0.3) | | |

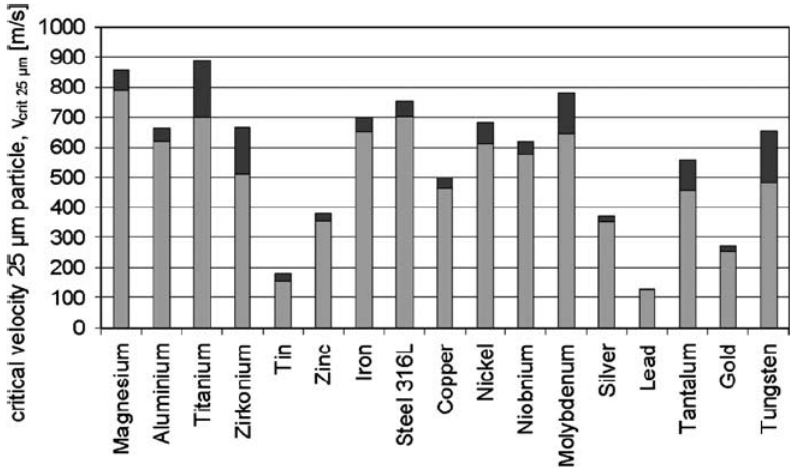


**Figure 14.** Critical impact velocities for several powder materials (Ø 25 µm) [24].

Particle size affects velocity by increasing it with decreasing particle size. Additionally, small particles have higher critical velocities due to the higher impurity content. Kang et al. [63] have

reported that higher oxygen content of powder in as-received state increases critical velocity of the powder. On the other hand, critical velocity can be decreased by increasing temperature. Particles having a higher temperature are in the softer state and thus, less kinetic energy is needed for the plastic deformation. [24]

#### 3.1.1.2 Particle velocity

Gas dynamics have an influence on the particle velocity and temperature on impact. The most important characteristics of gas flow are high-pressure shock wave layer formed near to the substrate, structure, and stability of the supersonic jet [6,27,64]. Bow shocks are observed with Schlieren imaging and are achieved in the supersonic velocity [28]. Velocity decreases in the shock wave (bow shock) layer, increasing gas mass density and therefore, increases drag forces on the particles [27]. In addition, bow shock decreases the gas velocity to subsonic velocity [65]. High pressure (as was already detected in Fig. 11), together with high density gas flow, generates formation of the shock wave layer near to the sprayed substrate, Fig. 15 [28,65,66]. This layer reduces the particle velocity and thus, particles should have enough velocity to go through the bow shock layer. In addition, shock wave increases gas pressure and temperature while gas velocity decreases [29]. The shock wave layer has more proper effect on the particle velocity of small particles [29,65,66]. Furthermore, bow shock is more evident with short spraying distances and could disappear with larger distances [28]. Moreover, a drag coefficient is lower with the spherical particles compared with the irregular particles [67,68]. Therefore, the irregular particles with high drag forces exhibit higher velocities [28].

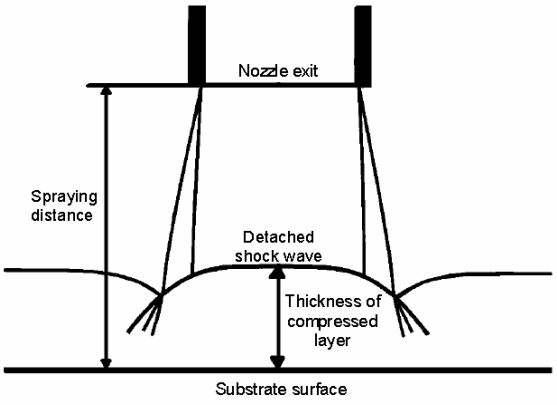


**Figure 15.** Schematic presentation of supersonic jet [66].

Particle impact velocity is also one of the crucial factors in the coating formation [69]. In cold spraying, solid particles impact on the sprayed surface with high velocities, 400-1200 m/s [24,40,70]. In the LPCS process, particle velocities are reported to be approximately from 350 to 700 m/s [71]. Obviously, particle size affects the particle velocity [70,72]. Large particles have lower velocity and also because of that, the degree of strain is slightly decreasing with increasing particle size [70]. Higher particle velocity, reportedly, improves coating quality [24,66]. In addition, the coating properties are improved by using higher preheating temperatures [39], resulting in higher particle temperature and hence, stronger deformability and adhesion [73]. Velocity increases in the throat of the nozzle and supersonic velocity is achieved in the divergent part of the nozzle. In the pressurized gas flow, powder particles reach the supersonic velocity as presented in Fig. 16. Due to the bow shock, particle velocity decreases in this area and thus, particles should have enough velocity and kinetic energy to go through the bow shock layer and to impact on the surface.

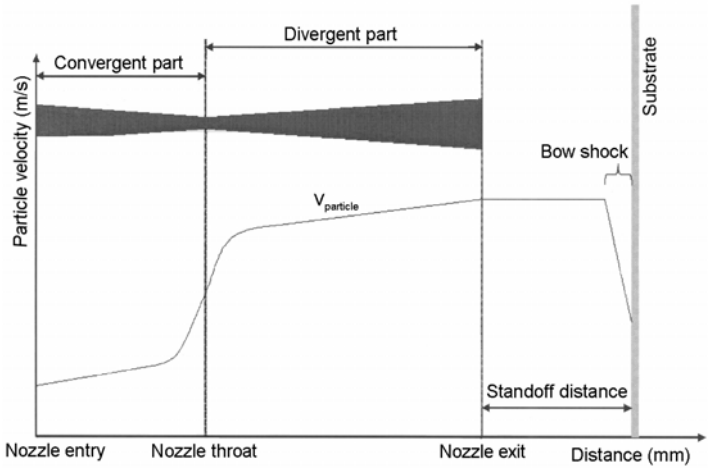


**Figure 16.** Schematic presentation of particle velocity behavior from nozzle entry to substrate surface. After Kairet [72].

Obviously, gas velocity also increases at the nozzle throat and in the diverging part of the nozzle. On the impact, the gas achieves higher velocities but lower temperatures than the particles [9]. The particle temperature increases near to the sprayed surface due to the bow shock formed near to the surface. The particle temperature from nozzle entry to the particle impact on the substrate is presented in Fig. 17. Temperatures of gas and particles are detected to have strong effect on the bonding between particles and particle-substrate [57]. On the other hand, the particle impact temperature can be increased by preheating the particles [40].

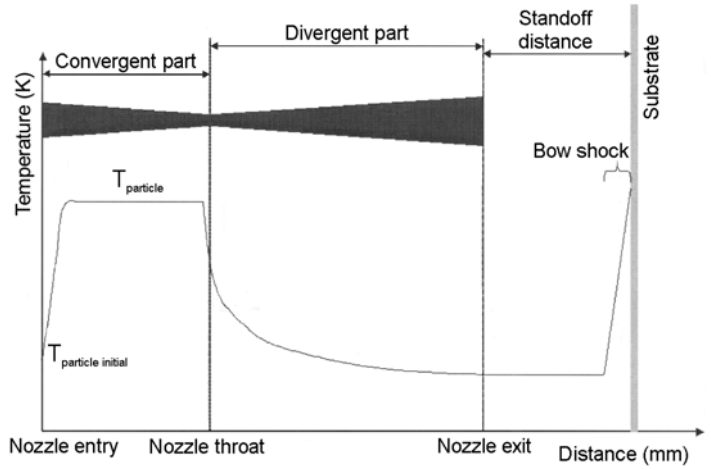


**Figure 17.** Schematic presentation of particle temperature behavior from nozzle entry to substrate surface. After Kairet [72].

As stated, the critical velocity is needed for the coating formation. However, if the velocity is too high, erosion occurs and coating is not formed [23]. Schmidt et al. [24] have presented a window of sprayability for the cold spraying, Fig. 18. Particle impact velocity should be higher than critical velocity $v_{crit}$ and on the other hand, lower than erosion velocity $v_{erosion}$. In addition, $v_{crit}$ and $v_{erosion}$ decrease with increasing particle impact temperature [24].

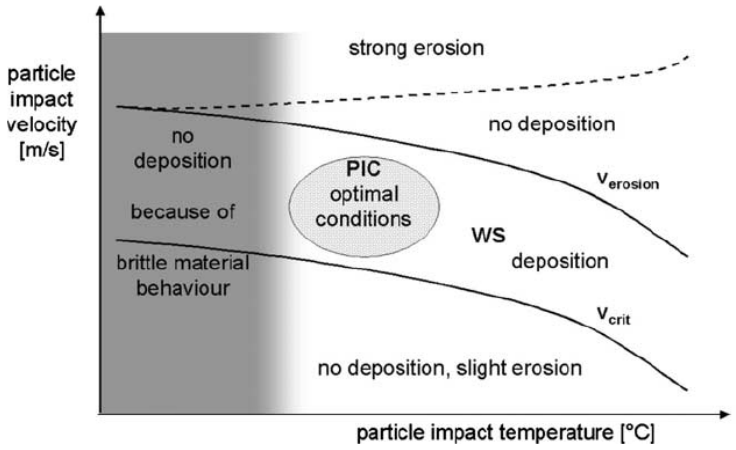


**Figure 18.** Window of sprayability (WS) and optimal impact conditions (PIC) for cold spraying as a function of particle impact velocity and particle impact temperature [24].

Particle velocity depends on particle size and density, gas pressure, gas temperature, gas molecular weight, and nozzle shape [4]. As stated, higher gas velocity generates higher particle velocity and for that purpose, gas is preheated in order to increase gas velocity and therefore, particle velocity [1,2,6]. In addition, lower molecular weight of the gas increases the velocity. [1,23] Typically, nitrogen, helium or air is used as a process gas. Molecular weights of $N_2$ and He are 28 and 4, respectively [74]. Lower weight increases the velocity. Ratio of specific heat for monatomic gas (He) is 1.66 and for diatomic gas ($N_2$, in addition, air is usually modeled as a diatomic gas (mixture of $N_2$ and $O_2$)), it is 1.4. Higher ratio of specific heat leads to higher velocity [4]. In addition, sonic velocity of air (80%$N_2$+20%$O_2$) is 343 m/s, of nitrogen 349 m/s and of helium 989 m/s, explaining the higher velocities produced by using helium as a process gas [1,75]. However, He is significantly more expensive gas which limits its use. The costs can be reduced by using a recycling system of He [1]. Moreover, the particle velocity increases with increasing temperature of the gas [65,76] and decreasing molecular weight of the gas [4]. Increasing pressure of the gas also increases particle velocity [76]; however, the effect of pressure is less significant than the effect of temperature [65]. Due to the lower molecular weight of He (4 versus 28), gas velocity of He is found to be twice as high as the velocity of $N_2$ exiting the nozzle, reflecting more acceleration effect of He on the particle velocity in the gas flow. In addition, larger particles have lower velocity than smaller ones [75].

### 3.1.2 Particle deformation

Due to the fact that coating formation depends on plastic deformation via particle impacts, particle deformation is an important factor in the coating deposition [5,6,9,23]. Particle deformation arising from plastic deformation, adiabatic shear instability, material jet formation, and adhesion of particle interfaces are discussed below.

#### 3.1.2.1 Plastic deformation

Plastic deformation is a permanent phenomenon and is caused by e.g., dislocation motion. Dislocation movements are also called slipping and therefore, dislocation lines as slip planes. In addition, plastic deformation can cause twinning in the structures. [77] Schematic presentations of deformation by slip and by twinning are clarified in Fig. 19 [78]. There again, high strain-rate deformation generates slipping and formation of the twins [5,78]. Plastic deformation is originated from dislocation movements caused by critical shear stress. In principle, plastic deformation occurs in each grain in the individual powder particle which means that particle boundaries can restrict the deformation of some grains. This indicates different levels of plastic deformations in the inter-particle structure and hence, through the coating structure. [79]

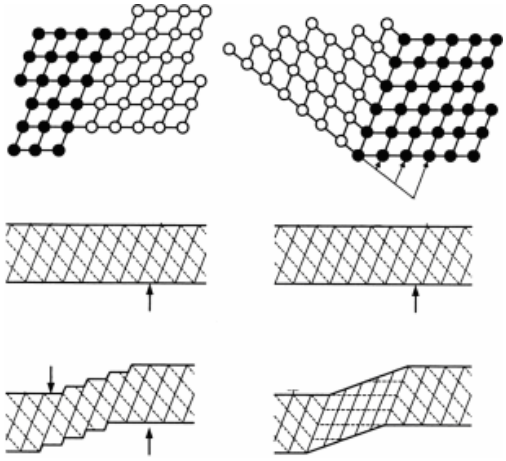


**Figure 19.** Schematic presentation of deformation a) by slip and b) by twinning [78].

In addition, coating structures' hardening mechanisms, work hardening and strain hardening, take place under high deformation [79]. Furthermore, hardness and strength of materials indicate their capability to resist this permanent deformation [77]. As it is known, in cold spraying, coating formation is based on plastic deformation. Plastic deformation is mostly concentrated on regions close to particle boundaries and therefore, material jets (of coating and substrate material) are formed in order to increase coating quality and adhesion [30]. On the other hand, generally, material properties depend on its microstructure which in turn, depends on grain structure and treatments. Typically, plastic deformation is detected from an etched microstructure of cold-sprayed coatings by a flattening degree of the particles. [79] Highly deformed particles have highly flattened shapes after impacts [80]. In turn, flattening degree depends, in addition to the deformation level, on the coating and substrate material combination. Flattening of the sprayed particle is higher on the impact on steel substrate compared with Cu substrate due to the higher hardness of steel substrate [31].

Particles deform more on impacts against hard substrates whereas on impacts against softer substrate, deformation of substrate material is stronger [81]. These effects are illustrated in Fig. 20 by the impacts of Al particles on Cu substrate (Fig. 20a) and Cu particles on Al substrate (Fig. 20b). During impact (increasing contact time), particle height-to-weight ratio obviously decreases together with increasing depth of cratering of substrate. However, it should be noticed that flattening of the particle is not so high in the case of Cu on Al than Al on Cu. It was assumed that differences are caused by larger kinetic energy of heavier Cu particles together with their higher strength. In addition, material jets are wider in the case of Cu impacts on Al compared with Al impacts on Cu. Interfacial instability is more pronounced on the impacts of Cu on Al, indicating also higher deposition efficiency (DE) for this situation. [82]

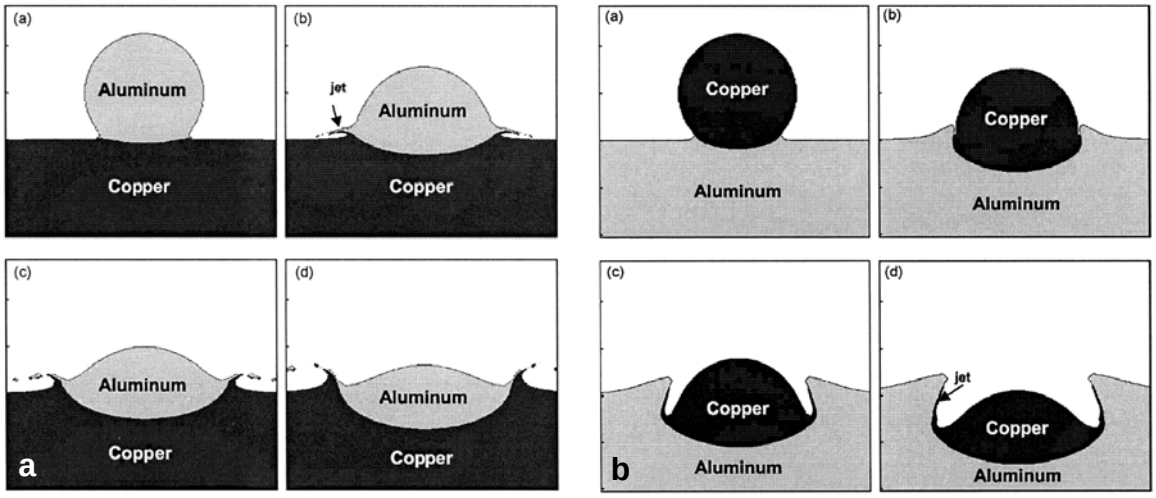


**Figure 20.** Particle impacts on the substrate at the velocity of 650 m/s: a) Al particle to the Cu substrate and b) Cu particle to the Al substrate as a function of impact time (a) 5 ns, (b) 20 ns, (c) 35 ns, and (d) 50 ns [82].

Plastic deformation under high strain rate conditions creates several microscopic features in the microstructure such as high amount of dislocations, dislocation wall formations, formation of elongated sub-grains, break-ups of sub-grains and recrystallization. At a solid state, under high strain rate, localized heating (material is still under melting point) generates adiabatic shearing instabilities at the interfaces, and then, formation of localized shear bands starts [26,67]. Borchers et al. [26] have illustrated microstructural defects such as vacancies and interstitials formed during or immediately after cold spray process. These defects are formed due to the temperature rises near melting point on the impacts and on the other hand, due to the strong deformation with very high strain rates. This, in turn, is caused by dislocations and their movements under high plastic deformation [26]. The structure with fine-sized grains without voids or oxide inclusions caused by dynamic recrystallization leads to a tight metal-metal bonding between particles [5,83]. Recrystallization due to high temperature during the collisions in the interfacial regions was observed [82].

#### 3.1.2.2 Adiabatic shear instability and material jets

Adiabatic shear instability due to the thermal softening leads to successful bonding in cold spraying [38]. Powder particles impact on the sprayed surface with high velocity under high pressure. On the impact, strain load is generated by pressure gradient caused on both interfaces during the collision (Fig. 21a). The pressure distribution during particle impact is also detected in Fig. 11. Shear load causes localized shear straining whereas plastic deformation, strain hardening, and thermal softening generate shear localization [67] and formation of shear bands [6]. Under the high impact conditions, this shear straining causes adiabatic shear instability due to the thermal softening and the influence is strongest at the interface by leading the jetting and thus, formation of material jets (Fig. 21b) [5,24,31]. Localized heating on the impact zone in the deformation region due to the high strain rate causes the formation of adiabatic shear bands [26,67]. On the other hand, strain is more compressive in the middle of the particle-substrate interface marked with gray arrow in Fig. 21b [26]. Additionally, locally deformed grains inside the powder particle can concentrate into shear bands. On the other hand, shear bands are produced by local dislocation reorganization which can generate elongated dislocation-free regions [67].

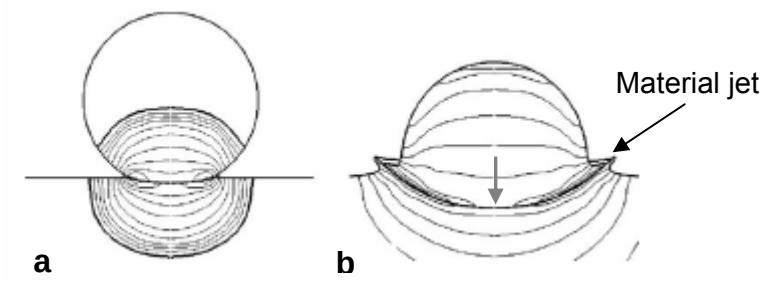


**Figure 21.** Particle impact: a) pressure distribution generation during particle impacts on the substrate and b) material jet formation [24].

Particle size is reported affecting the adiabatic shear instability behavior, attaining to the interface temperature, strain rate, and stress. Small particles have higher temperature gradients and thus, shear instability can be hindered by the high cooling rates. Additionally, smaller particles are more strain-rate hardened due to the high strain-rate. [24] Moreover, the effect of shock waves should be detected [28,66]. Localized heating near to the coating-substrate interface is clearly detected and it is the starting point for material jet formation. Moreover, higher particle velocities assist in the formation of higher material jets. [31]

High strain-rate deformation causes various microstructural details in the structure. Figure 22 shows these features of dynamic recrystallization. Randomly arranged dislocations (Fig. 22a) rearrange themselves to the dislocation cells (Fig. 22b) due to dynamic recovery. Then, severe deformation generates the formation of elongated subgrains (Fig. 22c). Furthermore, subgrains break-up (Fig. 22d) and finally, recrystallization of microstructure (Fig. 22e) takes place inside the structure [67].

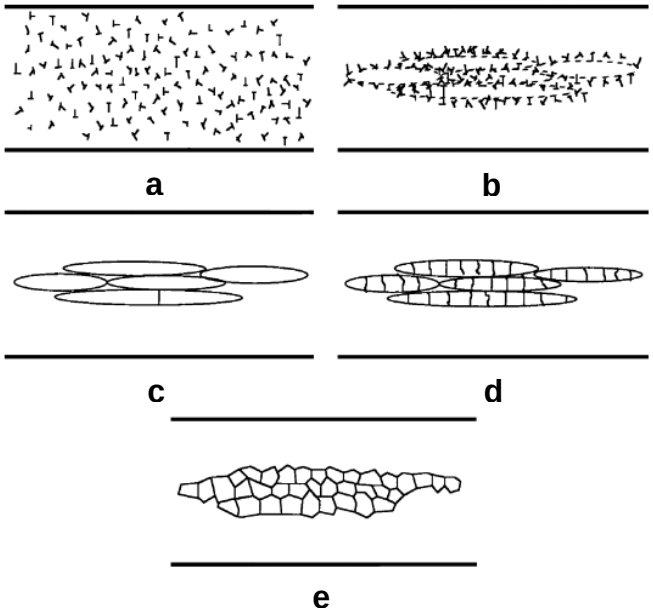


**Figure 22.** Microstructural details caused by high strain-rate deformation: a) randomly distributed dislocations, b) elongated dislocation cells, c) elongated subgrains, d) break-up of initial elongated subgrains, and e) recrystallized microstructure. After Meyers [67].

Generally speaking, several processes are able to occur during shearing. Meyers [67] has reported different mechanisms: *dynamic recovery, dynamic recrystallization, phase transformation, strain-induced precipitate dissolution, melting and resolidification, amorphization and crystallization*. Different processes can take place at the same time or separately. Structure inside the shear bands contains fine-sized and possibly recrystallized grains. [67] Borchers et al. [5] have shown recrystallized grain structure of the cold-sprayed Cu coating. In the cold spray process, dynamic recovery and recrystallization can play crucial roles in the shear localization caused by thermal softening in the case of metal materials. In turn, as for ceramic materials,

localized shearing can occur due to particle breaking-up or comminuting [67]. Grain refinement of the cold-sprayed particles together with non-uniform and randomly orientated fine-sized grains in the inter-particle structures is detected by TEM analysis [84,85]. Fine inter-particle grain size resulted from high plastic deformation whereas coarser grains appear in less deformed places [84].

Under high adiabatic shear instability, material jets form in the particle interfaces. The formation of these material jets is crucial for good and adherent particle-substrate and particle-particle bonding [5,31]. In addition, these material jets clean the surface, revealing a metal surface and further, a metal-metal bonding. In cold spraying, a phenomenon of material jet formation is comparable to the explosive welding [81]. For a dense coating and tight bonds between the particles, the metal-metal bonding is required. This requires clean contact surfaces under high pressure conditions [17,30,82]. Material jet formation is also one of the requirements for successful and tight bonding on impacts [82]. Fukumoto et al. [86] have described that material jetting can define coating properties. For that purpose, oxide layers of powder particles should be destroyed and removed from the metal surface on the impacts [1,3,53]. This is due to high plastic deformation and materials jets [1,4,17,30,82]. Removal of oxide layer can be illustrated with an egg-cell-model (during impact, particles behave like an egg, hard cell (oxide) breaks down and soft inside (metal) deforms). After oxide layer is broken down, gas flow removes oxides away. [1] In addition, fracturing of these oxide layers requires high impact velocity of the particles [23]. On the other hand, ceramic particles mixed with metallic powder can remove the oxide layers from the surfaces of metallic particles by activation, occurring on the collision of hard particles on the metallic region of the surfaces [87].

#### 3.1.2.3 Bonding

Particle-substrate and particle-particle bonding are compared with the explosive powder compaction where powder is loaded by strong shock waves with a high shock pressure. In the explosive powder compaction method, particles are welded and they form dense structure. Common for both methods is the highly localized interfacial deformation caused by material jets and also a highly elongated grain structure. [36] Reportedly, in the coating formation, the role of adhesive forces is not significant. After formation, however, these forces could have a role in the adhesion of the coating and the substrate. [23]

Adhesion caused by van der Waals and electrostatic forces is typically formed as sticking [57]. The adhesion depends on the size of interfacial area between particle and substrate [82]. In addition, one mechanism for the bonding is mechanical interlocking. It is usually present in the interfacial bonding [57]. Mechanical interlocking could be one bonding mechanism at the particle-substrate interface indicated by material jets and substrate deformation [86]. Interfacial instability is the driving force for the interlocking between coating and substrate [82]. Also, it should be noticed that repeated impacts have an influence on coating formation in cold spraying. This is also related to the activation by rebounded particles and, on the other hand, to the densifying effect of particles incoming next. In addition, sticking can become stronger during particle impacts and therefore, adhesion between particles is tighter [57]. On the contrary, adhesion by interlocking increases with increasing velocity and density of the sprayed particles. At the same time, increasing surface tension can degrade the adhesion [8]. In addition, oxide layers should be removed during impacts (by plastic deformation); revealing metal-metal contacts, pronounce metallic bonding between particles and substrate [86].

In cold spraying, bonding between particles and substrate and between particles can be said to be a combination of different bonding mechanisms. Localized metallurgical bonding was obtained and associated with impact fusion [88]. In addition, Hussain et al. [89] have reported that bonding is the combination of metallurgical bonding and interlocking. Furthermore, the bonding could be a combination of the metal-metal bonding, mechanical blocking, van der Waals adhesion, and diffusion. Diffusion was observed as a bonding mechanism between cold-sprayed Cu splats and Al substrate as the formation of intermetallic, nanocrystallized, thin layer at the interface [90]. In addition, Kairet [72] has found slight diffusion occurrence at Cu-Al interface. Furthermore, Guetta et al. [90] have suggested that local transient melting could occur

in the high-pressure and high-temperature impacts of Cu particles on Al surface. However, according to Grujicic et al. [82] atomic diffusion at the particle-substrate interface is not a dominant bonding mechanism. Accordingly, bonding is strongly influenced by the powder material, powder-substrate material combination together with the spraying parameters and heat treatments. For instance, bonding is influenced by substrate softening during impacts on the soft substrate materials, e.g., Cu impacts on Al substrate, making the strong adhesion between coating and substrate [72].

Melting of Cu particles was not found in the cold-sprayed or kinetically-sprayed Cu coatings when comparing feedstock structure with coating structure [5,23]. The coatings have anisotropic nature, having a flattened shape in the cross-sectional direction [23]. On the other hand, some localized melting in the particle interfaces was found with materials with low melting point, such as Zn and Al-12Si when using relatively high gas temperatures. Additionally, low thermal conductivity of powder material assists in local melting occurrence [88].

## 3.2 Coating properties

Coating properties depend on various factors. One important factor is the powder. Firstly, the effect of powder characteristics on coating properties is discussed. Secondly, structural and mechanical properties are discussed and finally, corrosion properties and potential applications are presented.

### 3.2.1 Effect of powders

The powder has a very crucial role in the coating formation and coating properties in the cold spray process. Firstly, powder material should be deformable and ductile. Thus, only metallic powder materials can be used in cold spray process. Furthermore, powder mixtures can be sprayed when at least one component of the powder mixture is a metallic powder. Therefore, metallic-ceramic powder mixtures can be used [23,91,92]. As a general trend, these powders are mostly used in the LPCS process. In addition, metal-metal powder mixtures are used in order to modify the coating properties. Secondly, powder characteristics, e.g., particle size, particle size distribution, particle morphology, and purity level affect the coating quality. Microstructural details of the powder mainly determine the microstructure of the coating [72]. In the LPCS process, brittleness of ceramic particles in powder mixture is compensated with ductile metallic particles [6]. Reportedly, thin deposits of hardmetals, e.g., WC-Co, are produced by using cold spray process. Furthermore, nano-sized structure of WC-Co was detected in the coating structure as well as in the initial powder structure, indicating no phase transformation occurrence during the cold spray process. [93,94]

Ductility of metallic powder or at least one component in the powder mixtures is required for flattening of the particles by plastic deformation. Thus, suitable powder material for spraying should endure plastic flow without fracturing in order to produce dense coatings by cold spraying [24]. Furthermore, it should be noticed that in composite mixture coatings, deposition efficiencies can vary in different components of the powder due to the possible differences on the critical velocities. Therefore, composition of coating and powder can differ strongly, depending on the initial powder composition [39]. Particle size has reportedly effect on coating formation. Small particles (5 μm) undergo shear instability. However, if impact temperature increases, shear instability does not necessarily occur. This is due to the high heat transfer over the particle volume and thus, high cooling rates which can hinder the occurrence of shear instability [24]. According to Schmidt et al. [24] if cooling and heating rates are close to each other, shear instability can be hindered or prevented.

Particle velocity depends on particle size. Powder contains certain particle size distribution and hence, it can be said that velocity of powder is composed of different velocities, depending on particle size distribution. Optimal particle size distribution should be determined particularly for each powder material and composition [24]. Production method of powder particles affects the oxygen content of particles. Gas-atomized particles are dense and have low oxygen content

whereas particles produced by direct reduction contain impurities in their structures. It is evident that coatings sprayed with higher oxygen content particles will have higher amount of oxygen in the coating structure as well. Trapped oxides have been found in the coating structures sprayed with higher oxygen content powder. [95] At the same time, flattening of Al particles was decreased with increased oxygen content of initial powder particles [63]. As known, particle velocity has strong effect on the coating formation. Higher velocities lead to higher coating quality. Therefore, powder characteristics affect the velocity and coating properties. Irregular particles have higher in-flight velocities compared with spherical particles. [69] However, it should be noted that irregular particles could contain higher amount of impurities in the as-received state due to the production method (water atomization or electrolytic production versus gas atomization).

For successful bonding, deposition conditions should be such that oxide layers on the particle surfaces are fractured during impact, revealing pure metallic contact [5,6]. In the optimal state, due to the highly strained interfaces, oxide cells are broken and clean metal surfaces are revealed for the tight bonding [24]. However, smaller particles typically contain more impurities arisen from higher surface area. This can lead to the higher critical velocities for smaller particles due to the fact that smaller particles have higher oxide content. Van Steenkiste et al. [23] have suggested that larger particles have more energy to fracture the oxide layers. In addition, more kinetic energy is required with increased thickness of oxide layers to remove oxides and for plastic deformation [63]. Moreover, inter-particle sliding can take place on the particle impacts during spraying [6].

Hard particles

Ceramic particles mixed with metallic powder affect the coating formation. Hard particles densify the metallic structure by assisting higher plastic deformation. $Al_2O_3$ particles mixed with e.g., Al powder have reportedly increased adhesion between coating and substrate, creating micro-asperities and increasing contact area [50]. Moreover, the addition of ceramic particles has been reported to improve the denseness of the LPCS Al coatings [96]. Coating properties depend on composite powder compositions [50]. On the other hand, metallic powder mixture can also increase plastic deformation. Maev et al. [97] have found out that Ni particles deform more intensively when they contain W particles in the initial powder mixture. One explanation can be higher kinetic energy of W particles due to their high density, when W particles impact on the Ni particles [97]. Ceramic particles embed in the soft metallic matrix or they can be fractured to small pieces in the structure during particle impacts [14,92]. Lee et al. [14] have reported no signs of cratering of soft Si substrate during impacts of hard ceramic $WO_3$ particles, in turn, ceramic particles embedded in the substrate and no erosion occurred.

The main function of the $Al_2O_3$ particle addition is to keep the nozzle of the gun clean. Furthermore, $Al_2O_3$ particles activate (clean and roughen) the sprayed surfaces, i.e., through activation the surface becomes cleaner and more adaptive to the sprayed particles, which then stick better to the surface. In addition to these, $Al_2O_3$ particles affect mechanically the coating by hammering the substrate/sprayed layers or by peening effect via particle impacts. [49] During particle impacts, collision of the ceramic particles also increases the deformation of the metallic particles (compacting effect) which in turn, affects the coating properties and deposition efficiency particularly in the LPCS process [51]. Papyrin et al. [55] have reported that hard particles (e.g., $Al_2O_3$) can affect the temperature (and thus, velocity) of soft metallic particles (e.g., Cu and Al) in the metallic-ceramic powder mixtures. Hard particles decrease the so-called critical temperature of metallic particles and therefore, also decrease critical velocity needed due to the activation of ceramic particles. This can explain the lower particle velocities in the LPCS process compared with the HPCS process [50,55].

### 3.2.2 Coating structure

Cold-sprayed coatings have a strongly deformed coating structure due to the high plastic deformation. Cold-sprayed coatings are reportedly dense without evidence of pores by microscopic analysis [9]. However, porosity level in the coatings depends strongly on sprayed materials as well as spraying parameters [18]. Rezaeian et al. [18] have shown porosity levels

for cold-sprayed Ti, Ni, and Cu coatings: 9-21 %, 1-4 %, and 0-8 %, respectively. Due to the high plastic deformation, particle structure is flattened and become pancake-like with flattening ratio of 3:1 or 5:1 [23]. Etching reveals the flattening of the powder particles which is extensively high due to the high plastic deformation [88]. Borchers et al. [5,26] have presented dense particle interfaces between cold-sprayed Cu particles and furthermore, high dislocation density areas, elongated grains, twins, and recrystallized grain structures, indicating unequal and nonuniform microstructure. Moreover, Zou et al. [98] have studied microstructures of cold-sprayed Ni coatings with EBSD and found clearly inhomogeneous structure with equiaxed and elongated grains. Ultra-fine grains were observed in the particle-particle interfaces [98]. Moreover, Kairet et al. [76] have found that cold-sprayed Cu coatings sprayed using fine particles have higher dislocation density than larger ones. Furthermore, heat treatments have an influence on the coating structures, e.g., porosity of the HPCS Cu coating (air used as process gas, dendritic particles as feedstock) was slightly decreased [73]. Figure 23 shows typical microstructures of the cold-sprayed coatings, cross-section of cold-sprayed Cu coating without any defects is in Fig. 23a [99], faultless interface between the Ni coating and grit-blasted steel substrate in Fig. 23b, etched structure of the Cu coating with flattened particle shapes in Fig. 23c, and elongated grain structure with localized deformation of the Ni-20Cr coating in Fig. 23d [100]. Elongation of highly deformed grains inside the flattened particles was also observed [83].

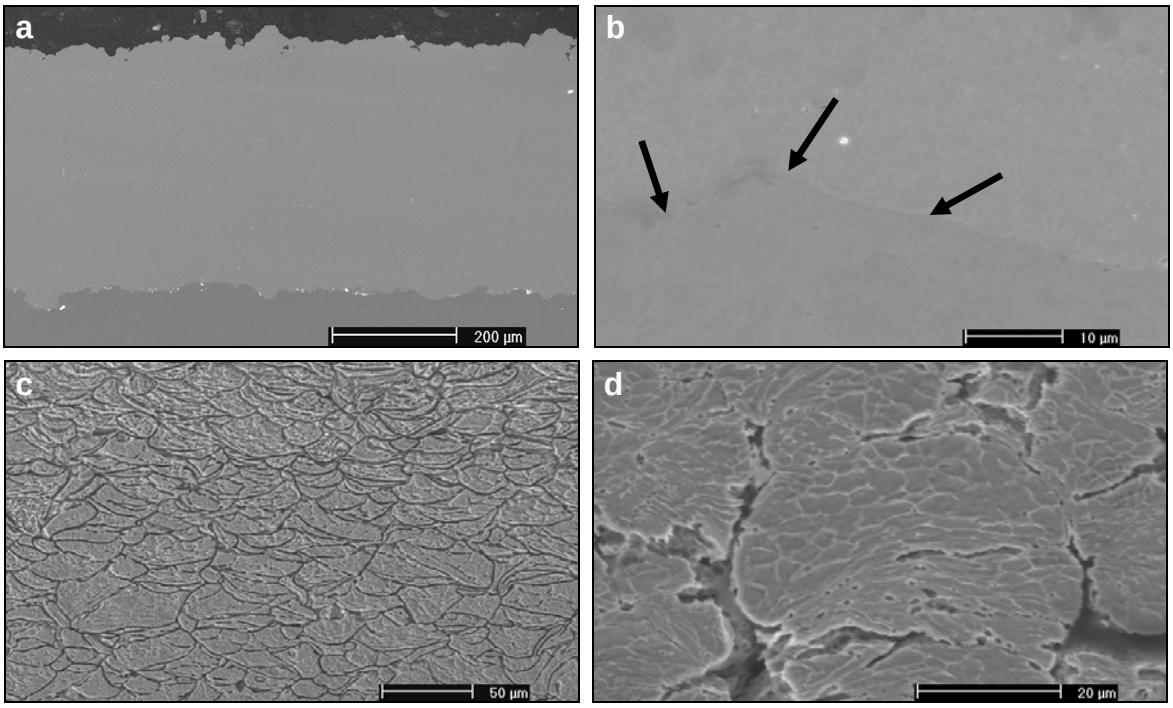


**Figure 23.** Cross-sectional structures of cold-sprayed coatings: a) Cu on grit-blasted steel substrate [99], b) interface (arrows) between Ni and grit-blasted steel substrate, c) etched Cu coating, and d) etched Ni-20Cr coating [100]. SEM images.

One advantage of cold spraying is to avoid the occurrence of oxidation and phase transformation caused by melting during spraying. This eliminates formation of undesirable phases and is material-dependent. However, interfacial boundaries of intermetallic phases (e.g., NiAl, $NiAl_3$, $Ni_3Al$) formed in the spraying of Al on Ni have been found [101]. In addition, Guetta et al. [90] have illustrated nanocrystallized phases, $Al_2Cu$ and $Al_4Cu_9$ phases, in the interface between cold-sprayed Cu splats and Al substrate by using TEM.

Heat treatments affect microstructural details of the cold-sprayed coatings by several mechanisms depending on heat treatment temperatures. Recovery, recrystallization and grain growth [80] occur in different temperature regions [102]. Figure 24 shows changes in the microstructure as a function of temperature. Refinement of grain structures after heat treatment due to the recrystallization was found in several studies. In addition, fracture behavior mostly

changes after heat treatments from the brittle (as-sprayed state) to ductile (heat-treated state). [103]

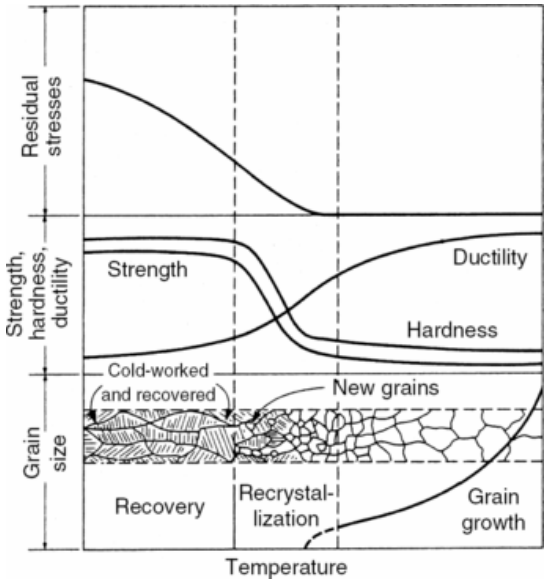


**Figure 24.** Cold-worked structure and properties. Effects of annealing temperature on recovery, recrystallization, and grain growth [102].

Shkodkin et al. [51] have reported increased bond strength and coating density with increasing ceramic particle addition. Amount of ceramic particles in the sprayed coating is low in comparison with the initial powder composition. Usually, coatings contain ceramic particles below 5 % from total amount of ceramic powder [51]. This indicates occurrence of erosion and activation by rebounded ceramic particles [51,104].

In addition, one way to improve the quality of LPCS Cu+$Al_2O_3$ coatings is to produce coatings with laser assistance. Laser-assisted low-pressure cold-sprayed (LALPCS) coatings have shown improved denseness. Nd:YAG and diode lasers were tested and they were installed to Dymet spraying gun [100,105]. Continuous laser irradiation with the LPCS spray spot preheated the substrate. Firstly, coating thicknesses were increased with increasing laser energy (temperatures measured using pyrometer). Secondly, the denseness improvement was detected with open-cell potential measurements and salt spray tests. The LALPCS Cu+$Al_2O_3$ coatings did not have through-porosity in their structures and results were similar with both lasers (diode and Nd:YAG). [105]

### 3.2.3 Mechanical properties

Cold-sprayed coatings have reportedly low residual stresses due to low heat input, rather high adhesion, and hardness normally higher than that of the corresponding bulk materials [2]. Mechanical properties of cold-sprayed coatings are shown here.

Hardness

Hardness is the property of a material to resist permanent indentation. During strain or work hardening, material becomes harder and stronger due to plastic deformation [77]. This explains the high hardness and thus, highly work-hardened structure of the cold-sprayed coatings. Higher velocity obtained with higher preheating temperature leads to higher hardness due to the higher level of plastic deformation and cold working. Additionally, hardness of the coating is somewhat higher that corresponding bulk material. [2,23] This is caused by high dislocation densities in the coating structure due to the high deformation occurrence on the high-velocity impacts [9]. Calla et al. [106] have reported that an increased particle velocity due to an increased driving pressure resulted in more cold working in the coating, leading to high hardness. Hardness values of the cold-sprayed Cu coatings are reportedly significantly higher than those of corresponding bulk material (160 versus 90 $HV_{0.2}$). This is explained by the high

work hardening effect and in addition to that, compressive residual stresses assist to increase the hardness of the coatings. [107]

According to Calla et al. [35] the reason for the high hardness of the cold-sprayed coatings is the very fine grain size and the significant micro-straining in the as-sprayed deposits. Cold-sprayed coatings have relatively high hardness due to the work hardening; however, annealing decreases the hardness [9,26,107]. Decrement of the hardness values was observed e.g., in the Al, Cu, Ni, and Ni-20Cr coatings [108]. Annealing at elevated temperatures affects the properties of cold-sprayed coatings. At temperatures of 300ºC and above for Cu, the dislocations in the grains rearrange, and recrystallization and further grain growth occur, usually reflecting decrement in the hardness [35]. The effect of annealing of cold-worked material is presented in Fig. 24. Cold-sprayed coatings could be expected to behave similarly.

Bond strength

Cold-sprayed coatings possess high adherence to base materials [23]. Reportedly, the bond strengths of HPCS Cu coatings on Al substrates are in the range of 35-40 MPa [9] or 20-60 MPa [76,89] and on steel and Cu substrates in the range of 30-40 MPa [5,31]. Additionally, in the other studies bond strengths were between 10 and 20 MPa [107,109]. Furthermore, the bond strengths of the LPCS coatings are reported to be in the range of 10-30 MPa [17]. Adhesion of soft metal coating is usually stronger on soft substrate than on hard substrate [109]. Higher values are measured in the coatings sprayed with higher gas velocities and particle velocities [31]. Adhesion of single splats also increases with higher impact velocity [90].

Meanwhile, high tensile strengths (cohesive strengths) of HPCS coatings between 85 and 150 MPa for Cu, are demonstrated [24]. Differences between adhesive strengths and cohesive strengths reflect the anisotropy of the coatings. Additionally, adhesion decreases with the increase of coating thickness. Furthermore, Schmidt et al. [110] have illustrated improvements of tensile strengths of the HPCS Cu coatings from 50 MPa to as high as 250 MPa with nozzle and spraying equipment developments. This is caused by the presence of internal stresses [26]. Annealing is reported to have influence on the ultimate strength of the HPCS Cu coatings by decreasing it significantly with increasing annealing temperature. In addition, stress-strain curves have revealed ductility increment with annealing, similar behavior is observed with cold-worked materials shown in Fig. 24. In addition, the same effect was demonstrated by using He instead of $N_2$. The adhesion between Cu and steel was increased also when He was used as a process gas, 57 MPa in the as-sprayed state [83]. Furthermore, more ductile fracture behavior was seen in SEM analysis. Using He as a process gas, particles were more work-hardened because of higher particle velocities [80]. It is also known that coating formation and coating properties depend on the combination of the powder material and substrate material. The influence is detected mostly on adhesion of the coatings. The adhesion is reportedly higher on soft substrate (e.g., aluminium) compared with hard substrate (e.g., steel). The bond strength of the cold-sprayed Cu coating (as-sprayed, $N_2$) on Al was 40 MPa whereas on steel it was 10 MPa [83]. Moreover, adhesion can be affected by substrate pre-treatments, e.g., by grit-blasting. Additionally, the adhesive strengths are improved with annealing, the bond strength of Cu on Al after 200ºC/1h was 45 MPa and on steel after the same annealing 28 MPa [83]. Hussain et al. [89] have also reported increased adhesion of Cu coating on Al substrate after heat treatment (adhesion strength increased from 57 MPa to > 69 MPa).

Ductility

Cold-sprayed coatings are relatively brittle in the as-sprayed state [1]. However, ductility increases with annealing as a post-treatment [111]. Furthermore, ductility of the coating can increase with increasing preheating temperature of the process gas [23]. Schmidt et al. [110] have shown significant ductile increment in the as-sprayed state by using a developed nozzle and an advanced spraying system. At the previous development states, ductile fracture behavior was less than 15 % and nowadays, with the improved system, it can be as high as 85-90 % [110].

Coating properties, both structural and mechanical, can be modified with heat treatments as post-treatments. Three different processes can occur during annealing: recovery,

recrystallization, and grain growth. Firstly, recovery relieves the strain energy and reduces amount of dislocations. Secondly, at higher temperature than in the case of recovery, recrystallization starts, forming new grains and rearranging grains inside the structure. Material becomes softer and more ductile during the recrystallization. After that at even higher temperature, grain growth takes place [77]. The effects of heat treatment on the mechanical and structural properties of cold-worked material are summarized in Fig. 24 [102].

Generally speaking, residual stresses start to release during recovery and are finally released during recrystallization. Furthermore, most significant differences between different properties occur during recrystallization. Hardness and strength decrease whereas ductility increases. Additionally, new grains are generated by recrystallization and further, in the grain growth region, grain size of these new grains is increased. Hardness and strength seemed to be relatively stable in the grain growth region whereas increment of ductility still continues. [102]

### 3.3 Corrosion resistance

Corrosion is defined as *an extractive metallurgy in reverse*. Corrosion is related to the chemical or electrochemical reaction between material (e.g., metal, coating) and its environment [112]. Therefore, one important technical issue is to manufacture corrosion resistant and protective materials and coatings with specific requirements, e.g., high reliability, quality, and low costs. Furthermore, corrosion resistance is necessary in several industries, in, e.g., chemical and process equipment, and energy production systems. Corrosion protection of metals is based on anodic protection by passivity or cathodic protection by sacrificial anode behavior. Therefore, metallic coatings can also give protection to the substrate in two ways: anodically or cathodically. Corrosion starts if protection fails or breaks down, making metal vulnerable to attacks of corrosion [113].

Corrosion can occur in different forms: e.g., uniform, pitting, crevice, and galvanic corrosion are typical forms of corrosion for coatings. The most common forms of localized corrosion are pitting and crevice corrosion in which corrosive conditions could penetrate relatively rapidly [112]. Pitting corrosion occurs if the passive layer of protecting material is locally damaged, pits form on the surface, and underlying metal is open for the attack [114]. Pitting corrosion causes highly localized damages [115]. For coatings, where structures are not totally adhering and uniform, pitting corrosion takes place quite easily. Porosity in the anodically protective coatings accelerates pitting type corrosion by opening the way for aqueous solution to penetrate inside the coating structure [116]. Crevice corrosion is said to be the one of the most damaging forms of corrosion. Crevice corrosion causes localized corrosion [117]. Galvanic corrosion occurs when two dissimilar metals form an electrical couple in the same electrolyte. In the electrical couple, corrosion starts in the less corrosion resistant material (more active) which becomes the anode whereas the more resistant material (nobler) will be cathode [118]. Metallographic structure and microstructural properties are also said to have an influence on corrosion [112].

In this study, corrosion resistance of cold-sprayed coatings is focused on anodically protective coating materials, i.e., Ta, Cu, Ni, Ni-Cu, and Ni-Cr coatings on steel substrates. Galvanic series of materials in seawater shows anodic-cathodic behavior of materials compared with each other. Galvanic series is presented in Table 3. The nobler the material, the higher it is on the order. Platinum is the noblest material. Cathodic materials protect less noble materials anodically whereas anodic materials give cathodic protection to the nobler material. Moreover, it is known that cathodic protection is based on sacrificial behavior of anodic material, e.g., Zn coating on steel substrate. In this study, nickel, nickel-30copper, and copper give anodic protection against the corrosion of steel substrate. [112] Nickel-chromium and tantalum are also nobler than steel [119].

**Table 3.** Galvanic series in seawater [112,119].

| Cathodic (noble) |
|---|
| Platinum |
| Gold |
| Graphite |
| Titanium |
| Silver |
| Zirconium |
| AISI Type 316, 317 Stainless steel (passive) |
| AISI Type 304 Stainless steel (passive) |
| AISI Type 430 Stainless steel (passive) |
| Nickel (passive) |
| Copper-Nickel (70-30) |
| Bronzes |
| Copper |
| Brasses |
| Tantalum [119] |
| Chromium [119] |
| Nickel (active) |
| Naval Brass |
| Tin |
| Lead |
| AISI Type 316, 317 stainless steel (active) |
| AISI Type 304 stainless steel (active) |
| Cast Iron |
| Steel or Iron |
| Aluminum alloy 2024 |
| Cadmium |
| Aluminum alloy 1100 |
| Zinc |
| Magnesium and Magnesium alloys |
| Anodic (active) |

Figure 25 shows the schematic presentation of the corrosion behavior in the cases of anodically protective coating (tin on steel) and cathodically protective coating (zinc on steel). Steel is more active than tin and thus, when a tin layer is broken, steel is attacked. In the other case, steel is nobler than zinc and damaged zinc acts as sacrificial anode and reforms the protective layer again [116]. Therefore, porosity is not critical with cathodically protective coatings whereas in the anodically protective coatings, impermeability of the coating and passive layer on its surface is critical for corrosion resistance.

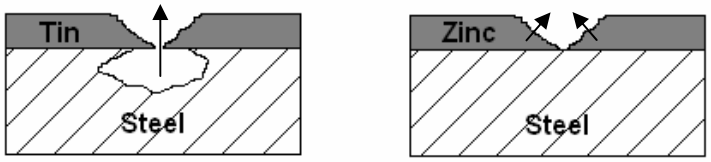


**Figure 25.** Corrosion behavior of a) anodically protective coating and b) cathodically protective coating in the case of galvanic corrosion at the damaged coatings. Steel is more active than tin and thus, steel corrodes strongly. Damaged zinc coating acts as a sacrificial anode and thus, steel does not corrode whereas zinc does due to the fact that steel is nobler than zinc. [116]

The best way to protect steel samples (active metal) is to deposit the protective coating on the steel surface [113]. For that purpose, cold spraying enables the production of dense coatings for corrosion resistance applications. In addition, denseness of the anodically protective coatings is the first criterion required for corrosion protection [120]. Common for all materials used in this study is that they give anodic protection to the steel substrate. Anodic protection is based on passivation of metals. Therefore, existing of passive film is the requirement for corrosion

protection. [121] Passivation is based on a formation of thin, protective oxide layer, acting as a corrosion barrier film [112]. Some metals can form a protective film on their surface which inhibits interactions between metal and corrosive atmosphere due to passivation. Coverage of passive layer is crucial because if it is not or passive layer breaks down, corrosion can damage the structure. Metals' passivity is usually based on the formation of thin oxide layer typically in the air. It is very important to have a continuous and coherent oxide film. Nickel, nickel-chromium and copper are passivating metals. [113] Figure 26 presents anodic polarization curve where active, passive, and transpassive areas are observed. In passivated metals, passivation potential $E_p$ indicates critical potential and above that corrosion rate of metal decreases. The area is called passivation range. Below $E_p$ corrosion occurs at a higher rate. If the passive layer fractures, it opens the way for localized forms of corrosion [112]. Anodic polarization behavior shows material active-passive behavior and therefore, corrosion protection [115]. Furthermore, the passivity and protectiveness of metals can be studied from their active-passive-transpassive behavior in anodic polarization curves [112].

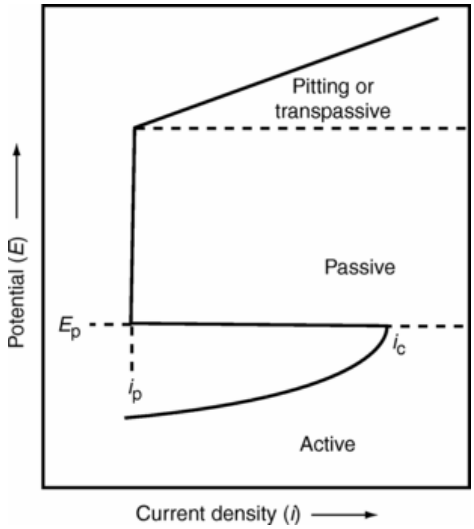


**Figure 26.** Example of anodic polarization curve. $E_p$ is passivation potential, $i_p$ passivation current density and $i_c$ critical passivation current density [121].

Denseness, or in other words impermeability, is the criterion for good corrosion resistance [9]. Open-cell potential measurements and salt spray (fog) tests as wet corrosion tests are relevant methods to evaluate the denseness of coatings on corrodible substrate (e.g., carbon steel in saltwater conditions). Additionally, salt spray (fog) testing is a commonly used test method to evaluate the quality of various coatings. This particular test enables the use of different corrosive solutions and different test temperatures in a controlled test condition [122]. Corrosion protectiveness and corrosion rates can be estimated with polarization behavior of the coatings. Furthermore, active-passive behavior is clearly detected from anodic polarization measurements [115].

Figure 27 illustrates the potential behavior of coating, substrate and porous coating. If the coating contains interconnected porosity, potential behavior is composed of potentials of both coating and substrate which is seen as mixed potential. This is the basic idea for the open-cell potential measurements used in this study to evaluate existing interconnected porosity, in the other words, through-porosity or open-porosity.

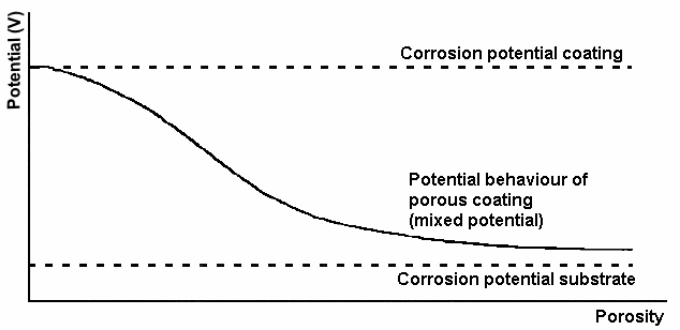


**Figure 27.** Potential behavior of the coating as a function of porosity [123].

Tantalum has extraordinary corrosion resistance [124] due to the formation of highly stable passivating layer [115]. Tantalum resists corrosion effectively in acids (not HF), salts, and organic chemicals even at elevated temperatures [124]. Furthermore, tantalum as a dense coating acts like corrosion barrier coating on a steel substrate, providing high corrosion resistance in many environments [112]. While, copper is a corrosion resistant material against seawater, waters, dilute sulfuric acid, phosphoric acid, acetic acid and other non-oxidizing acids and in addition, generally atmospheric exposure. Monel 400 (Ni-30Cu) has good corrosion resistance in sulfuric, hydrochloric, phosphoric, and hydrofluoric acids. In Monel alloy, Cu improves corrosion resistance better than pure Ni. [115] Usually, thermally-sprayed nickel-chromium alloy coatings are used for applications where corrosion and oxidation resistance is needed and additionally, for repairs and bond coats [125]. Protective $Ta_2O_5$ (tantalum pentoxide) layer forms on the surface of tantalum [115,124], protective $Cu_2O$ layer, also called patina, forms on copper [115], and protective NiO layer on nickel surface [112].

Corrosion properties of the cold-sprayed coatings are reported rather briefly in other studies. These studies are more concentrated on the corrosion protection of materials which give cathodic protection based on sacrificial behavior, e.g., Zn and Al [126]. Blose et al. [126] have reported the corrosion protection of steel substrates with cold-sprayed Zn, Al, and Zn-Al coatings against wet corrosion. Furthermore, Karthikeyan et al. [53] have shown that corrosion resistance of the cold-sprayed Al coatings was higher than that of Al bulk material analyzed using polarization measurements. Repassivation was observed at higher potentials [53]. In addition, the cold-sprayed Al+$Al_2O_3$ coatings performed improved anti-corrosion ability compared with Al bulk material in the polarization measurements [127]. Furthermore, LPCS Al coatings act as sacrificial anode and protect the AA2024 substrate, reflecting possibility to be used for corrosion protection in atmospheric and seawater conditions [128].

## 3.4 Potential applications of cold-sprayed coatings

Corrosion resistance

There is high potential to use cold spray processes in the production of corrosion barrier coatings (low porosity) [2]. However, with some materials, optimization and improvement are still needed. The cold-sprayed Al and Zn coatings [6,129] and LPCS Zn/Al/$Al_2O_3$ coatings [49] are able to be used for corrosion protection. In addition, Zn, Ni, Ta, stainless steel, and brass coatings with low porosity in their structures are reported to have potential for corrosion resistance applications. In addition, Ta coatings could be optimal as chemical resistant materials in chemical industry and Ni coatings for replacing the electroplating. [130] It is also possible to use cold-sprayed coatings as anti-corrosion coatings on welds [57]. Additionally, cold-sprayed Ta, Zr, and Ti coatings are used to protect the substrates in the corrosion resistance applications [131].

Electrical and thermal conductivity

Based on high purity and oxide-free structures of the coatings, cold spraying can optionally be used in applications, where either electrical or thermal conductivity is needed [129]. Cold-sprayed Cu coatings can be used in connecting plates, Cu and Al coatings on heat sinks in electronics [6,130] and cooling devices [129]. Electrical conductivity of the cold-sprayed Cu coating can be as high as 95 % of the value of the bulk Cu [129]. In addition, one possibility is to use cold-sprayed coatings as thermal barrier coatings, e.g., in aluminum piston heads, disc brakes [6] or as electrically conducting or insulating coatings in applications in aerospace industry [57]. Again, one of the key properties of the cold-sprayed coatings is conductivity [6,11], thus, it is ideal for conductors and thermal management, e.g., as electric screening coatings on plastics or as conductive coatings on non-metal substrates [130].

Repairing

LPCS coatings can be used in metal restoration, repairing [17,48,51] and sealing, e.g., in engine blocks, castings, molds, and body repair [6,49] and repairing parts [57], e.g., pistons, bearing components, seals [2]. In addition, one advantage is the ability to repair Al structures by using HPCS Al coating for the reclamation purposes [53]. Additionally, cold spraying is reported to be used for repair parts by using Al, Cu, steel, Ni, and various alloy coatings [130,131]. Cast iron and steel substrates can be repaired by using LPCS Cu-W-Zn or Ni-TiC composite coatings [132] and damaged surfaces of chill cast by using HPCS coatings [129].

Functional coatings

In addition to the applications above, cold-sprayed coatings could be used as functional coatings where anti-stick and magnetic properties are required, in soldering of electronic components [6,49,129,130], and for implants [6]. With cold-sprayed coatings, strengthening and hardening can be added and near-net shapes and compact pieces, e.g., Ti and Ti-based coatings can be produced [1,2]. In addition, Ni coatings can be used as base or intermediate layers in sandwich structures [130]. Furthermore, Ni, pure Fe [129], and other magnetic materials are suitable for cooking applications for induction heating. Composite materials, powder mixtures with functional properties, e.g., layers for thermal management, wear protection, bearing or solder layers are reported. [130] Cold-sprayed ceramic and metal-matrix composite ($Al_2O_3$, $Al_2O_3$-$Ti_2O$, $WO_3$, Ta-$MnO_2$, Al-$MnO_2$) thin films (mostly particle penetrations) can be used as surface treatments for functional applications, e.g., catalytic coatings [12]. Cold-sprayed braze and Zn coatings can also be used for engraving surfaces in printing industry, and Ta, Nb, and TiMo coatings as sputtering targets [131].

## 4 AIM OF THE STUDY

The aim of this work was to characterize the microstructural and mechanical properties of cold-sprayed coatings and to find out affecting factors in order to produce overall dense coatings. Figure 28 shows the structure of the research topics and affecting factors. The research is focused on evaluation of the microscopic and macroscopic properties of high-pressure and low-pressure cold-sprayed coatings. The main goal was to find correlation between different properties including microstructure, grain structure, bonding, and mechanical properties, and the most important, denseness. In addition, corrosion resistance of overall dense coatings was investigated.

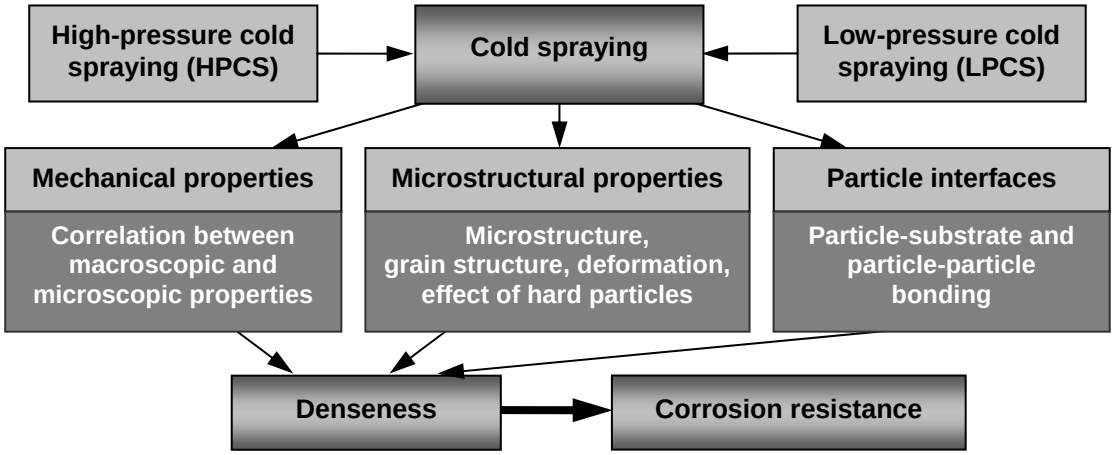


**Figure 28.** The structure of the research work.

The research was focused on the evaluation of powders, spraying parameters, substrates, post-treatments, and optimal combinations of these factors. Denseness of the coatings is a requirement for corrosion protection and for that, it was important to characterize microstructural details, denseness, and corrosion properties more specifically. This work is composed of the seven publications. The relationship between these publications is presented in Fig. 29.

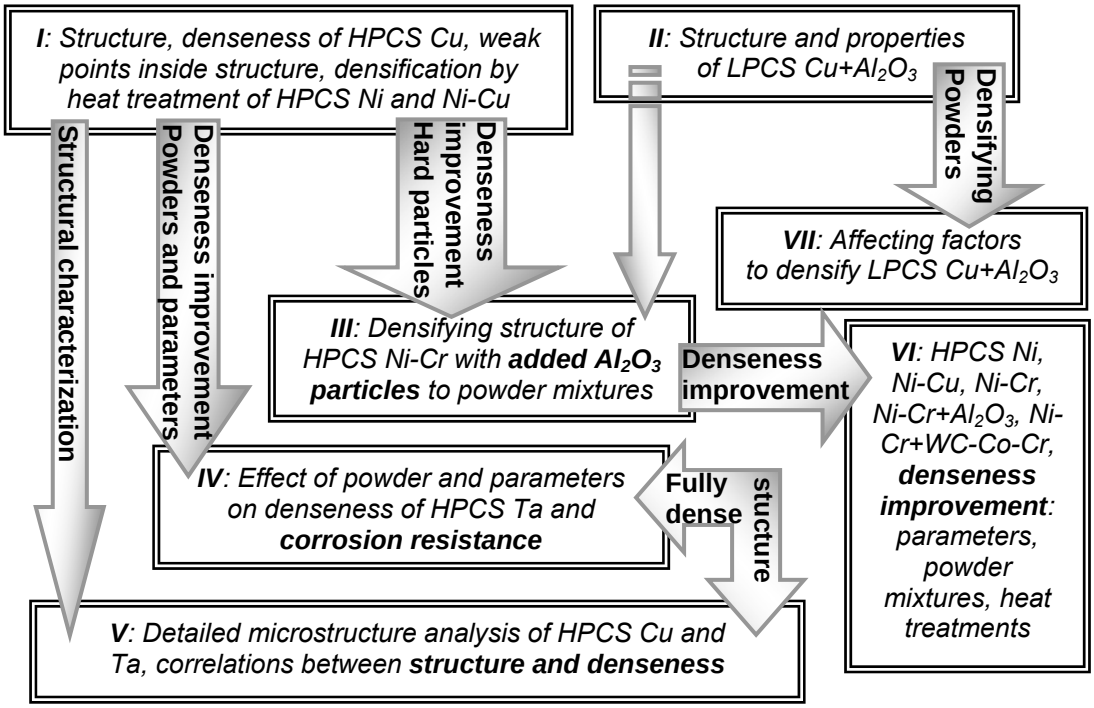


**Figure 29.** Relationship between research topics, main research results, and published papers (I-VII).

## 5 MATERIALS

Various powder materials were used. Metallic powders and metallic-ceramic powder mixtures were tested with different compositions and with different powder properties, e.g., particle size and particle morphology. Common feature for all these metallic materials is that they give anodic protection for the steel substrate. Copper was chosen as coating material due to its good electrical and thermal conductivity [133] and corrosion resistance in atmospheric conditions [115]. Nickel [134,135], nickel-chromium [135], nickel-copper [135] and tantalum [124] were chosen for their corrosion resistance in various corrosive environments.

### 5.1 Powder materials

Cu, Ta, Ni, Ni-20/30Cu, Ni-20Cr, Ni-20Cr+$Al_2O_3$, and Ni-20Cr+WC-10Co-4Cr coatings were manufactured using the HPCS system whereas Cu and Cu+$Al_2O_3$ coatings were produced using the LPCS system. Table 4 summarizes the powder characteristics. Spherical particles are produced by using gas atomization, dendritic particles by using electrolytical production method, and blocky-shaped particles by fusing and crushing. In Table 4, after each powder material also the publication where the particular powder was used is stated.

**Table 4.** Characteristics of powders used in HPCS and LPCS processes.

| Powder material | Particle size (µm) | Morphology | Spraying process used |
|---|---|---|---|
| Cu[I] | -22+5 | Spherical | HPCS |
| Cu[I] | -30+10 | Spherical | HPCS |
| Cu[V] | -35+15 | Spherical | HPCS |
| Cu[I] | -38+11 | Spherical | HPCS |
| Cu[VII] | -25+5 | Spherical | LPCS |
| Cu+ $Al_2O_3$[II, VII] | - | Dendritic<br>Blocky | LPCS |
| Cu+ (10, 30, 50%)$Al_2O_3$[VII] | -25+5<br>-22+5 | Spherical<br>Blocky | LPCS |
| Cu+ (10, 30, 50%)$Al_2O_3$[VII] | < 63<br>-22+5 | Dendritic<br>Blocky | LPCS |
| Ni[I] | -25+5 | Spherical | HPCS |
| Ni[VI] | -30+10 | Spherical | HPCS |
| Ni-20Cr[I, III] | -22+5 | Spherical | HPCS |
| Ni-20Cr[IV, VI] | -30+10 | Spherical | HPCS |
| Ni-20Cr+ (30, 50%)$Al_2O_3$[III] | -22+5<br>-90+45, -45+22, -22+5 | Spherical<br>Blocky | HPCS |
| Ni-20Cr+ 50%$Al_2O_3$[VI] | -30+10<br>-90+45 | Spherical<br>Blocky | HPCS |
| Ni-20Cr+ 30%WC10Cr4Co[VI] | -30+10<br>-45+15 | Spherical<br>Blocky | HPCS |
| Ni-20Cu[VI] | -30+10 | Spherical | HPCS |
| Ni-30Cu[I] | -38+16 | Spherical | HPCS |
| Ta[IV, V] | -30+10 | Blocky | HPCS |
| Ta[IV] | -38+10 | Blocky | HPCS |

### 5.2 Substrate materials

Grit-blasted (mesh 18 (HPCS) or mesh 24 (LPCS) $Al_2O_3$ grits) carbon steel, Fe52 (cold-rolled) and copper (cold-rolled) sheets were used as substrate materials. Coatings were sprayed on steel substrate for denseness evaluations.

# 6 METHODS

In this work, two different spraying systems were used. High-pressure cold spray systems were used at Linde AG Linde Gas Division (Unterschleissheim, Germany) whereas low-pressure cold spray system was used at Tampere University of Technology (Tampere, Finland). Spraying methods, characterization methods and post-treatments are described here.

## 6.1 Spraying methods

### 6.1.1 High-pressure cold spray system

HPCS coatings were prepared with Cold Gas Technology's (CGT) Kinetiks 3000 and Kinetiks 4000 spraying systems. Nitrogen was used as a process gas. Kinetiks 4000 is an advanced spraying system (Fig. 30) which enables the use of pressure of max. 40 bar and preheating temperature of max. 800ºC whereas for Kinetiks 3000, pressure max. 30 bar and preheating temperature max. 600ºC. In addition, two heating systems can be used with Kinetiks 4000. Kinetiks 3000 (in publications I and IV) and Kinetiks 4000 (in publications III, IV, V, and VI) with electrical power of 47 kW and a standard MOC-nozzle were used in this study. Spraying parameters used are presented in the following publications: Cu, Ni, and Ni-30Cu [I], Ni-20Cr and Ni-20Cr+$Al_2O_3$ [III], Ta [IV], Cu and Ta [V], Ni, Ni-20Cu, Ni-20Cr, Ni-20Cr+$Al_2O_3$, and Ni-20Cr+WC-10Co-4Cr [VI].

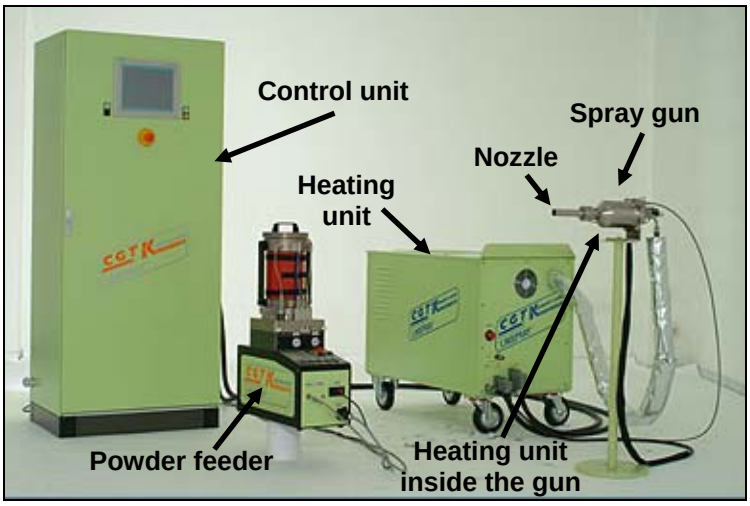


**Figure 30.** Cold Gas Technology GmbH (CGT) Kinetiks 4000 high-pressure cold spray system [136].

In both Kinetiks 3000 (20 kW) and Kinetiks 4000 systems, spraying conditions (e.g., powder feed, pressure, gas feed, and temperature) are controlled [137]. In Kinetiks 4000 equipment, 17 kW, 34 kW, and 47 kW heating power can be used. The system with 17 kW heating power is typically used with soft and low melting point materials, e.g., Al and Zn with maximum temperature of $N_2$ 550ºC whereas 34 kW and 47 kW heating systems offer possibility to use preheating temperature of $N_2$ 800ºC. These models are suitable for most of the materials used in cold spraying. In addition, for these two models, heating consists of two heating systems: a filament inside the nozzle and a separate heating unit with 17 kW or 30 kW power, depending on the model used [131].

### 6.1.2 Low-pressure cold spray system

LPCS coatings were prepared with a DYMET 304K equipment (Obninsk Center for Powder Spraying, OCPS). Compressed air was used as process gas. Maximum pressure is 9 bar and preheating temperature is 650ºC. Both round and tubular nozzles can be used. In this study, a round (Ø 5 mm) stainless steel nozzle was used. The DYMET 304K (Fig. 31) is a portable cold

spray system, and it can be operated manually or with a robot or x-y manipulator. Spraying parameters used are presented in the following publications: Cu+$Al_2O_3$ [II], and Cu and Cu+$Al_2O_3$ [VII].


**Figure 31.** Obninsk Center for Powder Spraying (OCPS) DYMET 304K low-pressure cold spray system [56].

## 6.2 Characterization methods

Various characterization methods were used in order to find relationships between powders, spraying parameters, and post-treatments and structural characteristic and corrosion properties of the HPCS and LPCS coatings.

### 6.2.1 Microscopic techniques

Electron microscopes and a stereomicroscope were used in the characterization of the macro-, micro- and grain structures of the cold-sprayed coatings. Microscopes used are described below.

Scanning Electron Microscope (SEM)

Structures of the cold-sprayed coatings and powder morphologies were characterized using a scanning electron microscope (SEM, Philips XL30). Secondary (SE) and backscattering (BSE) detectors were used. The structures were analyzed from unetched and etched metallographic cross-sectional coating samples. Furthermore, cross-sectional analysis was performed after corrosion tests. HPCS coating samples were prepared by grinding them first with 600-4000 SiC papers and then by polishing with SiO polishing liquid (OP-U, Struers). LPCS coating samples were grinded with 600-1200 SiC papers, 5 µm $Al_2O_3$ paste and 1 µm $Al_2O_3$ liquid. Final polishing was done with SiO polishing liquid. Etching procedure is presented in publication [I].

Field-Emission Scanning Electron Microscope (FESEM)

The unetched microstructures and fracture surfaces were analyzed with an ultra high resolution field-emission scanning electron microscope (FESEM, Zeiss ULTRAplus). Metallographic cross-sectional samples were prepared with the same procedure as SEM samples. Coating samples were bent up to rupture for fracture surface analysis.

Transmission Electron Microscope (TEM)

The inter-particle structures were characterized using an analytical transmission electron microscope (TEM) with an energy dispersive X-ray spectrometer (EDS) (TEM (Jeol JEM 2010)+EDS (Noran Vantage)). In TEM characterization, samples were analyzed both from top-view and cross-section directions. Samples were either electrolytically prepared with twin jet electrolytical polisher (Struers Tenu-Pol-5) using a solution of nitric acid in methanol (1:2) or samples were prethinned by hand, then thinned with dimple grinder (Gatan Dimpler 656) and finally thinned with precision ion polishing system (Gatan PIPS 691).

Stereomicroscope (SM)

After corrosion tests, coating surfaces were analyzed with a stereomicroscope (SM, Leica MZ7.5). The coating samples were cleaned with water and ethanol prior to the surface analysis with stereomicroscope.

### 6.2.2 Corrosion tests

Denseness of the cold-sprayed coatings was evaluated with open-cell potential measurements and with salt spray tests. These tests reveal impermeability or existing through-porosity inside the coating structures. In addition, corrosion properties of the coatings were studied by using anodic polarization measurements. Corrosion tests used are presented below.

Open-cell potential measurements

The corrosion behavior and denseness, i.e., impermeability or existing through-porosity of the coatings, were tested with electrochemical open-cell potential measurements. The electrochemical cell used in the open-cell potential measurements consisted of a plastic tube of diameter 20 mm and volume 12 ml, glued on the surface of the coating specimen. A 3.5 wt.-% NaCl solution was placed in the tube for 9-, 18-, or 60-day measurements, taken with a Fluke 79 III true RMS multimeter. A silver/silver chloride electrode (Ag/AgCl) was used as a reference electrode. Bulk (cold-rolled metal sheets) materials were also tested as a reference.

Salt spray test

The salt spray tests were conducted according to the ASTM B117 standard. Substrates were masked with epoxy paint before testing in order to allow only the coating surfaces to be in contact with the corroding salt spray. A 5 wt.-% NaCl solution was used with an exposure time of 48, 96, or 240 h, a temperature of 35-40°C, a solution pH of 6.3, and a solution accumulation of 0.04 ml/cm$^2$h. The salt spray tests in publications I and II, were done at Tampere University of Technology whereas tests in publications III, IV, VI, and VII, were carried out at Technology Centre KETEK (Kokkola, Finland).

Anodic polarization measurements

Polarization measurements were carried out in order to evaluate the corrosion resistance of the cold-sprayed Ta coatings. Polarization behavior is usually studied in order to estimate corrosion protection and corrosion rates. Furthermore, active-passive behavior is clearly detected from anodic polarization measurements [115]. The anodic polarization tests were carried out adapting the standard ASTM G59. The polarization tests were run in a flat specimen cell with a rubber O-ring used as gasket. Tests were conducted in 3.5 wt.-% NaCl and 40 wt.-% $H_2SO_4$ water solutions at room temperature (RT) of 22ºC and at elevated temperature of 80ºC. Potential was scanned from 0.6 V below the resting potential ($E_0$) to potential of 3 V at a scanning rate of 2 mV/s. A saturated calomel electrode (SCE) was used for reference. The tests were done at Technology Centre KETEK (Kokkola, Finland).

### 6.2.3 Mechanical testing methods

Hardnesses and bond strengths of the cold-sprayed coatings were investigated in order to evaluate mechanical behavior and to find correlation between macroscopic properties and microscopic details.

Microhardness

Vickers hardness ($HV_{0.3}$) was measured as an average of ten measurements from the cross-sections of coatings with a Matsuzawa MMT-X7 hardness tester. The weight of the load was 300 g. In hardness measurements, the indentations were taken from the metallic coating areas of the coatings with hard particles to evaluate the mechanical behavior of the metallic particles.

Bond strength

Bond strength values were determined according to standard EN582 in a tensile pull test (Instron 1185 mechanical testing machine) as an average of three measurements. The coating samples were glued between two rods which were grit-blasted prior to gluing. The glue used was 3M Scott-Weld DP-460.

### 6.2.4 Other methods

In addition to the above methods, image analysis, particle size distribution measurements and chemical analysis were carried out.

Image analysis

The image analyses were done using ImageJ program. The hard particle fractions were calculated from cross-sectional samples of the coating using image analysis. In addition, the amount of corrosion spots on the coating surfaces after corrosion tests were calculated.

Particle size measurements

The particle size distributions of Ta powders were measured with Symantec Helos analysis in wet conditions (Sucell). Measurements are based on laser diffraction.

Chemical analysis

Oxygen contents of Ta powders (in publication IV) were measured with chemical analyzers (Leco TC-436DR and Leco TC-136) at Outotec Research, Pori, Finland.

## 6.3 Post-treatments

Heat treatments were done as post-treatments in order to densify the structures of HPCS Cu, Ni, Ni-20/30Cu, Ni-20Cr, Ni-20Cr+$Al_2O_3$, and Ni-20Cr+WC-10Co-4Cr coatings. In publication I, the heat treatments were done in a Carbolite 3-zone controlled atmosphere furnace using Ar as protective gas. Holding time at the annealing temperature was 5 hours and annealing temperatures were 200, 400, 600, 800, and 1000ºC, depending on the coating materials. In addition, in publication VI, heat treatments were done using a furnace in a protective (Ar-3%$H_2$) atmosphere with the holding time of 2 hours at 600ºC annealing temperature. In both heat treatment procedures, samples were under protective atmospheres during temperature rising, holding and cooling.

# 7 RESULTS AND DISCUSSION

The focus point of this study was to produce overall and fully dense cold-sprayed coatings and characterize the microscopic and macroscopic features of the coatings which affected the coating denseness. The denseness of the coatings strongly depends on powder characteristics together with spraying parameters. Microstructural properties (microstructure, grain structure, fracture surfaces, and particle bonding) were analyzed to gain the microstructure-denseness dependence. Corrosion properties and especially, impermeability were evaluated in order to estimate the capability of the coatings for corrosion protection.

## 7.1 Microscopic properties of cold-sprayed coatings

Structures of the cold-sprayed coatings as well as microstructures and grain structures of the dense coatings are shown here. It can be said that microstructure of the coatings defines their corrosion protection capability, denseness being the key factor.

### 7.1.1 Microstructure

Typically, the structure of cold-sprayed coatings is dense (without pores or with low porosity level) according to microscopic characterization. Figure 32a shows an example of the cross-sectional structure of HPCS Ta coating on grit-blasted steel substrate. This is the typical structure of a dense cold-sprayed metallic coating. In addition, the interface between the coating and substrate is clean and voidless. Furthermore, etching reveals the detailed microstructure of the coatings. Microscopic details; particle boundaries, partly inter-particle structure, particle deformation, and flattening are seen in the etched cross-sectional microstructure of HPCS Cu coating, Fig. 32b. Examples of slip planes caused by localized deformation are marked with arrows. Particles are highly flattened on the impacts due to the high level of plastic deformation. Furthermore, high deformation leads to high denseness [31]. The microstructures of HPCS Cu coatings are presented in [I, V], HPCS Ni in [I, VI], HPCS Ni-20/30Cu in [I, VI], HPCS Ni-20Cr and Ni-20Cr+$Al_2O_3$ [III, VI], HPCS Ni-20Cr+WC-10Co-4Cr [VI], and Ta in [IV, V].

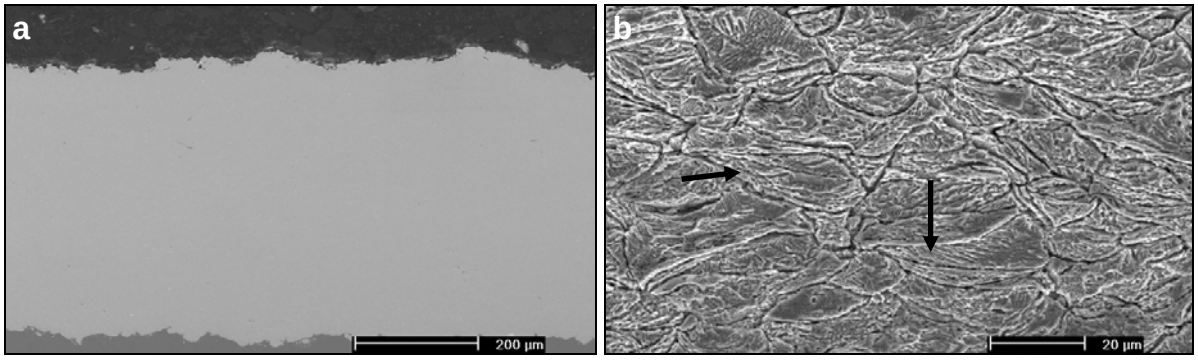


**Figure 32.** Cross-sectional structure of HPCS a) Ta coating on grit-blasted steel substrate, unetched [IV] and b) Cu coating, etched structure [I]. SEM images.

Metallic-ceramic powder mixtures are usually used in the LPCS process. Ceramic particles keep the nozzle clean, activate the sprayed surface, and densify the coating structures. Figure 33a shows the typical cross-sectional structure of LPCS Cu+$Al_2O_3$ coating. Black particles in the structure are $Al_2O_3$ particles arisen from an initial powder mixture. Coatings are visually dense, particles are plastically deformed; however, some oxidized particle boundaries are present, seen in Fig. 33b (SEM (BSE) image) as darker gray boundaries (arrows). Obviously, dendritic powder particles present relatively high number of oxidized particle boundaries due to the fact that primary particles contain irregular, dendritic structures. The etching reveals primary particle boundaries which are clearly visible in Fig. 33c. Powder particle boundaries are not detected in the structure and this is caused by break-down of powder particles on the high-velocity impact. In addition, the high level of plastic deformation of primary particles is detected in the etched

microstructure as flattened particle shapes (Fig. 33c). The microstructures of LPCS Cu and Cu+$Al_2O_3$ coatings are presented in [II, VII].

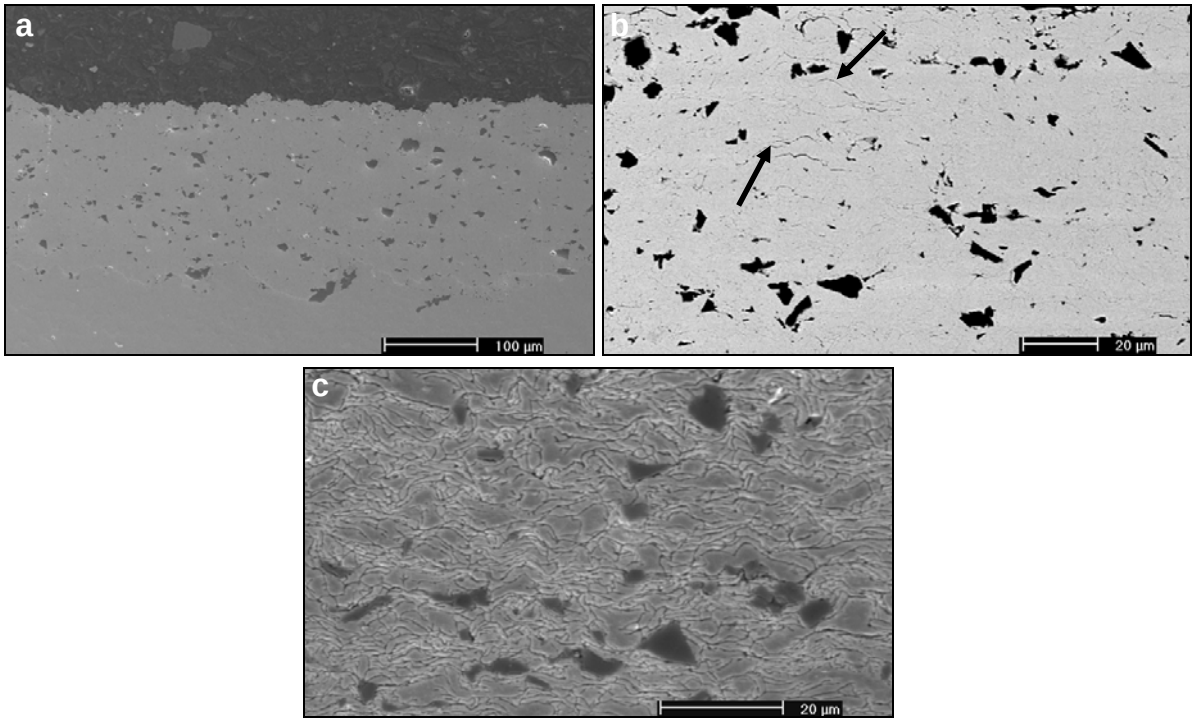


**Figure 33.** Cross-section of LPCS Cu+$Al_2O_3$ coating: a) unetched structure, coating on grit-blasted steel substrate (SE image), b) unetched microstructure (BSE image), oxidized particle boundaries are shown with arrows, and c) etched microstructure (SE image). SEM images. [II]

Powder characteristics have a strong influence on the coating formation and hence, the coating properties [1] also in the LPCS process. Two different types of Cu powders were studied in order to find affecting factors to densify the structures of LPCS Cu and Cu+$Al_2O_3$ coatings [VII]. An amount of 50% $Al_2O_3$ particles mixed with dendritic Cu powder showed the densest structure according to microscopic evaluation in the comparison between 0, 10, and 30% $Al_2O_3$ additions in the case of this powder. Figure 34 presents the cross-section of LPCS Cu+50$Al_2O_3$ prepared from Ecka dendritic powder. In this study, the highest amount of $Al_2O_3$ showed clearly decreased porosity and pores were mostly concentrated on the top of the coatings. However, some oxidized boundaries were still detected in the detailed structure (Fig. 34b), indicating that oxide layers of initial primary particles were not totally removed during impacts. Furthermore, the dendritic powder particles had large surface area due to the dendritic shape and thus, the high number of oxidized primary particle boundaries appears already in the as-sprayed state.

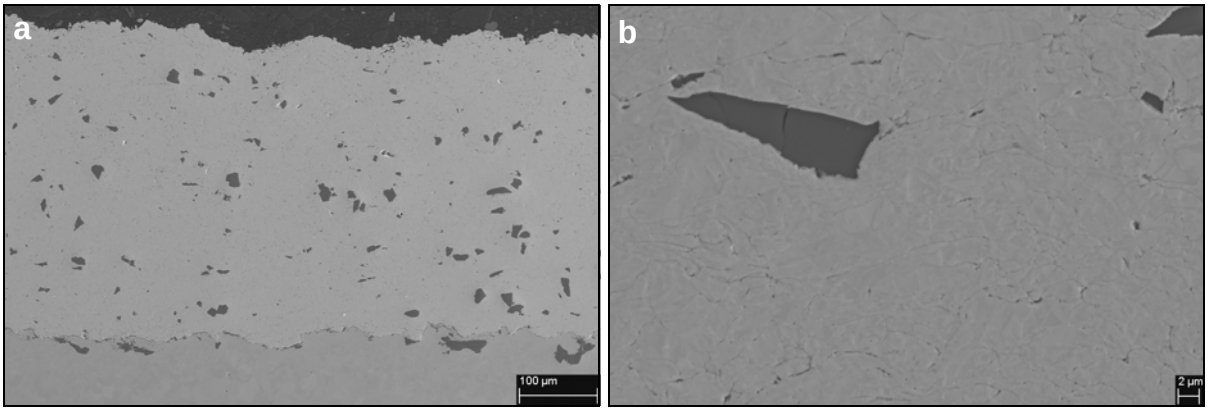


**Figure 34.** Cross-section of LPCS Cu+50%$Al_2O_3$ coating prepared from dendritic Cu powder particles (Ecka M15) mixed with $Al_2O_3$ particles: a) coating on grit-blasted steel substrate and b) unetched detailed microstructure. FESEM images. [VII]

On the other hand, one solution to decrease porosity and to increase denseness of the LPCS Cu coatings was gained by using spherical Cu particles. The spherical particles have lower number of particle boundaries compared with dendritic particles due to powder morphology and primary particle size. The relatively dense LPCS Cu coating without any hard particle addition was gained by using spherical Cu powder. In addition, 10% $Al_2O_3$ particle addition clearly densified the structure. Figure 35 shows the cross-section and detailed microstructure of LPCS Cu+10$Al_2O_3$ coating prepared from Osprey spherical powder. Only a few oxidized boundaries were detected in the structure. Additionally, the amount of these boundaries in this coating was lower than in other LPCS Cu and LPCS Cu+$Al_2O_3$ coatings.

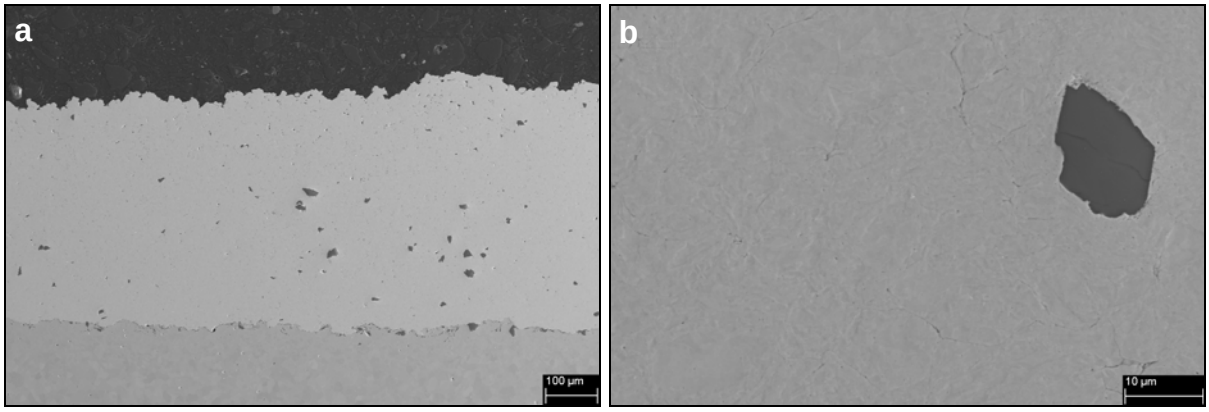


**Figure 35.** Cross-sectional structure of LPCS Cu+10%$Al_2O_3$ coating prepared from spherical Cu powder particles (Osprey) mixed with $Al_2O_3$ particles: a) coating on grit-blasted steel substrate and b) unetched detailed microstructure. FESEM images. [VII]

The hard particle addition has also shown its potential to densify the metallic structure of HPCS Ni-20Cr coatings. The cross-sections of HPCS Ni-20Cr+50$Al_2O_3$ and Ni-20Cr+30WC-10Co-4Cr are presented in Figs. 36a and 36b, respectively. The coating structures are visually dense without pores or other defects inside. Black particles in Fig. 36a are $Al_2O_3$ particles whereas light gray particles are WC-10Co-4Cr particles in Fig. 36b. The proportions of hard particles in the coatings are 5 % and 18 %, respectively. [VI]

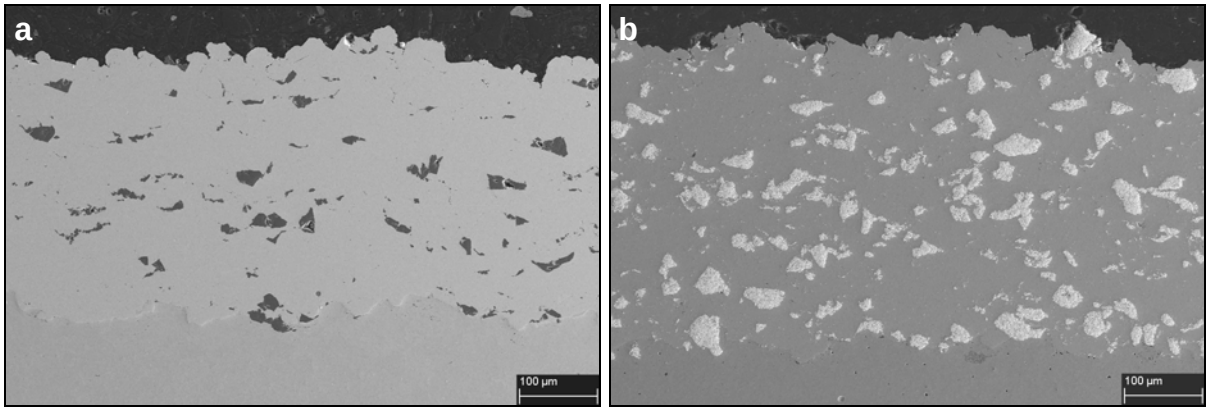


**Figure 36.** Cross-sectional structures of HPCS a) Ni-20Cr+50$Al_2O_3$ and b) Ni-20Cr+30WC-10Co-4Cr coatings on grit-blasted steel substrates. FESEM images. [VI]

As a summary, the microstructures of HPCS coatings are dense and oxide-free due to the highly plastically deformed structure caused by high-velocity particle impacts. For the dense structure formation, presence of pores, voids and other impurities should be eliminated. The high level of plastic deformation makes it possible to eliminate defects inside the structure by e.g., breaking down the oxide layers of initial powder particles. In addition, porosity is eliminated with high particle deformation. Typically, weak points in the cold-sprayed structures were concentrated on the particle boundaries at the connecting point of several particles. When

particles are deformed enough, porosity is eliminated due to the localized deformation and formation of material jets.

With the HPCS Ta coatings, denseness improvement was detected with the optimal combination of powder (improved powder: particle size, particle size distribution, purity) and spraying conditions (advanced spray equipment). High preheating temperature affects coating quality [131] by increasing particle velocity and temperature which in turn, increases the particle deformation and forms a tighter structure [41]. The denseness improvement by optimal combination of powder and spraying parameters and its effect on particle deformation is schematically presented in Fig. 37, case 1. The optimal powder properties and further, spraying parameters are material-dependent. In the other case, denseness of the coatings was improved with the addition of hard particles. Firstly, it enables the use of higher process temperatures (without nozzle clogging) which in turn, improves coating quality [32,41]. Secondly, hard particles densify the structure due to hammering and tamping effects [49]. This is demonstrated in Fig. 37, case 2.

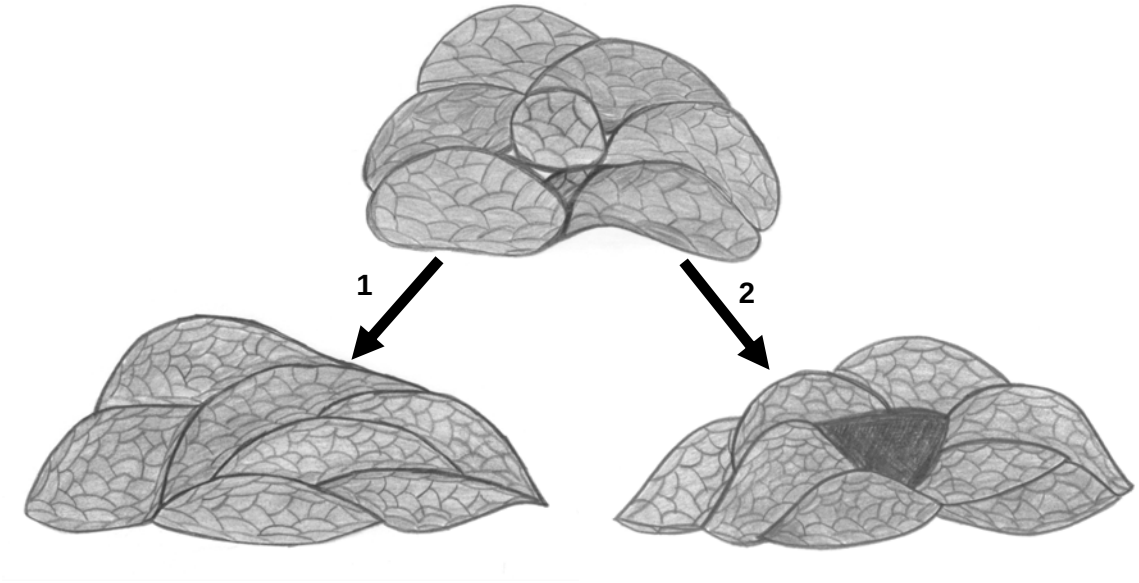


**Figure 37.** Schematic presentation of particle structure of coating with porosity and coatings with dense structure due to the high level of deformation. Number 1 indicates denseness improvement by choosing optimal combination of powder and spraying parameters and number 2 by adding hard particles to densify the metallic structure.

### 7.1.2 Grain structure

The FESEM characterization shows a dense structure and in addition to that, a grain structure with highly deformed grains. Tight bonding between the HPCS Ta particles as well as a metal-metal contact between particles is observed in Fig. 38. Metal-metal bonding is the requirement for tight bonds and therefore, overall dense coating structure. Figure 38a shows a very fine grain structure detected near to the particle-particle interface and additionally, elongated grains due to the high deformation. Furthermore, materials jets are reportedly crucial for the high coating quality [5,30,31,82]. Arrow shows material jet formed between two Ta particles (Fig. 38b). Powder characteristics together with optimized spraying parameters lead to the formation of highly dense coatings by cold spraying. In addition, purity of the powder is crucial for the metal-metal bonding, depending on oxide layer removal. Powder particles with high purity have thinner oxide layers on the particle surfaces, promoting tendency to get the metal-metal bonding on the impact. If the oxide layer is thick, removal of this layer is more difficult on the impacts and thus, there is possibility that oxides stay at particle boundaries in the structure and decrease the metal-metal bonding [1]. Localized deformation is due to the adiabatic shear instability and thermal softening [24,30,31]. High plastic deformation is needed to destroy oxide layers of the particles and thus, enabling the formation of the metal-metal bonding between particles.

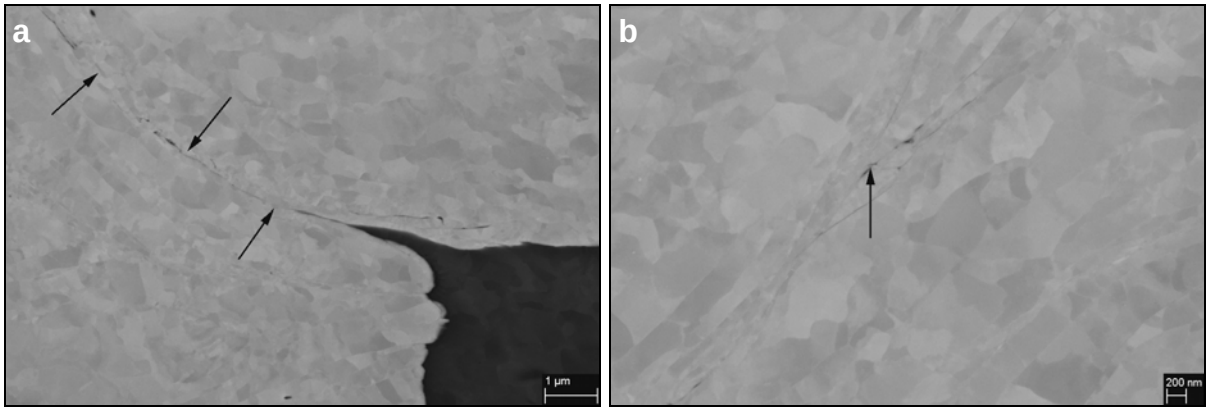


**Figure 38.** Cross-sectional microstructure of HPCS Ta coating: a) particle-particle and particle (gray area)-substrate (black area) interfaces (arrows indicate particle boundary) and b) metal-metal bonding between Ta particles (arrow indicates material jet). FESEM images. [V]

Plastic deformation is known to be related to dislocations (i.e., microstructural defects) in the structure. Under high strain, dislocation movement cause plastic flow and, hence permanent deformation. Even further, dislocation movement causes work hardening. In the microstructure, plastic flow can be seen in the presence of slip planes due the sliding [79] and of shear bands due to the adiabatic shear localization [67]. High dislocation density indicates high plastic strain and hence, high level of deformation [79]. In addition to the high dislocation density, twinning, i.e., formation of twins causes permanent deformation in the material.

High plastic deformation together with adiabatic localization is detected by microscopic characterization from the structure by various nanoscale features. In addition, the cold-sprayed Cu coatings had non-uniform structures [138] due to the localized deformation. Localization of the grain deformation inside the particle structure is strongly concentrated on the region near to the particle interfaces. The strongest deformation is due the adiabatic shearing and thus, the elongation of grains. Moreover, high dislocation density together with a formation of shear bands, slip planes, and twins causes different levels of deformation in different part of particles. Figure 39a reveals shear bands and twins, indicating localized grain deformation on the impacts. Deformation and inter-particle structure from top-view direction of Ta particles are shown in Fig. 39b. High dislocation density areas are observed in the TEM images. Figure 39b shows elongated grains with high dislocation density.

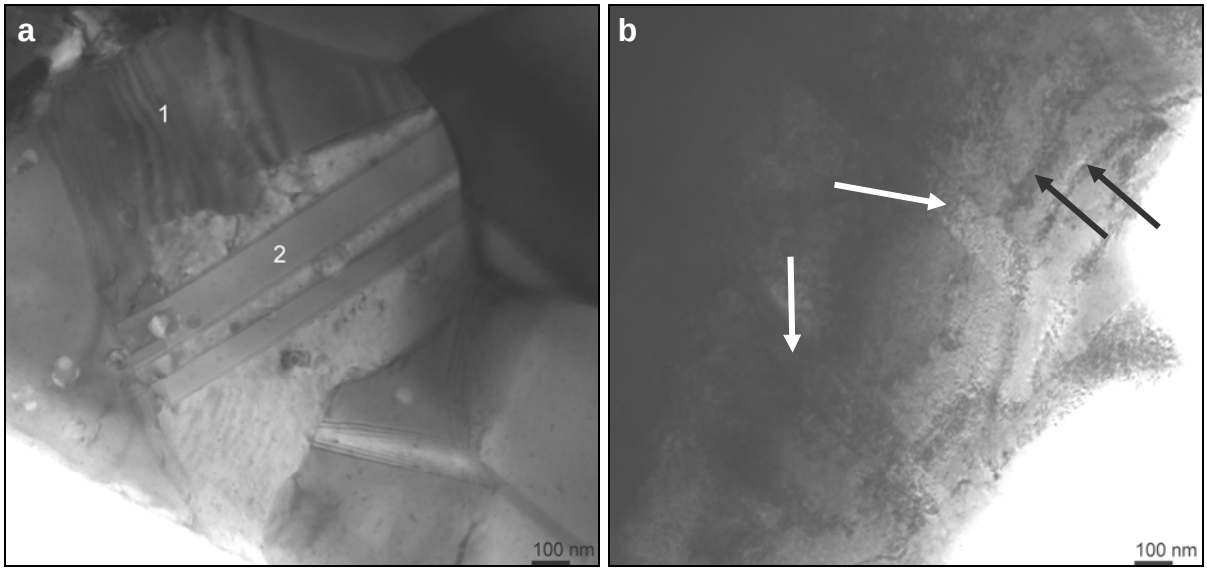


**Figure 39.** Inter-particle structure of HPCS a) Cu, 1 indicates shear bands and 2 twins, and b) Ta coatings with elongated grains (white arrows) and dislocation walls (black arrows). TEM images. [V]

## 7.2 Particle interfaces

In this work, also particle interfaces and bonding between metallic and metallic-ceramic particles were studied. Particle bonds are tight in the dense coating structure and metal-metal bonds are dominant in the metallic coatings. In addition, in the metallic-ceramic mixture coatings, ceramic particles reinforce the structure and mechanical bonding between metallic and ceramic particles has been observed.

### 7.2.1 Metal-metal particle bonding

As already mentioned, typical weak points in the cold-sprayed coating are concentrated on particle interfaces due to the weak particle boundaries. Weak bonds between particles caused by undeformed or only slightly deformed particle together with insufficiently removed oxide layers on the particle surfaces can compose porosity [85]. In addition, in some cases, e.g., in Ni-20Cr coatings, porous layer on the top of the coatings is formed due to the absence of tamping effect of next incoming particles [85,111]. Figure 40a shows porosity (black area) in the structure of HPCS Ni-20Cr coating and oxide layers between particles (darker gray areas, marked with arrows). Furthermore, open particle boundaries are observed in the structure of HPCS Ni-30Cu coating after salt spray test as shown in Fig. 40b, indicating a weak structure with local defects and thus, non-protective coating. In addition, the most critical areas in the particle bonding are the connection points between several particles. For tight bonding without weak bonds and local defects, metal-metal bonding is required and it is able to be attained with high particle deformation on the particle impacts by removing the oxides from the surfaces while gas flow removes them away.

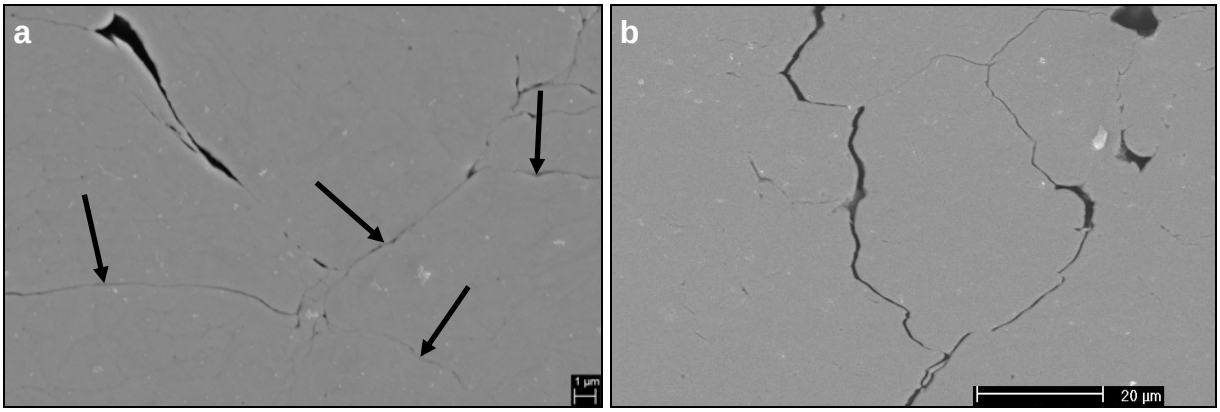


**Figure 40.** Cross-sectional structure of HPCS a) Ni-20Cr coating with weak particle boundaries (arrows indicate oxidized particle boundaries), FESEM image [VI] and b) Ni-30Cu coating after salt spray test, SEM image [I].

Examples of tight, dense, and oxide-free particle interfaces are presented in Fig. 41. Arrows indicate the connection points between particles: Ni-Ni and Cu-Cu, in Figs. 41a and 41b, respectively. In addition, randomly aligned grains are detected inside the structure of HPCS Cu coating (Fig. 41b).

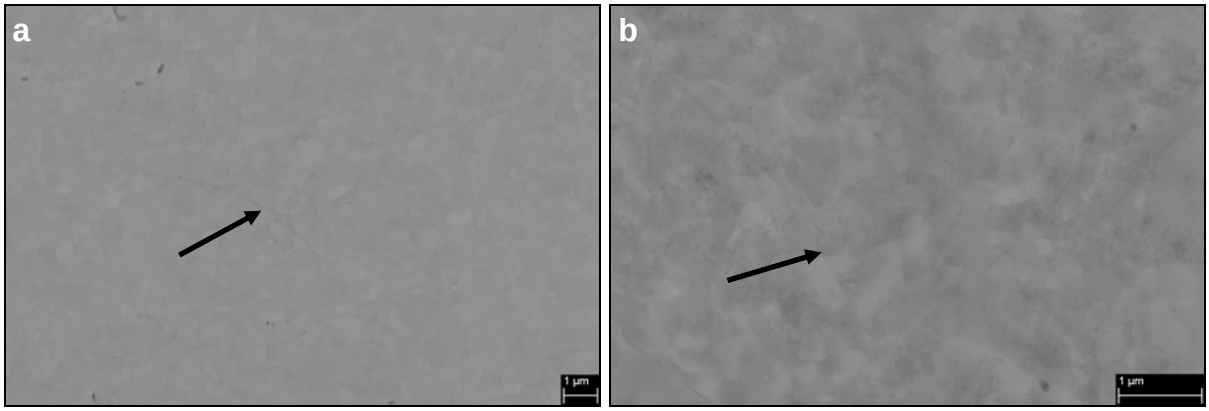


**Figure 41.** Cross-sectional microstructure of HPCS a) Ni [VI] and b) Cu [V] coatings. Dense coatings have tight particle bonds. Arrows indicate bonding between three particles. FESEM images.

Also TEM characterization reveals the tight particle bonds. Figure 42a shows the inter-particle structure and particle interface of HPCS Cu particle in the cross-sectional direction whereas the inter-particle structure of HPCS Ta particle from top-view direction is presented in Fig. 42b. In Fig. 42a, holes in the structure arisen from ion milling are designated as weaker particle boundaries whereas other parts of the boundaries were tight. In addition, removal of oxides from initial powder particle was observed with TEM+EDS analysis. The EDS analysis revealed the oxygen contents at the selected points in the structure of HPCS Cu: 1) 1.9 wt.-%, 2) 2.6 wt.-%, 3) 0.9 wt.-%, and 4) 0.5 wt.-%, as shown in Fig. 42a. These analyses show the oxygen contents at the selected points and they do not reflect to the total amount of oxygen in the structure. Values are given here in order to have comparison between different regions inside the coatings. The EDS analysis revealed that the oxygen content was lower inside the particle (points 3 and 4 in Fig. 42a) than at the particle boundary (points 1 and 2). Additionally, the oxygen content was lower at point 1 than at point 2, indicating tighter bonding region (point 1). On the other hand, it is possible that higher oxygen content in the open boundary (point 2) compared with the tight boundary (point 1) reflects to the fact that the oxide layers were not totally removed. As a conclusion, there are still some weak points in the structures of the dense HPCS Cu coating, however, tight bonds are dominant and thus, coating has impermeable cross-sectional structure. This was also verified with corrosion tests.

Figure 42b shows the microstructural details of HPCS Ta coating, e.g., tight particle bonds with shear bands (white arrows indicate particle boundaries whereas black arrow shows shear bands). The EDS analysis from selected points revealed low oxygen contents both at the particle boundary and in the inter-particle structure: 1) 0.7 wt.-%, 2) 0.7 wt.-%, 3) 0.5 wt.-%, and 4) 0.6 wt.-%, as shown in Fig. 42b. This indicates pure metal-metal bonding between the particles. The HPCS Ta coating had very dense and highly deformed structure with tight bonds. This coating contained a high amount of dislocations and especially dislocation walls. Moreover, the elongated grains indicate high plastic deformation and localized deformation due to the localized adiabatic shearing and thermal softening.

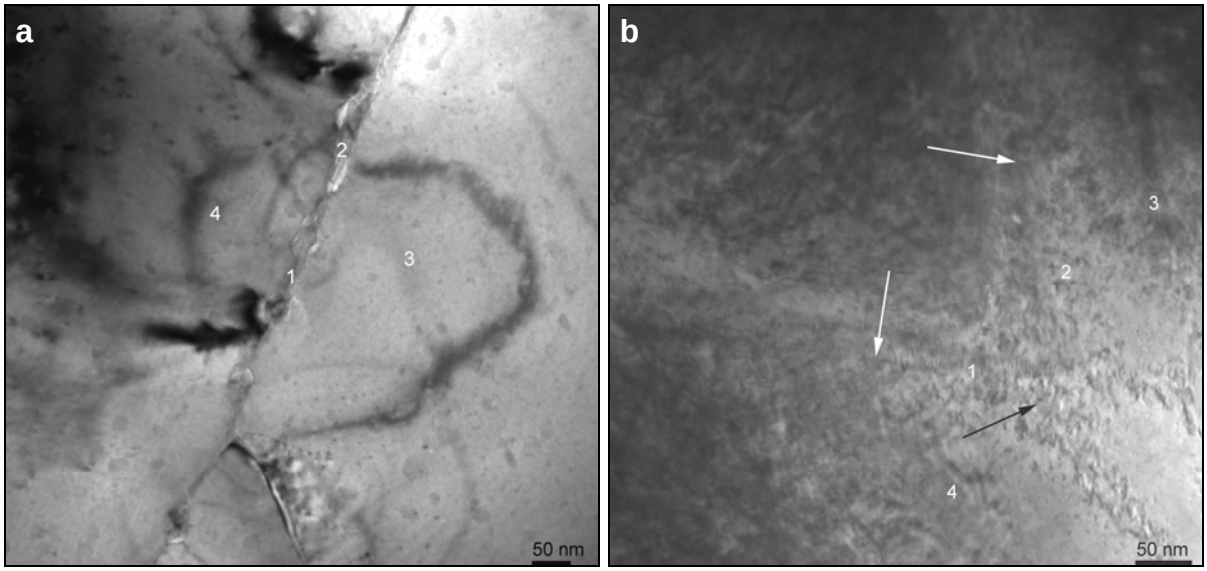


**Figure 42.** Particle boundaries between HPCS a) Cu particles (cross-sectional direction) and b) Ta particles (top-view direction). EDS analyses taken from places 1-4. Particle boundaries are indicated with white arrows and example of shear bands with black arrow. TEM images. [V]

### 7.2.2 Metal-ceramic particle bonding

One solution to densify the coating structure of HPCS metallic coating is to use metallic-ceramic powder mixtures. The experiments revealed technical spraying limitations when spraying Ni-20Cr powder. At higher temperature (600ºC/700ºC versus 500ºC) Ni-20Cr particles clogged the nozzle. This was possibly caused by the Ni-20Cr particles which were in softer state and thus, they stuck more easily to the surface of the nozzle [III]. To solve such problems, metallic powders were mixed with ceramic particles. Hard particles in the metallic powder have three functions: 1) to keep the nozzle clean, 2) to activate the sprayed surface, and 3) to densify the coating structure. Hard ceramic particles, $Al_2O_3$, were added into the metallic Ni-20Cr powder in order to improve coating quality and denseness together with possibility to use higher process temperature. Figure 43 shows bonding between Ni-20Cr and $Al_2O_3$ particles in the metallographic cross-section (Fig. 43a) and in the fracture surface (Fig. 43b). $Al_2O_3$ particles were mostly embedded into the softer metallic matrix and they were stuck to the surface. The particle interface seemed to be dense without visually detectable pores. In addition, the high level of plastic deformation of Ni-20Cr particle with material jets is observed from fracture surface in Fig. 43b. Hard particle hammers the previous particle, densifing the entire structure. In addition, $Al_2O_3$ particles were slightly fractured instead of deformation. It has been reported that fracturing of ceramic particles can be necessary for the coating formation [23,92].

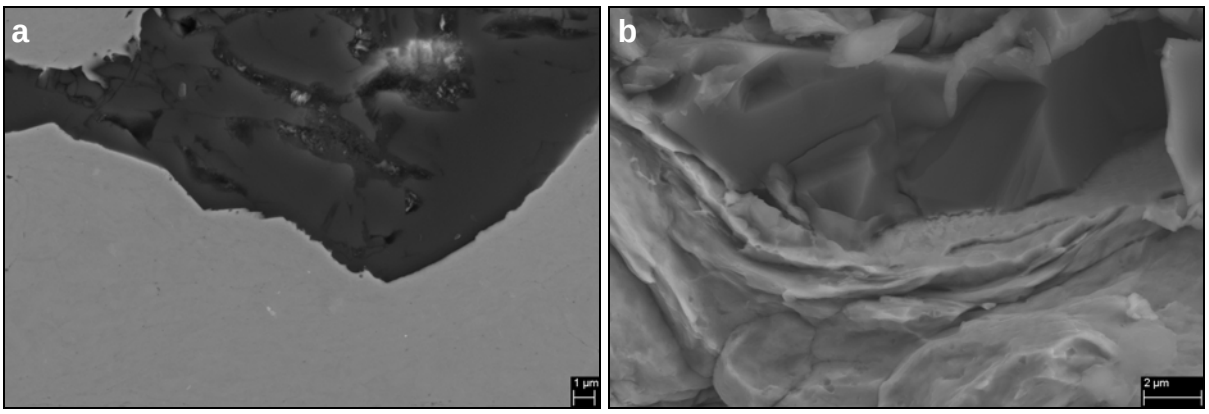


**Figure 43.** HPCS Ni-20Cr+50$Al_2O_3$ coating: a) cross-sectional structure and b) fracture surface. Bonding between Ni-20Cr (lighter gray) and $Al_2O_3$ (darker gray) particles. FESEM images. [VI]

In addition to the $Al_2O_3$ particle addition, hardmetal particle addition showed the denseness improvement in HPCS Ni-20Cr coatings. WC-10Co-4Cr particles were added into the Ni-20Cr powder. The cross-sectional structure of HPCS Ni-20Cr+WC-10Co-4Cr mixture coating is presented in Fig. 44a and fracture surface in Fig. 44b. WC-Co-Cr particles were broken down and scattered inside the structure on the particle impact and then, fragmented. The hammering effect of WC-Co-Cr particles on the deformation of Ni-20Cr particles was also noticeable.

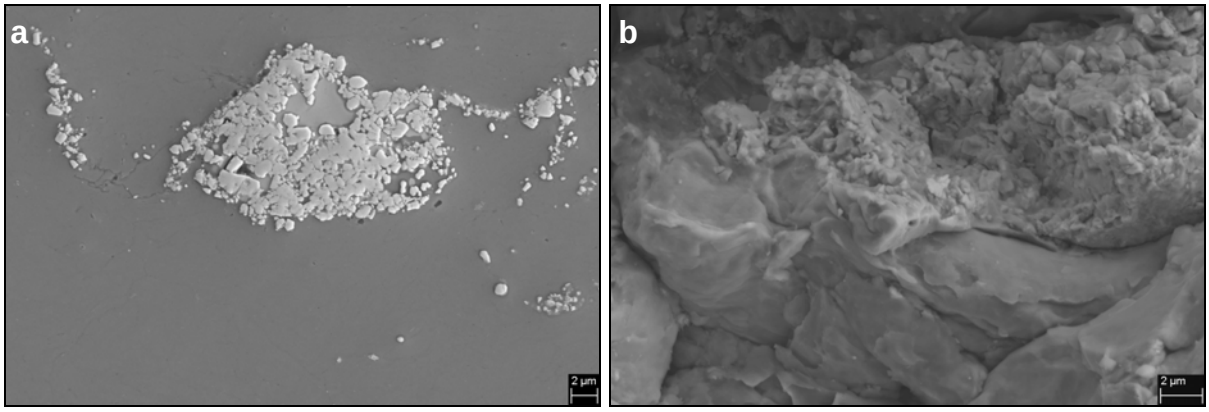


**Figure 44.** HPCS Ni-20Cr+30WC-10Co-4Cr coating: a) cross-sectional structure (heat-treated) and b) fracture surface. WC-Co-Cr particles broke down on the impact. FESEM images. [VI]

Bonding between dendritic Cu particles and hard $Al_2O_3$ particles is presented in fracture surface of LPCS Cu+$Al_2O_3$ coating in Fig. 45. Ceramic particles reinforced the structure by hammering and tamping the impacted surface and some of hard particles stuck to the surface. Localized deformation of Cu primary particles is observed in Fig. 45. However, also less deformed primary particles are detected in the structure of LPCS Cu+$Al_2O_3$ coating due to the fact that dendritic particles contain significantly finer primary particle size and thus, there are more particle boundaries for the deformation (more initial oxide layers to be removed). Moreover, powder particle boundaries were not clearly seen whereas primary particles were observed. [VII]

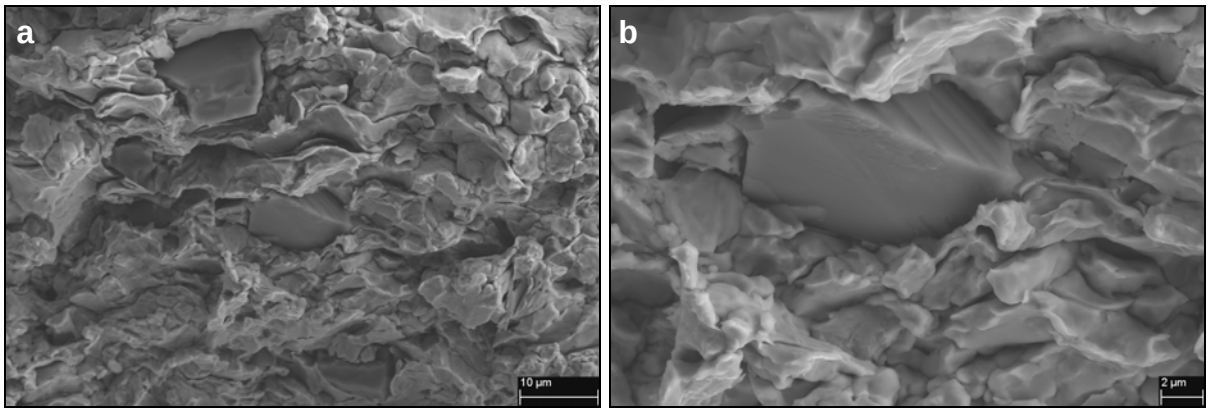


**Figure 45.** Fracture surfaces of LPCS Cu+$Al_2O_3$ coating: a) general overview and b) bonding between Cu and $Al_2O_3$ particles. FESEM images. [VII]

### 7.2.3 Particle deformation

In addition to the fracture behavior, fracture surface analysis reveals particle deformation. The dense coating structure contains highly deformed microstructure and inter-particle structures. The fracture surface of the fully dense HPCS Cu coating is presented in Fig. 46a. The fracture is partly brittle and partly ductile. In addition to the ductile behavior, due to the dynamic recrystallization [138] recrystallized grains are observed [V]. The HPCS Ta coating also had an overall dense structure. Figure 46b shows the high level of particle flattening due to the high deformation. However, grains inside differ from those inside the Cu particles; the Ta particles

have columnar shapes. Material differences together with different powder types of Cu and Ta leads to different inter-particle behavior (recrystallized grains versus columnar grains).

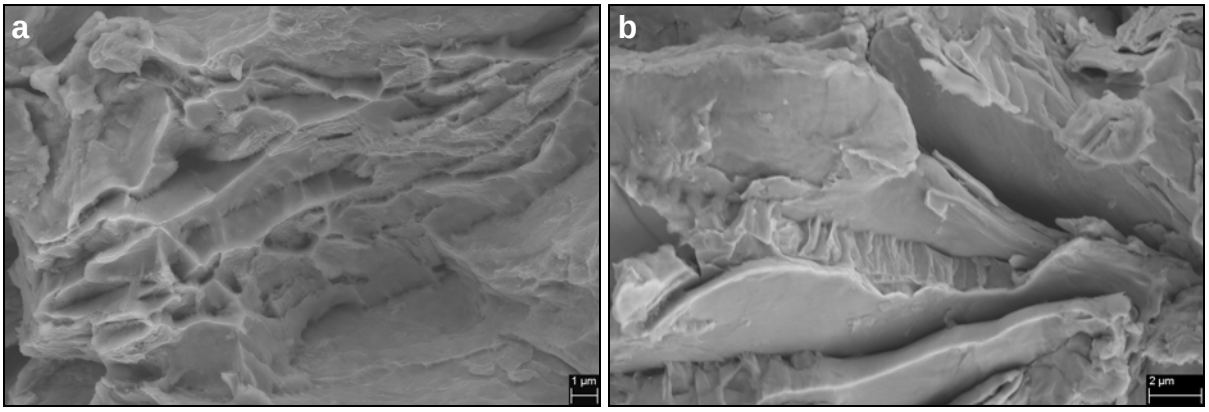


**Figure 46.** Fracture surfaces of HPCS a) Cu and b) Ta coatings. Highly deformed particles. FESEM images. [V]

The crossing points of HPCS Ni particles in as-sprayed and heat-treated state in the fracture surfaces are presented in Fig. 47. The structure became significantly more ductile after heat treatment due to recrystallization. Additionally, small-sized grains are detected in the fracture surface of heat-treated Ni coating, Fig. 47b. The same influence of heat treatment on the fracture behavior is observed in the case of Ni-20Cu coating, shown in Fig. 48. In the as-sprayed state, fracture is mostly brittle-type, whereas in the heat-treated state, it is mostly ductile-type (Fig. 48b). In addition, coating structure was densified during heat treatment due to the void reduction and recrystallization. [VI]

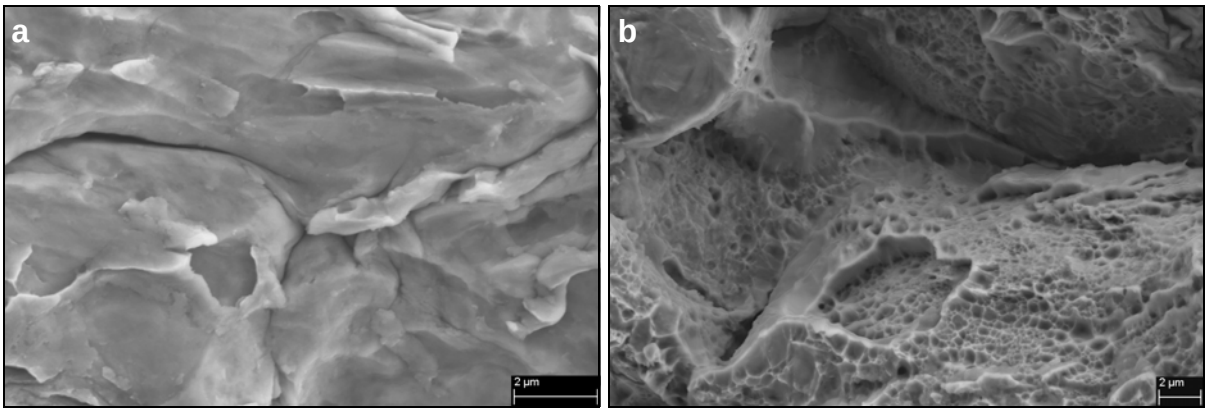


**Figure 47.** Fracture surface of HPCS Ni coating in a) as-sprayed and b) heat-treated state. Structure became more ductile during heat treatment. [VI]

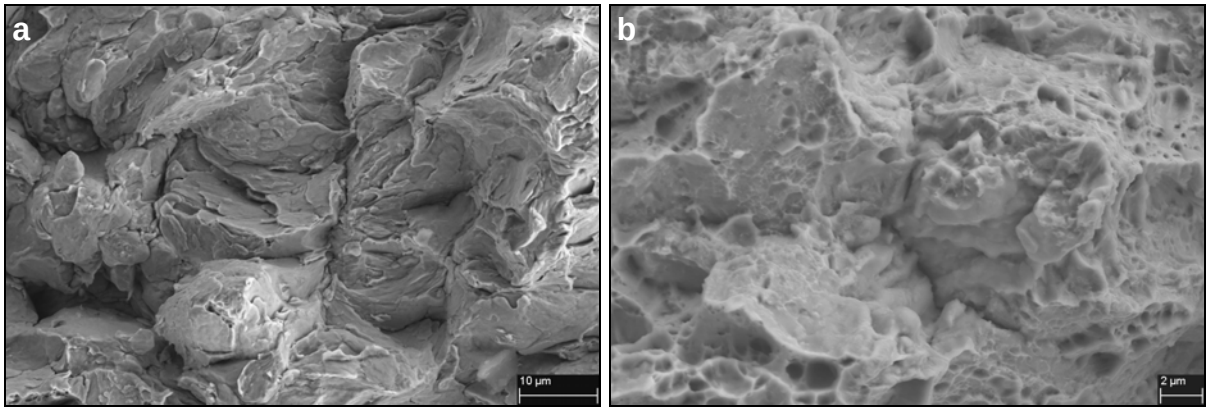


**Figure 48.** Fracture surface of HPCS Ni-20Cu coating in a) as-sprayed (mostly brittle-type fracture) and b) heat-treated (mostly ductile-type fracture) state. Structure is highly deformed. FESEM images. [VI]

Comparison between the coating structures of LPCS Cu coatings prepared from dendritic and spherical particles are shown in Figs. 49a and 49b, respectively. The fracture surface of dendritic Cu coating reveals the high number of primary particle boundaries and less deformed particles in the structure. Whereas spherical Cu particles are more deformed with flattened shapes and the coating contains less particle boundaries due to larger primary particle size. It should be noticed that these coatings are sprayed from pure Cu powders without $Al_2O_3$ addition. Furthermore, the hard particle addition leads to denser coating structure with higher deformation level of Cu particles due to the hammering effect of $Al_2O_3$ particles. The effect was stronger in the case of dendritic Cu particles than in the case of spherical Cu particles.

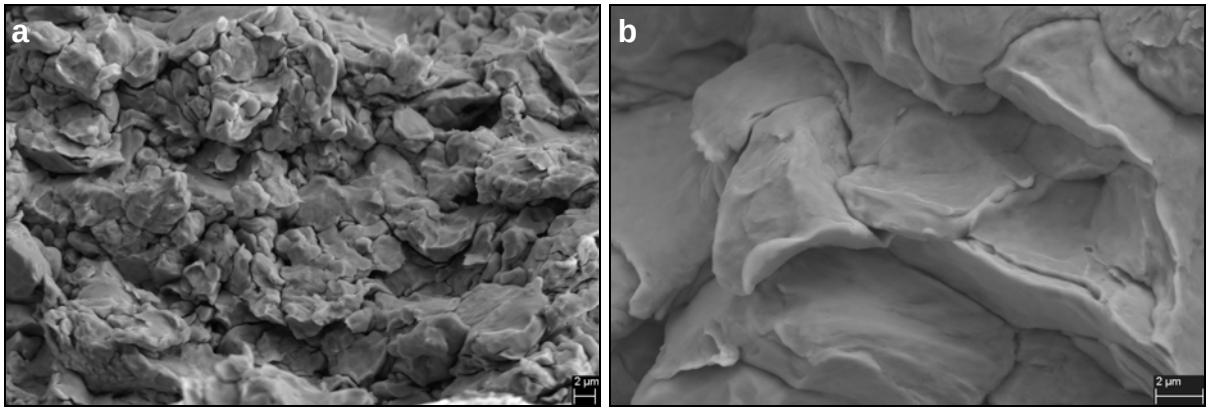


**Figure 49.** Fracture surfaces of LPCS Cu coatings a) prepared from dendritic Cu powder (Ecka) and b) prepared from spherical Cu powder (Osprey). FESEM images. [VII]

On particle impacts, particle deformation is a very crucial factor in order to produce dense coating structures. One important factor is the disruption and removal of continuous oxide layers from the particle surfaces. Adhesion between particles is tighter between metal-metal surfaces compared with the metal-oxide layer surfaces. Thus, metal-metal bonds should be dominant bonding mechanism for dense coatings. Oxide layers are removed from the surfaces in the gas flow, presuming the disruption of the layer. The TEM characterization proves a slight amount of oxygen (by EDS analysis) in some parts of the particle boundaries. However, pure metallic bonding was dominant and hence, the coating structure was tight and dense.

Metal-metal bonding performed tight and adherent particle boundaries. This is due to the localized particle and grain deformation. Adiabatic shear instability due to high contact pressure impact and thermal softening possesses formation of material jets to the connecting points of particle-substrate or particle-particle. In addition, material jets assist in the disruption of oxide layers from initial powder particle surfaces. Furthermore, one way to densify the metallic structure of cold-sprayed coatings was to add hard particles into the metallic powder. Densification was clearly detected both in the HPCS and LPCS coatings. Obviously, bonds

between metallic particles are tighter than metallic-ceramic bonds; however, ceramic particles increase particle deformation of metallic particles by hammering the structure and by activating the sprayed surface. Due to the fact that the amount of ceramic particles is relatively low in the coating in comparison with the initial powder mixture, most of the ceramic particles rebound and do not adhere to the structure and thus, they activate the surface. Furthermore, attached hard particles are stuck to the metallic matrix of the coating. To sum up, low amount of parts of oxide layers and few embedded hard particles do not hinder the impermeability of the coating structure as long as the most dominant particle bonding is metal-metal bonding.

## 7.3 Macroscopic properties of cold-sprayed coatings

Here, mechanical properties, hardness, and bond strength, are presented. These macroscopic properties reflect to deformation level generated during spraying due to work and strain hardening and plastic deformation.

### 7.3.1 Microhardness

Highly deformed and tightly bonded structures of the HPCS Cu and Ta coatings were observed with FESEM and TEM characterizations. In addition to these, a high level of plastic deformation causes work hardening in the coating structure. While, high hardness indicates work hardening. Hardness of the HPCS Ta coating was 230 $HV_{0.3}$ and of Ta bulk material 100 $HV_{0.3}$ [139]. The same trend was detected also with the HPCS Cu compared with the Cu bulk material, 150 $HV_{0.3}$ versus 80 $HV_{0.3}$ [139]. In both coatings, increment of the coatings' hardness was significant, indicating strain hardening and work hardening resulted from plastic deformation. In hardened material, dislocation density increases, making connection between work hardening (increased hardness) and highly deformed microstructure (high dislocation density). [77]

For the HPCS Ni-20Cr coating, hardness was 240 $HV_{0.3}$ and between 320 - 340 $HV_{0.3}$ for the HPCS Ni-20Cr+$Al_2O_3$ coatings [III]. The $Al_2O_3$ particles affected the hardness by increasing its value; this effect arises from hardening and reinforcing by the hard particles. This effect was clearly detected. In hardness measurements, the indentations were taken from the metallic coating areas in order to evaluate the behavior of the metallic Ni-20Cr particles. High hardness of the Ni-20Cr+$Al_2O_3$ coatings can be reflected to their high work hardening level [106]. More hardening (compacting effect of $Al_2O_3$ particles) occurred at higher particle velocities [43] caused by high gas temperature. Comparison of the Ni-20Cr and Ni-20Cr+$Al_2O_3$ coatings revealed that, the $Al_2O_3$ particle addition together with a high gas temperature had a pronounced effect on microstructural properties and on hardness values.

Hardness of the Ni bulk material was 118 $HV_{0.3}$, of Ni-20Cr bulk material 202 $HV_{0.3}$, and of Ni-30Cu bulk material 147 $HV_{0.3}$. In every case, the HPCS coatings have significantly higher hardness, Table 5, compared with corresponding bulk materials, shown above. It should be noticed that the HPCS Ni-20Cr coating had not as high hardness increment than Ni and Ni-20Cu coatings had. However, with hard particle addition, hardness of metallic part increased due to the densifying effect of hard particles by hammering the structure for higher plastic deformation. As detected in the microstructural characterization, the Ni-20Cr coating contained porosity in its structure. In addition, the hardness of Ni and Ni-20Cu coatings was significantly decreased after heat treatment due to the fact that coatings were in a softer state caused by recovery and recrystallization. However, the hardness of Ni-20Cr, Ni-20Cr+50$Al_2O_3$, and Ni-20Cr+30WC-10Co-4Cr coatings were at the same level when comparing the as-sprayed and heat-treated coatings with each other. This is possibly caused by the oxygen content of the coatings resulting in weak points in the particle boundaries. The effect of oxidized areas was probably higher than recovery and thus, hardness was not decreased after heat treatments. Moreover, the hardness of Ni-20Cr with added hard particles was higher than that of pure Ni-20Cr (measurements were done from the metallic part of the coating), indicating the hardening by hard particles.

**Table 5.** Vickers hardness ($HV_{0.3}$) of HPCS Ni, Ni-20Cu, Ni-20Cr, Ni-20Cr+50$Al_2O_3$, and Ni-20Cr+30WC-10Co-4Cr coatings in as-sprayed and heat-treated states. [VI]

| | Vickers hardness $HV_{0.3}$ | |
|---|---|---|
| **Coating** | **As-sprayed** | **Heat-treated** |
| HPCS Ni | 238 | 124 |
| HPCS Ni-20Cu | 266 | 185 |
| HPCS Ni-20Cr | 247 | 308 |
| HPCS Ni-20Cr+50$Al_2O_3$ | 398 | 372 |
| HPCS Ni-20Cr+30WC-10Co-4Cr | 388 | 387 |

The powder type and composition have a strong effect on hardening of the powder particles in the LPCS process, Table 6. It should be noticed that an indentation was taken from a metallic area of the coating in order to analyze the behavior of metallic Cu particles and the effect of $Al_2O_3$ particles on it. The LPCS Cu coating prepared from dendritic Cu (E_Cu) particles has lower hardness than the coating sprayed from spherical Cu (O_Cu) particles. Furthermore, hardness increases with increasing amount of $Al_2O_3$ particle addition, indicating high deformation and thus, higher hardening effect. Denser powder particles with higher primary particle size can explain this effect due to the fact that spherical particles undergo higher level of plastic deformation. Thus, probability to have a lower number of weak particle boundaries is higher due to higher particle size.

**Table 6.** Vickers hardness ($HV_{0.3}$) of LPCS Cu and Cu+$Al_2O_3$ coatings. [VII]

| **Coating** | **Vickers hardness $HV_{0.3}$** |
|---|---|
| E_Cu (dendritic) | 83 |
| E_Cu+10$Al_2O_3$ | 95 |
| E_Cu+30$Al_2O_3$ | 96 |
| E_Cu+50$Al_2O_3$ | 103 |
| O_Cu (spherical) | 106 |
| O_Cu+10$Al_2O_3$ | 113 |
| O_Cu+30$Al_2O_3$ | 127 |
| O_Cu+50$Al_2O_3$ | 127 |

In cold spray processes, powder particles undergo relatively high level of plastic deformation which is reflected to the high hardness values of the coatings. The high hardness is proven with comparison between coatings and bulk materials. Also, the addition of hard particles increases the hardness of the metallic regions of the coatings by hammering and tamping the structure. This effect of hard particles on the hardness and thus, on work hardening and deformation level is clearly observed with all metallic-ceramic mixture coatings independently on the spraying process.

### 7.3.2 Bond strength

The bond strengths (adhesion strengths) of the Ni-20Cr+$Al_2O_3$ coatings were 25 - 38 MPa [III], and for Ni-20Cr, it was 31 MPa [99]. In all cases, failure occurred at the interface between coating and substrate, indicating the adhesive-type bond strengths. Because $Al_2O_3$ particle addition to the metallic Ni-20Cr powder only slightly affected the adhesion strength, it can be concluded that in all cases, with and without the addition of $Al_2O_3$ particles, the adhesion strengths between the Ni-20Cr coatings and substrates were acceptable, indicating a reasonable adhesion between coatings and substrates. Bond strength of HPCS Ni was 20 MPa, of Ni-20Cu, it was 25 MPa, and for Ni-20Cr+30WC-10Co-4Cr coating 32 MPa. In addition, the bond strength of the HPCS Ta coating was 32 MPa [120]. Meanwhile, the bond strengths of the HPCS Cu were 29-36 MPa on Cu substrate [99]. Also these bond strengths are reasonable,

indicating rather good bonding between the coating and substrate. Furthermore, it should be noticed that failure occurred at the coating-substrate interfaces in the HPCS coatings, them being the weakest points in the coating-substrate combination. This indicates higher strength between particles (cohesive strength) than these adhesion strengths.

Bond strengths of the LPCS Cu and Cu+$Al_2O_3$ coatings were also reasonable and increased with the increasing amount of added $Al_2O_3$ particles. In addition, bond strengths of the Cu coatings prepared from spherical particles were higher than those of coatings sprayed with dendritic Cu powder. In addition, bond strengths were cohesive or cohesive/adhesive-type in dendritic coatings, whereas fractures occurred at the coating-substrate interface in the coatings prepared from spherical particles, indicating adhesive-type bond strength. Bond strength of LPCS Cu prepared from dendritic powder was 8 MPa and with 50% $Al_2O_3$ particle addition, 18 MPa. Meanwhile, bond strength of LPCS Cu prepared from spherical powder was 13 MPa and with 50% $Al_2O_3$ particle addition it was 32 MPa. Improvement of adhesion was significant and therefore, bond strengths of Cu+$Al_2O_3$ mixture coatings are reasonable, in the range of 20-30 MPa. [VII] The $Al_2O_3$ particle addition has activation effect, causing cratering of the substrate which in turn, helps to achieve higher adhesion between coating and substrate by increasing the impact surface [91].

## 7.4 Corrosion resistance of cold-sprayed coatings

Denseness is the first criterion for the corrosion resistance of coatings which are nobler than substrate material. In this study, all coating materials (Cu, Ta, Ni, Ni-Cu, and Ni-Cr) are nobler than steel substrate. Denseness means impermeability of the coatings, indicating coating structures without existing through-porosity. Denseness, or on the other hand, existing through-porosity, is identified by using corrosion tests. The open-cell potential measurements and salt spray (fog) tests were chosen for the denseness evaluations. Because coatings used in this study are not corroded by seawater whereas substrate material does [115], the open-cell potential measurements using salt solution and salt spray tests are good methods for testing coating's impermeability. In addition, anodic polarization measurements were carried out in order to indicate corrosion resistance and corrosion properties of the HPCS Ta coatings.

### 7.4.1 Denseness

Open-cell potential measurements show existence of through-porosity in the coating structures. If the open-cell potential value of the coating approaches the value of the corresponding bulk material, it indicates impermeable and dense coating structure. However, if the value of the coating approaches the value of the substrate material (here Fe52), it reflects the through-porosity in the coating structure. In such situation, testing liquid has an open access to penetrate from the surface of the coating to the interface between coating and substrate, it will corrode the substrate, and corrosion products will come up to the surface. Figure 50 indicates overall dense coating structures of the HPCS Cu (-35+15 µm) and Ta coatings, having a similar open-cell potential behavior with corresponding bulk materials. According to microscopic analysis and corrosion tests, the structure of these coatings is fully dense resulting from the optimal combination of powder and spraying parameters. The coatings remained stable in the long-time exposure, indicating their structural durability [V]. In addition, fully dense structures of HPCS Cu coatings prepared from two other powders (-38+11 µm and -30+10 µm) were also verified with open-cell potential measurements in [I]. In addition, salt spray tests showed an overall dense structure of HPCS Ta coating, no changes were detected on the coating surface after 240-h exposure [IV].

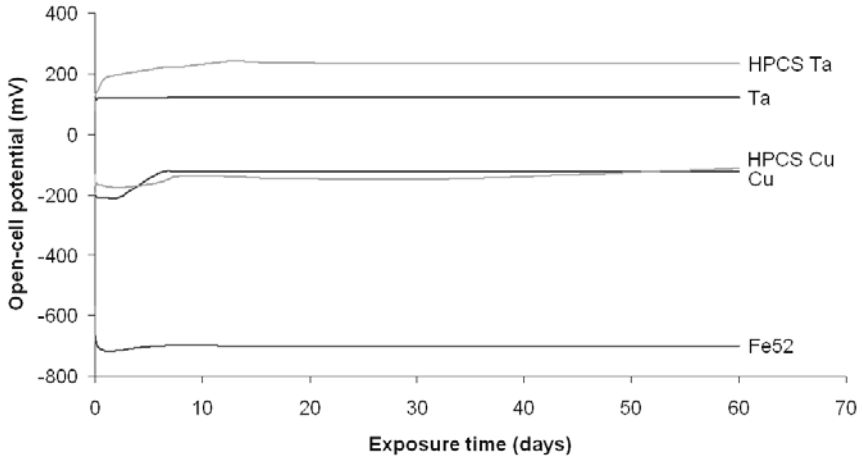


**Figure 50.** Open-cell potentials of HPCS Ta and Cu coatings, Ta and Cu bulk materials and Fe52 substrate material as a function of exposure time in 3.5%NaCl solution. Ag/AgCl reference electrode. [V]

Open-cell potentials of as-sprayed and heat-treated HPCS Ni and Ni-20Cu coatings are also closer to the bulk materials (Ni and Ni-30Cu) than to the substrate material (Fe52), Fig. 51. In addition, the denseness of these coatings was improved with heat treatments, which is also seen in the open-cell potential behavior; values of these coatings are even closer to the bulk materials. Heat treatment densified the coating structures due to recovery, recrystallization, and void reduction by the softening and rearrangement of grains [I, VI]. Number 2 indicates the optimized spraying parameters used. More information about effect of spraying parameters on the denseness of HPCS Ni and Ni-20Cu coatings can be found in [VI]. The denseness of HPCS Ni coatings was improved with right spraying parameters, more details in [VI]. With lower traverse speed together with higher beam distance (distance between two adjacent spray beads), the structure became denser due to the fact that this combination induced high particle deformation and thus, tight particle boundaries (without weak bonds) into the structures. In addition, the denseness improvement of HPCS Ni coating by heat treatment was detected [I].

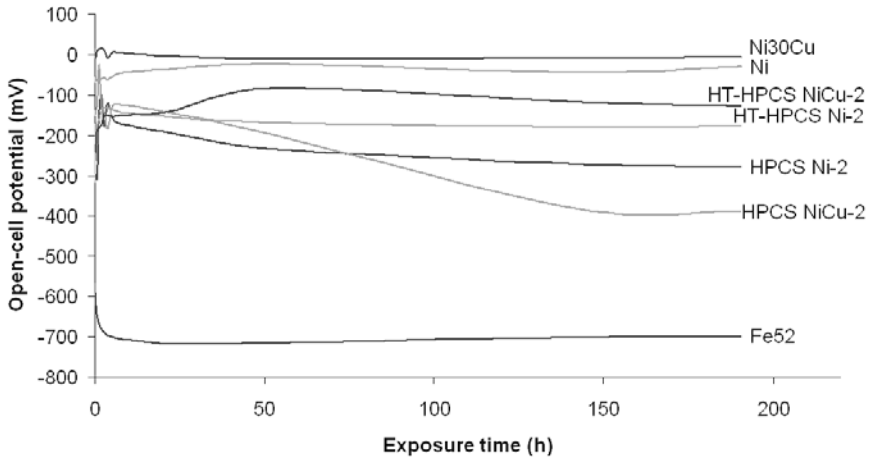


**Figure 51.** Open-cell potentials of as-sprayed and heat-treated HPCS Ni and Ni-20Cu coatings, Ni and Ni-30Cu bulk materials and Fe52 substrate material as a function of exposure time in 3.5%NaCl solution. Ag/AgCl reference electrode. [VI]

Nickel alloy coatings give protection against wet corrosion to steel substrate; however, due to their behavior as nobler material than steel, giving the anodic protection, dense coating structure is required. Figure 52 shows open-cell potentials of HPCS Ni-20Cr, Ni-20Cr+50$Al_2O_3$, and Ni-20Cr+30WC-10Co-4Cr coatings in the as-sprayed and heat-treated state. The HPCS Ni-20Cr coating contained through-porosity. Moreover, heat treatment did not densify the structure

of the Ni-20Cr coating. Their open-cell potentials were close to that of Fe52 substrate material. One way to improve the denseness of the Ni-20Cr coating was to add hard particles into the metallic powder. Addition of $Al_2O_3$ and WC-10Co-4Cr particles showed significant improvement of denseness of the Ni-20Cr coatings. In addition, heat treatment increased the denseness of Ni-20Cr+$Al_2O_3$ coating whereas heat treatment did not affect the denseness of the Ni-20Cr+WC-10Co-4Cr coating, as seen in Fig. 52. [VI] WC-Co-Cr was chosen because of it has better corrosion resistance than WC-Co [140].

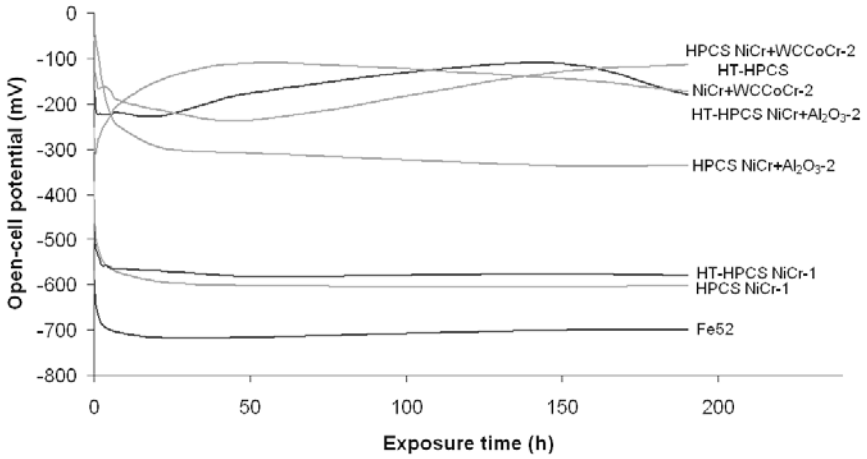


**Figure 52.** Open-cell potentials of as-sprayed and heat-treated HPCS Ni-20Cr+30WC-10Co-4Cr, Ni-20Cr+50$Al_2O_3$ and NiCr coatings and Fe52 substrate material as a function of exposure time in 3.5%NaCl solution. Ag/AgCl reference electrode. [VI]

Salt spray test is the complementary test to evaluate existing through-porosity in the coating structures. As was observed in the open-cell potential measurements [III], Ni-20Cr coating contained through-porosity. On the other hand, densifying effect of $Al_2O_3$ particle addition was noticeable after salt spray test. Figure 53 shows the coating surfaces of Ni-20Cr and Ni-20Cr+50$Al_2O_3$ coatings after 48-h salt spray test [III]. The amount of corrosion spots on the surface was significantly decreased with Ni-20Cr+$Al_2O_3$ mixture coating from 45.5% (Ni-20Cr) to 0.8% (Ni-20Cr+50$Al_2O_3$, -90+45 µm) [III].

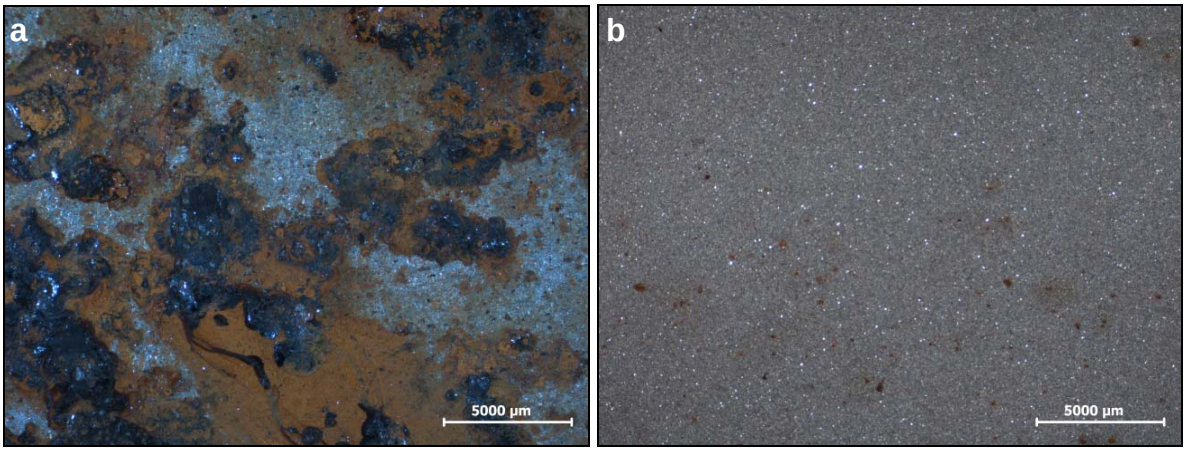


**Figure 53.** Coating surfaces of HPCS a) Ni-20Cr and b) Ni-20Cr+50$Al_2O_3$ coatings after 48-h salt spray test. SM images. [III]

The HPCS Ni coating was dense according to salt spray test, having very low amount of corrosion spots on its surface whereas Ni-20Cu coating became denser after heat treatment. The amounts of corrosion spots on the coating surfaces after 96-h salt spray test by image analysis (ImageJ) are summarized in Table 7. The HPCS Ni-20Cr coating was totally corroded; however, densifing effect of hard particles was clearly observed with $Al_2O_3$ particle addition.

Heat treatment densified the structure of HPCS Ni, Ni-20Cu, and Ni-20Cr+50$Al_2O_3$ coatings which is detected in the amount of corrosion spots on the surfaces after salt spray tests. The HPCS Ni-20Cr coatings contained over-amount defects in their structures and thus, not even heat treatment was able to densify the structure. Heat treatment did not densified the HPCS Ni-20Cr+WC-Co-Cr coatings whereas process parameters had strong influence on denseness of these coatings (is shown in publication VI). The denseness (through-porosity) behavior of HPCS Ni-20Cr+30WC-Co-Cr coatings after heat treatments needs further investigations to explain different behavior compared with Ni-20Cr coatings with the addition of $Al_2O_3$ particles.

**Table 7.** Amount (%) of corrosion spots on the surface of the HPCS Ni, Ni-20Cu, Ni-20Cr, Ni-20Cr+50$Al_2O_3$, and Ni-20Cr+30WC-10Co-4Cr coatings after 96-h salt spray test by image analysis. [VI]

| | Corrosion spots (%) | |
|---|---|---|
| **HPCS coating** | **As-sprayed** | **Heat-treated** |
| Ni | 0.8 | 0.1 |
| Ni-20Cu | 34.7 | 11.3 |
| Ni-20Cr | 98.5 | 98.9 |
| Ni-20Cr+50$Al_2O_3$ | 12.7 | 8.5 |
| Ni-20Cr+30WC-10Co-4Cr | 24.7 | 30.0 |

Summing up, the HPCS Ni coating has a highly dense structure and it was further densified by heat treatments. Also in the case of HPCS Ni-20Cu coating, heat treatment significantly densified the structure. However, the structure still contains some weak points which can be explained by oxidized particle boundaries, in other words, some parts were not deformed enough in order to remove oxide layers from initial powder particles. In spite of that, the denseness improvement was remarkable. In addition, the hard particle addition mixed with Ni-20Cr powder showed notable denseness improvement as analyzed by corrosion tests. [VI]

The open-cell potential measurements and salt spray tests showed that the LPCS Cu and Cu+$Al_2O_3$ coatings contained through-porosity in their structures. Open-cell potentials of the coatings were close to the values of Fe52 substrate material [II, VII]. Regardless, in the LPCS process, powder type and composition had strong influence on the denseness of the Cu and Cu+$Al_2O_3$ coatings. Denseness of the coatings was improved with $Al_2O_3$ particle addition. Table 8 summarizes the amounts of corrosion spots after salt spray test on the coating surfaces analyzed by image analysis (ImageJ). In the E_Cu and E_Cu+$Al_2O_3$ coatings, denritic Cu particles were used, whereas spherical Cu particles were used in O_Cu and O_Cu+$Al_2O_3$ coatings. The LPCS Cu coatings prepared from spherical feedstock had a denser structure compared with coatings prepared from dendritic feedstock. These results indicate that bonds between particles were tighter in these O_Cu coatings than in E_Cu coatings. Moreover, the denseness was improved most with 10 vol.-% $Al_2O_3$ particle addition to the spherical powder and with 30 vol.-% $Al_2O_3$ particle addition to the dendritic powder. This indicates that optimal composition of metallic and ceramic particles in the powder mixture depends on sprayed material combination and powder type of metallic particles.

**Table 8.** Amount (%) of corrosion spots on the surface of the LPCS Cu and Cu+$Al_2O_3$ coatings after 96-h salt spray test by image analysis. [VII]

| Sample | Corrosion spots (%) |
|---|---|
| E_Cu (dendritic) | 94.5 |
| E_Cu+10 vol.%$Al_2O_3$ | 73.0 |
| E_Cu+30 vol.%$Al_2O_3$ | 59.4 |
| E_Cu+50 vol.%$Al_2O_3$ | 68.5 |
| O_Cu (spherical) | 38.9 |
| O_Cu+10 vol.%$Al_2O_3$ | 19.2 |
| O_Cu+30 vol.%$Al_2O_3$ | 32.1 |
| O_Cu+50 vol.%$Al_2O_3$ | 31.3 |

### 7.4.2 Corrosion properties

The anodic polarization measurements were performed in order to characterize the polarization behavior of the HPCS Ta coating in comparison with Ta bulk material. Open-cell potential measurements and salt spray fog tests already confirmed an overall dense structure of the HPCS Ta coating (CS Ta2 [IV]). The CS Ta1 coating with through-porosity was also tested for a comparison between dense coating (CS Ta2) and coating (CS Ta1) with through-porosity. Figure 54 shows polarization behavior in 3.5% NaCl and Fig. 55 in 40%$H_2SO_4$ solutions.

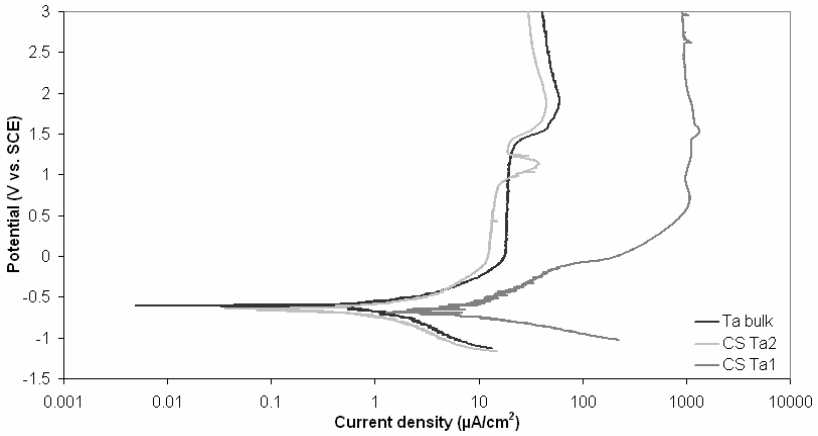


**Figure 54.** Polarization behavior of tantalum bulk material and HPCS Ta coatings in 3.5-wt.% NaCl solution at 22ºC. CS Ta2 is an improved coating and CS Ta1 a standard coating. [IV]

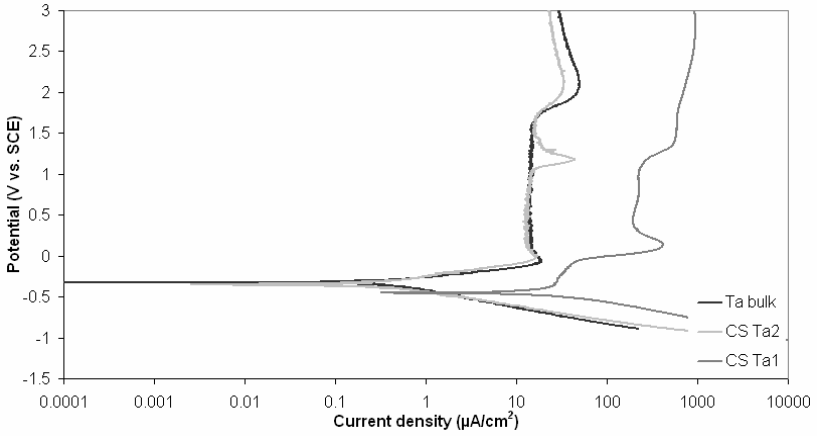


**Figure 55.** Polarization behavior of tantalum bulk material and HPCS Ta coatings in 40-wt.% $H_2SO_4$ solution at 22ºC. CS Ta2 is an improved coating and CS Ta1 a standard coating. [IV]

Tantalum gets passivated rapidly, as shown by its polarization curves in NaCl and $H_2SO_4$ solutions, transforming linearly and quickly from active to passive with increasing potential, indicating material stability. The CS Ta2 coating behaved like the bulk material. However, the CS Ta1 coating did not behave in a stable manner because of its through-porosity. Test solution reacted the steel substrate, thus anodic polarization was resulted from combination of behavior of steel substrate and CS Ta1 coating. This indicates possible instability of the passivation layer and thus, provides poor corrosion protection. Ta bulk material and dense HPCS Ta coating got passivated rapidly, and above their passivation potential, corrosion rate falls to very low value in the passive area due to the stable passive layer [112].

Tafel extrapolation was done to determine the corrosion potential $E_{corr}$, passivation potential $E_{pp}$, corrosion current density $i_{corr}$, and the passivation current density $i_{pp}$ of the tantalum bulk material and the HPCS Ta (CS Ta2) coating in both NaCl and $H_2SO_4$ solutions at 22ºC and at 80ºC. Results are shown in Table 9.

**Table 9.** Corrosion potential $E_{corr}$, corrosion current density $i_{corr}$, passivation potential $E_{pp}$, and passivation current density $i_{pp}$ of tantalum bulk material and CS coatings in 3.5-wt.% NaCl and 40-wt.% $H_2SO_4$ solutions analyzed by Tafel extrapolation. [IV]

| Sample | Solution | T (ºC) | $E_{corr}$ (V) | $i_{corr}$ (μA/cm$^2$) | $E_{pp}$ (V) | $i_{pp}$ (μA/cm$^2$) |
|---|---|---|---|---|---|---|
| Ta bulk | NaCl | 22 | -0.66 | 1.1 | 0 | 16 |
| HPCS Ta | NaCl | 22 | -0.67 | 1.1 | 0.05 | 11 |
| Ta bulk | NaCl | 80 | -0.68 | 0.5 | -0.25 | 20 |
| HPCS Ta | NaCl | 80 | -0.66 | 0.6 | 0.05 | 13 |
| Ta bulk | $H_2SO_4$ | 22 | -0.32 | 0.4 | 0.08 | 12 |
| HPCS Ta | $H_2SO_4$ | 22 | -0.33 | 0.3 | 0.10 | 12 |
| Ta bulk | $H_2SO_4$ | 80 | -0.34 | 0.8 | 0.04 | 15 |
| HPCS Ta | $H_2SO_4$ | 80 | -0.30 | 2.0 | 0.05 | 15 |

The HPCS Ta coating, prepared from improved powder with advanced spraying equipment, behaved like bulk tantalum, indicating resistance to corrosion. The HPCS Ta coating and bulk material showed wide-ranging passivation, characteristic of stable passive behavior [141]. According to the polarization curves in both NaCl and $H_2SO_4$ solutions at room temperature and elevated temperature, the passivation of dense HPCS Ta coating was first linear, then curving slightly (possibly because of pit corrosion), followed by another stretch of linear passivation at higher potential (passive layer formation). This is due to the materials' ability to be repassivated. A pit may result from a failure in the passive layer [112,115], but when pits are insignificant, reparation or repassivation and thus, re-protection may occur in the protective passive layer [115]. At a high potential of about 1.2 V, coating (CS Ta2) showed unstable passivation; however, at an even higher potential the coating got repassivated. Balani et al. [37] have reported similar repassivation of cold-sprayed aluminum coatings. In fact, pitting corrosion may occur also in a transpassive area [141], and impurities may cause breaks in the passive layer [113]. With some metals, passivation depends on pH and the potential [113], but the highly protective oxide layer of tantalum remains stable at all pH and potential values [112].

In summary, overall and fully dense and impermeable Ta coatings can be produced by using the HPCS system. This will be a major advantage for corrosion resistance. The HPCS Ta coatings act like real corrosion barrier coatings and can thus, be used in applications where corrosion protection is needed.

# 8 CONCLUDING REMARKS AND SUGGESTIONS FOR FUTURE WORK

Cold spraying enables the production of overall dense coatings with porosity-free and pure (without oxidation) coating structures. Cold-sprayed coatings with impermeable structures have high potential to be used in corrosion protection. In this work, denseness improvement was performed in three ways: 1) by optimized powder-spraying parameters combination (Cu, Ta, Ni), 2) by adding hard particles to metallic powder (Ni-20Cr+$Al_2O_3$, Ni-20Cr+WC-10Co-4Cr, Cu+$Al_2O_3$), and 3) by heat treatments (Ni-20Cu). High plastic deformation together with metal-metal bonding is required for the denseness of cold-sprayed coatings. Although structure appears dense by microscopic evaluation, corrosion tests reveal impermeability, showing the existence/absence of through-porosity. Impermeability of the coatings is crucial and therefore, it could be said that microstructure defines corrosion protection capability of the cold-sprayed coatings. As a conclusion, cold-sprayed coatings have dense structures, high hardness due to the work hardening and reasonable bond strengths. Furthermore, it is worth noticing that hard particle addition affects in addition to structure, also the mechanical properties by increasing hardness of the metallic parts of the coatings and by improving bond strengths.

1) Optimized powder-spraying parameters combination

The HPCS Cu and Ta coatings possessed fully dense and overall impermeable coating structures according to both microstructural characterization and corrosion tests. In addition, the HPCS Ni coating had a dense structure. These are significant advantages, having possibility to use them in applications where corrosion resistance is needed. Powder characteristics had a very strong influence on the coating formation and hence, on the coating structure. The overall dense coating structure requires high level of plastic deformation, adiabatic shear instability conditions on the impacts and thus, material jet formation. In addition, tight bonds between particles and metal-metal bonding are required for the production of dense coatings and furthermore, acting as real corrosion barrier coatings. The optimal combination is material-dependent and process-dependent and it should be optimized separately for each case depending on the desired properties and functions of the coatings. In addition to the corrosion protectiveness, HPCS Ta coating behaved like the tantalum bulk material in the anodic polarization tests with rapid passivation and high passivation range, indicative of its corrosion resistance. Generally, Ta is typically used when extreme corrosion resistance is required and for that, denseness of the coatings is the first criterion for real corrosion protection. Therefore, it can be said that high-pressure cold spraying proves its potential in the production of uniformly dense and corrosion protective coatings. On the other hand, cold-sprayed Cu coatings are typically used in applications where electrical or thermal conductivity is needed. For applications of this kind, high purity and denseness of the coatings are advantageous properties.

Due to the fact that coating properties, especially denseness, depend strongly on powders and process parameters, the further development will focus on continuing optimization. The key words in future work are tailored powders with advanced methods. The powder development is going towards high purity and narrow particle size distribution whereas the development of the process itself is going towards even higher process temperatures and effectiveness (e.g., the latest development stage: Kinetiks 8000 with 1000ºC preheating temperature of $N_2$ [136]). Future work will concentrate on finding new materials and powders from which it is possible to produce fully dense cold-sprayed coatings with the optimal powder-spraying parameters combinations. In addition, the corrosion research of the cold-sprayed coatings and testing with more aggressive environments would be one of next steps.

2) Hard particle addition

The structures of the HPCS Ni-20Cr coatings showed prevalent through-porosity, as demonstrated by corrosion tests. The solution for that was to add hard particles into the Ni-20Cr powder. The hard particle addition ($Al_2O_3$ and WC-10Co-4Cr particles) into the metallic powder showed significant denseness improvement. Generally, the composition of the powder depends on the desired properties required for the coating. Addition of ceramic particles affected the properties of the coating deposited by HPCS process. On the other hand, $Al_2O_3$ particles mixed with metal alloy powder also had a spraying technical effect on the process parameters, enabling the use of higher gas temperatures without nozzle clogging. Hard particle addition has three functions: 1) to keep the nozzle clean, 2) to activate the sprayed surface, and 3) to reinforce the sprayed coating structure. Moreover, it was found that $Al_2O_3$ particles embedded into the structure of Ni-20Cr coatings whereas WC-Co-Cr particles broke down and stuck into the structure. However, both particle additions made the structure of the HPCS Ni-20Cr coating denser due to the fact that higher gas temperature could be used and due to the hammering and tamping the coating structure.

The LPCS process is a relevant method of preparing Cu and Cu+$Al_2O_3$ coatings. Also in here, powder characteristics and compositions affected the denseness. LPCS Cu and Cu+$Al_2O_3$ coatings prepared from spherical Cu particles contained less through-porosity in their structures compared with coatings prepared from dendritic particles, indicating denser coating structures. The dendritic particles have more boundaries in their structures, increasing the probability of weak bonds between the particles. Denser powder particles with higher primary particle size can be explained with the higher level of plastic deformation of the spherical particles. Thus, probability to have a lower number of weak particle boundaries is higher due to higher particle size. Moreover, it was also possible to produce pure Cu coatings from both spherical and dendritic feedstock by using the LPCS process. All in all, with the hard particle addition coating quality can be improved. This work clearly showed more deformed and denser coating structure of the LPCS Cu+$Al_2O_3$ coatings compared with the LPCS Cu coatings.

As stated, it is not always possible to manufacture overall dense microstructures of pure metallic coatings by using cold spraying. One solution to improve denseness is to add hard particles or to use powder mixtures in order to improve the quality of the coatings. In future, research will focus on finding new material compositions and powder mixtures for the production of composite coatings with optimal properties. In addition, powder and material mixing can open new possibilities with combined properties from all components.

3) Heat treatments

Cold spraying has proven to be an optimal thermal spray method in order to prepare fully dense or low-porosity coatings from metallic or metallic-ceramic composite mixture powder feedstock. In an optimal situation, fully dense coating structures can be manufactured with the optimal combination of powder and spraying parameters. In the contrast to this, if the optimal combination is not achieved, structural details could be improved with post-treatments. Denseness of HPCS Ni and Ni-20Cu coatings was improved with heat treatments. Heat-treated Ni and Ni-20Cu coatings were in a softer state due to void reduction, recovery and recrystallization. In addition, the degree of through-porosity was significantly reduced after heat treatments. Densification and denseness improvement by heat treatments were illustrated with the corrosion tests. Next, a possibility to improve the denseness of LPCS coatings with heat treatments will be investigated.

## REFERENCES


[1] V. Champagne, Ed., 2007, *The Cold Spray Materials Deposition Process: Fundamentals and Applications*, Woodhead Publishing Ltd., Cambridge, England, 362 p

[2] A. Papyrin, V. Kosarev, S. Klinkov, A. Alkimov, V. Fomin, 2007 *Cold Spray Technology*, 1st ed., Elsevier, printed in the Netherlands, 328 p

[3] M. Grujicic, C. Zhao, C. Tong, W. DeRosset, D. Helfritch, Analysis of the impact velocity of powder particles in the cold-gas dynamic-spray process, *Mat. Sci. Eng. A*, 368, 2004, p 222-230

[4] R. Dykhuizen, M. Smith, Gas Dynamic Principles of Cold Spray, *J. Therm. Spray Technol.*, 7(2), 1998, p 205- 212

[5] C. Borchers, F. Gärtner, T. Stoltenhoff, H. Assadi, H. Kreye, Microstructural and Macroscopic Properties of Cold Sprayed Copper Coatings, *J. Appl. Phys.*, 93(12), 2003, p 10064-10070

[6] R. Maev, V. Leshchynsky, Air Gas Dynamic Spraying of Powder Mixtures: Theory and Application, *J. Therm. Spray Technol.*, 15(2), 2006, p 198-205

[7] T. Van Steenkiste, J. Smith, R. Teets, J. Moleski, D. Gorkiewicz, R. Tison, D. Marantz, K. Kowalsky, W. Riggs, II, P. Zajchowski, B. Pilsner, R. McCune, K. Barnett, Kinetic spray coatings, *Surf. Coat. Technol.*, 111, 1999, p 62-71

[8] V. Sobolev, J. Guilemany, J. Nutting, 2004, *High Velocity Oxy-Fuel Spraying, Theory, Structure-Property Relationships and Applications*, Maney Publishing, London, UK, 397 p

[9] T. Stoltenhoff, H. Kreye, H. Richter, An Analysis of the Cold Spray Process and its Coatings, *J. Therm. Spray Technol.*, 11(4), 2001, p 542-550

[10] Cordon England, website, http://www.gordonengland.co.uk/tsc.htm, referred 2009.

[11] L. Pawlowski, 1995, *The Science and Engineering of Thermal Spray Coatings*, John Wiley & Sons Ltd., New York, USA, 414 p

[12] S. Veräjänkorva, J. Lagerbom, P. Vuoristo, Influence of Powder Type and Properties on Ceramic Layer Deposition by Cold Spraying, *Thermal Spray 2006: Building on 100 Years of Success*, B. Marple, M. Hyland, Y.-C. Lau, R. Lima, J. Voyer (Eds.), May 15-18 (Seattle, Washington, USA), ASM International, 6 p

[13] J. Vlcek, L. Gimeno, H. Huber, A Systematic Approach to Material Eligibility for the Cold Spray Process, *Thermal Spray 2003: Advancing the Science & Applying the Technology*, C. Moreau, B. Marple (Eds.), May 5-8, (Orlando, Florida; USA), ASM International, p 37-44

[14] H.-Y. Lee, Y-H. Yu, Y.-C. Lee, Y.-P. Hong, K.-H. Ko, Interfacial studies between cold-sprayed $WO_3$, $Y_2O_3$ films and Si substrate, *Appl. Surf. Sci.*, 227, 2004, p 244-249

[15] C.-J. Li, G.-J. Yang, X.-C. Huang, W.-Y. Li, A. Ohmori, Formation of $TiO_2$ photocatalyst through cold spraying, *Thermal Spray 2004: Advances in Technology and Application*, May 10-12 (Osaka, Japan), ASM International

[16] Y. Ichikawa, K. Sakaguchi, K. Ogawa, T. Shoji, S. Barradas, M. Jeandin, M. Boustie, Deposition Mechanisms of Cold Gas Dynamic Sprayed MCrAlY Coatings, *Thermal Spray 2007: Global Coating Solutions*, B. Marple, M. Hyland, Y. Lau, C.-J. Li, R. Lima, G. Montavon (Eds.), May 14-16 (Beijing, China), ASM International, p 54-59

[17] R. Maev, V. Leshchynsky, 2008, *Introduction to Low Pressure Gas Dynamic Spray, Physics & Technology*, Wiley-VCH Verlag GmbH&Co, KGaA, Weinheim, Germany, 328 p

[18] A. Rezaeain, R. Chromik, S. Yue, E. Irissou, J.-G. Legoux, Characterization of cold-sprayed Ni, Ti and Cu coating properties for their optimizations, *Thermal Spray 2008: Thermal Spray Crossing Borders*, E. Lugscheider (Ed.), June 2-4 (Maastricht, The Netherlands), DVS, p 854-860

[19] L. Pawlowski, 2008, *The Science and Engineering of Thermal Spray Coatings*, 2nd edition, John Wiley & Sons Ltd., New York, USA, 656 p

[20] J. Davis (Ed.), 2004, *Handbook of Thermal Spray Technology*, ASM International, printed in the United States of America, 346 p

[21] A. Alkhimov, A. Papyrin, V. Kosarev, N. Nesterovich, M. Shushpanov, Gas-Dynamic Spray Method for Applying a Coating, U.S. Patent 5 302 414, 12 April 1994

[22] A. Alkhimov, A. Papyrin, V. Kosarev, N. Nesterovich, M. Shushpanov, Method and Device for Coating, European Patent 0 484 533 B1, 25 January 1995

[23] T. Van Steenkiste, J. Smith, R. Teets, Aluminum Coatings via Kinetic Spray with Relatively Large Powder Particles, *Surf. Coat. Technol.*, 154, 2002, p 237-252

[24] T. Schmidt, F. Gärtner, H. Assadi, H. Kreye, Development of a generalized parameter window for cold spray deposition, *Acta Mater.*, 54, 2006, p 729-742

[25] C.-J. Li, W.-Y. Li, Examination of the critical velocity for deposition of particles in cold spraying, *Thermal Spray 2005: Explore its surfacing potential!*, ASM International, May 2-4, 2005 (Basel, Switzerland), ASM International, p 217-224

[26] C. Borchers, F. Gärtner, T. Stoltenhoff, H. Kreye, Formation of persistent dislocation loops by ultra-high strain-rate deformation during cold spraying, *Acta Mater.*, 53, 2005, p 2991-3000

[27] B. Jodoin, Effects of Shock Waves on Impact Velocity of Cold Spray Particles, *Thermal Spray 2001: New Surfaces for a New Millennium*, C. Berndt, K. Khor, E. Lugscheider (Eds.), May 28-30 (Singapore), ASM International, p 399-407

[28] J. Pattison, S. Celotto, A. Khan, W. O'Neill, Standoff distance and bow shock phenomena in the Cold Spray process, *Surf. Coat. Technol.*, 202, 2008, p 1443-1454

[29] D. Helfritch, V. Champagne, Optimal Particle Size for the Cold Spray Process, *Thermal Spray 2006: Building on 100 Years of Success*, B. Marple, M. Hyland, Y.-C. Lau, R. Lima, J. Voyer (Eds.), May 15-18 (Seattle, Washington, USA), ASM International

[30] M. Grujicic, C.L. Zhao, W.S. DeRosset, D. Helfritch, Adiabatic shear instability based mechanism for particles/substrate bonding in the cold-gas dynamic-spray process, *Mater. Design*, 25, 2004, p 681-688

[31] H. Assadi, F. Gärtner, T. Stoltenhoff, H. Kreye, Bonding mechanism in cold gas spraying, *Acta Mater.*, 51, 2003, p 4379-4394

[32] P. Richter, H. Höll, Latest Technology for Commercially Available Cold Spray Systems, *Thermal Spray 2006: Building on 100 Years of Success*, B. Marple, M. Hyland, Y.-C. Lau, R. Lima, J. Voyer (Eds.), May 15-18 (Seattle, Washington, USA), ASM International

[33] T. Van Steenkiste, D. Gorkiewicz, Analysis of Tantalum Coatings Produced by the Kinetic Spray Process, *J. Therm. Spray Technol.*, 13(2), 2004, p 265-273

[34] T. Price, P. Shipway, D. McCartney, E. Calla, D. Zhang, A Method for Characterizing the Degree of Inter-particle Bond Formation in Cold Sprayed Coatings, *J. Therm. Spray Technol.*, 16(4), 2007, p 566-570

[35] E. Calla, D. McGartney, P. Shipway, Effect of Heat Treatment on the Structure and Properties of Cold Sprayed Copper, *Thermal Spray 2005: Explore its surfacing potential!*, , May 2-4 (Basel, Switzerland), ASM International

[36] T. Schmidt, F. Gärtner, H. Kreye, High Strain Rate Deformation Phenomena in Explosive Powder Compaction and Cold Gas Spraying, *Thermal Spray 2003: Advancing the Science & Applying the Technology*, C. Moreau, B. Marple (Eds.), May 5-8 (Orlando, Florida, USA), ASM International, p 9-18

[37] K. Balani, T. Laha, A. Agarwal, J. Karthikeyan, N. Munroe, Effect of Carrier Gases on Microstructural and Electrochemical Behavior of Cold-sprayed 1100 Aluminum Coating, *Surf. Coat. Technol.*, 195, 2005, p 272-279

[38] F. Gärtner, C. Borchers, T. Stoltenhoff, H. Kreye, H. Assadi, Numerical and Microstructural Investigations of the Bonding Mechanisms in Cold Spraying, *Thermal Spray 2003: Advancing the Science & Applying the Technology*, C. Moreau, B. Marple (Eds.), May 5-8 (Orlando, Florida, USA), ASM International, p 1-8

[39] S. Shin, S. Yoon, Y. Kim, C. Lee, Effect of particle parameters on the deposition characteristics of a hard/soft-particles composite in kinetic spraying, *Surf. Coat. Technol.*, 201, 2006, p 3457-3461

[40] T. Schmidt, H. Assadi, F. Gärtner, H. Richter, T. Stoltenhoff, H. Kreye, T. Klassen, From Particle Acceleration to Impact and Bonding in Cold Spraying, *J. Therm. Spray Technol.*, 18(5-6), 2009, p 794-808

[41] H. Kreye, T. Schmidt, F. Gärtner, T. Stoltenhoff, The Cold Spray Process and Its Optimization, *Thermal Spray 2006: Building on 100 Years of Success*, B. Marple, M. Hyland, Y.-C. Lau, R. Lima, J. Voyer (Eds.), May 15-18 (Seattle, Washington, USA), ASM International

[42] F. Gärtner, T. Stoltenhoff, T. Schmidt, H. Kreye, The Cold Spray Process and Its Potential for Industrial Applications, *J. Therm. Spray Technol.*, 15(2), 2006, p 223-232

[43] T. Schmidt, F. Gärtner, H. Kreye, New Developments in Cold Spray Based on Higher Gas- and Particle Temperatures, *J. Therm. Spray Technol.*, 15(4), 2006, p 488-494

[44] K. Sakaki, T. Tajima, H. Li, S. Shinkai, Y. Shimizu, Influence of Substrate Conditions and Traverse Speed on Cold Sprayed Coatings, *Thermal Spray 2004: Advances in Technology and Application*, May 10-12 (Osaka, Japan), ASM International

[45] J. Legoux, E. Irissou, C. Moreau, Effect of Substrate Temperature on the Formation Mechanism of Cold Sprayed Aluminum, Zinc and Tin Coatings, *Thermal Spray 2007: Global Coating Solutions*, B. Marple, M. Hyland, Y. Lau, C.-J. Li, R. Lima, G. Montavon (Eds.), May 14-16 (Beijing, China), ASM International, p 48-53

[46] Ktech Corp. website, http://www.ktech.com/Advanced_Manufacturing/Design_Build/Cold_Spray_System.html, referred 2009.

[47] http://www.cmit.csiro.au/innovation/2003-08/cold_spray.cfm, referred 2004.

[48] A. Kashirin, O. Klyuev, T. Buzdygar, A. Shkodkin, DYMET Technology Evolution and Application, *Thermal Spray 2007: Global Coating Solutions*, B. Marple, M. Hyland, Y. Lau, C.-J. Li, R. Lima, G. Montavon (Eds.), May 14-16 (Beijing, China), ASM International, p 141-145

[49] B. Djordjevic, R. Maev, SIMAT™ Application for Aerospace Corrosion Protection and Structural Repair, *Thermal Spray 2006: Building on 100 Years of Success*, B. Marple, M. Hyland, Y.-C. Lau, R. Lima, J. Voyer (Eds.), May 15-18 (Seattle, Washington, USA), ASM International

[50] A. Sova, A. Papyrin, I. Smurov, Influence of Ceramic Powder Size on Process of Cermet Coating Formation by Cold Spray, *J. Therm. Spray Technol.*, 18(4), 2009, p 633-641

[51] A. Shkodkin, A. Kashirin, O. Klyuev, T. Buzdygar, The Basic Principles of DYMET Technology, *Thermal Spray 2006: Building on 100 Years of Success*, B. Marple, M. Hyland, Y.-C. Lau, R. Lima, J. Voyer (Eds.), May 15-18 (Seattle, Washington, USA), ASM International

[52] A. Shkodkin, A. Kashirin, Determination of the parameters of the process of gas-dynamic deposition of metallic coatings, *Weld. Internat.*, 20(2), 2006, p 161-164

[53] J. Karthikeyan, T. Laha, A. Agarwal, N. Munroe, Microstructural and Electrochemical Characterization of Cold-Sprayed 1100 Aluminum Coating, *Thermal Spray 2004: Advances in Technology and Application*, May 10-12 (Osaka, Japan), ASM International

[54] H. Weinert, E. Maeva, E. Leshchynsky, Low Pressure Gas Dynamic Spray Forming Near-net Shape Parts, *Thermal Spray 2006: Building on 100 Years of Success*, B. Marple, M. Hyland, Y.-C. Lau, R. Lima, J. Voyer (Eds.), May 15-18 (Seattle, Washington, USA), ASM International

[55] A. Papyrin, V. Kosarev, S. Klinkov, A. Sova, I. Smurov, P. Bertrand, Investigation of composites: metal - ceramics and metal - metal coatings produced with cold spray equipment with ejector, *Thermal Spray 2008: Thermal Spray Crossing Borders*, E. Lugscheider (Ed.), June 2-4 (Maastricht, The Netherlands), DVS, p 611-615

[56] Obninsk Center for Powder Spraying (OCPS, Russia) website, http://dymet.amazonit.ru/eindex.html, referred 2009.

[57] S. Klinkov, V. Kosarev, M. Rein, Cold spray deposition: Significance of particle impact phenomena, *Aerospace Sci. Technol.*, 9, 2005, p 582-591

[58] A. Papyrin, S. Klinkov, V. Kosarev, Effect of the substrate surface activation on the process of cold spray coating formation, *Thermal Spray 2005: Explore its surfacing potential!*, May 2-4 (Basel, Switzerland), ASM International, p 145-150

[59] T. Schmidt, Kaltgasspritzen, Eine Analyse des Materialverhaltens beim Partikelaufprall und die daraus abgeleitete Prozessoptimierung, Werkstofftechnik, Shaker Verlag, Hamburg, Germany, 2007, in Germany

[60] H. Katanoda, M. Fukuhara, N. Iino, Numerical Study of Combination Parameters for Particle Impact Velocity and Temperature in Cold Spray, *J. Therm. Spray Technol.*, 16(5-6), 2007, p 627-633

[61] A. Papyrin, S. Klinkov, V. Kosarev, Modelling of particle-substrate adhesive interaction under the cold spray process, *Thermal Spray 2003: Advancing the Science & Applying the Technology*, C. Moreau, B. Marple (Eds.), May 5-8 (Orlando, Florida, USA), ASM International, p. 27-?

[62] F. Raletz, M. Vardelle, G. Ezo'o, Critical particle velocity under cold spray conditions, *Surf. Coat. Technol.*, 201, 2006, p 1942-1947

[63] K. Kang, S. Yoon, Y. Ji, C. Lee, Oxidation Effects on the Critical Velocity of Pure Al Feedstock Deposition in the Kinetic Spraying Process, *Thermal Spray 2007: Global Coating Solutions*, B. Marple, M. Hyland, Y. Lau, C.-J. Li, R. Lima, G. Montavon (Eds.), May 14-16 (Beijing, China), ASM International, p 66-71

[64] V. Kosarev, S. Klinkov, A. Alkhimov, A. Papyrin, On Some Aspects of Gas Dynamics of the Cold Spray Process, *J. Therm. Spray Technol.*, 12(2), 2003, p 265-281

[65] T. Han, Z. Zhao, B. Gillispie, J. Smith, A fundamental study of the kinetic spray process, *Thermal Spray 2004: Advances in Technology and Application*, May 10-12 (Osaka, Japan), ASM International

[66] A. Alkhimov, V. Kosarev, S. Klinkov, The Features of Cold Spray Nozzle Design, *J. Therm. Spray Technol.*, 10(2), 2001, p 375-381

[67] M. Meyers, Plasticity: Adiabatic Shear Localization, *Encyclop. Mat.: Sci. Technol.*, p 7093-7103

[68] B. Jodoin, L. Ajdelsztajn, E. Sansoucy, A.Zúñiga, P. Richter, E. Lavernia, Effect of particle size, morphology, and hardness on cold gas dynamic sprayed aluminum alloy coatings, *Surf. Coat. Technol.*, 201, 2006, p 3422-3429

[69] H. Fukanuma, N. Ohno, B. Sun, R. Huang, The Influence of Particle Morphology on In-flight Particle Velocity in Cold Spray, *Thermal Spray 2006: Building on 100 Years of Success*, B. Marple, M. Hyland, Y.-C. Lau, R. Lima, J. Voyer (Eds.), May 15-18 (Seattle, Washington, USA), ASM International

[70] A. Alkhimov, S. Klinkov, V. Kosarev, Experimental Study of Deformation and Attachment of Microparticles to an Obstacle upon High-Rate Impact, *J. Appl. Mech. Techn. Phys.*, 41(2), 2000, p 245-250

[71] X.-J. Ning, X-J., J.-H. Jang, H.-J. Kim, C.-J. Li, C. Lee, Cold Spraying of Al-Sn Binary Alloy: Coating Characteristics and Particle Bonding Features, *Surf. Coat. Technol.*, 202(9), 2008, p 1681-1687

[72] T. Kairet, A contribution to the study of cold gas dynamic spraying of copper: Influence of the powder characteristics on the mechanical properties of the coating, Doctoral Thesis, Université Libre de Bruxelles, Belgium, 2007

[73] P. Sudharshan Phani, D. Srinivasa Rao, S. Joshl, G. Sundararajan, Effect of Process Parameters and Heat Treatments on Properties of Cold Sprayed Copper Coatings, *J. Therm. Spray Technol.*, 16(3), 2007, p 425-434

[74] S. Zumdahl, 1998, *Chemical Principles*, 3rd ed., Houghton Mifflin Company, Boston, New York, USA, 1040 p

[75] X.-J. Ning, J.-H. Jang, H.-J. Kim, The Effects of Powder Properties on In-Flight Particle Velocity and Deposition Process during Low Pressure Cold Spray Process, *Appl. Surf. Sci.*, 253(18), 2007, p 7449-7455

[76] T. Kairet, G. Di Stefano, M. Degrez, F. Campana, J.-P. Janssen, Comparison Between Coatings from two Different Copper Powders: Mechanical Properties, Hardness and Bond

Strength, *Thermal Spray 2006: Building on 100 Years of Success*, B. Marple, M. Hyland, Y.-C. Lau, R. Lima, J. Voyer (Eds.), May 15-18 (Seattle, Washington, USA), ASM International

[77] W. Callister, Jr., 2000, *Materials science and engineering, an introduction*, 5th ed., John Wiley &Sons Inc., printed in United State of America, 871 p

[78] ASM Metals Handbook, Vol. 14A, Metalworking: Bulk Forming, Plastic Deformation Structures, Plastic Deformation in Crystals, ASM international, 2005, p 539-551

[79] T. H. Courtney, 2000, *Mechanical Behavior of Materials*, McGrae-Hill Publishing Company, 2nd ed., (Singapore), 733 p

[80] F. Gärtner, T. Stoltenhoff, J. Voyer, H. Kreye, S. Riekehr, M. Kocak, Mechanical properties of cold-sprayed and thermally sprayed copper coatings, *Surf. Coat. Technol.*, 200, 2006, p 6770-6782

[81] D. Zhang, P. Shipway, D. McCartney, Particle-Substrate Interactions in Cold Gas Dynamic Spraying, *Thermal Spray 2003: Advancing the Science & Applying the Technology*, C. Moreau, B. Marple (Eds.), May 5-8 (Orlando, Florida, USA), ASM International, p 45-52

[82] M. Grujicic, J. Saylor, D. Beasley, W. DeRosset, D. Helfritch, Computational analysis of the interfacial bonding between feed-powder particles and the substrate in the cold-gas dynamic-spray process, *Appl. Surf. Sci.*, 219, 2003, p 211-227

[83] T. Stoltenhoff, C. Borchers, F. Gärtner, H. Kreye, Microstructures and key properties of cold-sprayed and thermally sprayed copper coatings, *Surf. Coat. Technol.*, 200, 2006, p 4947-4960

[84] P. Richter, A.Zúñiga, M. Yandouzi, B. Jodoin, CoNiCrAlY microstructural changes induced during Cold Gas Dynamic Spraying, *Surf. Coat. Technol.*, 203(3-4), 2008, p 364-371

[85] L. Ajdelsztajn, B. Jodoin, J. Schoenung, Synthesis and mechanical properties of nanocrystallize Ni coatings produced by cold gas dynamic spraying, *Surf. Coat. Technol.*, 201(3-4), 2006, p 1166-1172

[86] M. Fukumoto, M. Mashiko, M. Yamada, E. Yamaguchi, Deposition Behavior of Copper Particles onto Flat Substrate Surface in Cold Spraying, *Thermal Spray 2009: Expanding Thermal Spray Performance to New Markets and Applications*, B. Marple, M. Hyland, Y.-C. Lau, C.-J. Li, R. Lima, G. Montavon (Eds.), May 4-7 (Las Vegas, Nevada, USA), ASM International, p 273-278

[87] S. Klinkov, V. Kosarev, A. Sova, I. Smurov, Calculation of Particle Parameters for Cold Spray Spraying of Metal-Ceramic Mixtures, *J. Therm. Spray Technol.*, 18(5-6), 2009, p 944-956

[88] W.-Y. Li, C. Zhang, X. Guo, C.-J. Li, H. Liao, C. Coddet, Study on impact fusion at particle interfaces and its effect on coating microstructure in cold spraying, *Appl. Surf. Sci.*, 254, 2007, p 517-526

[89] T. Hussain, D. McCartney, P. Shipway, D. Zhang, Bonding Mechanisms in Cold Spraying: The Contributions of Metallurgical and Mechanical Components, *J. Therm. Spray Technol.*, 18(3), 2009, p 364-379

[90] S. Guetta, M. Berger, F. Borit, V. Guipont, M. Jeandin, M. Boustie, Y. Ichikawa, K. Sakaguchi, K. Ogawa, Influence of Particle Velocity on Adhesion of Cold-Sprayed Splats, *J. Therm. Spray Technol.*, 18(3), 2009, p 331-342

[91] H. Lee, S. Jung, S. Lee, Y. You, K. Ko, Correlation between $Al_2O_3$ particles and interface of Al-$Al_2O_3$ coatings by cold spray, *Appl. Surf. Sci.*, 252, 2005, p 1891-1898

[92] H. Lee, Y. Yu, Y. Lee, Y. Hong, K. Ko, Cold Spray of SiC and $Al_2O_3$ With Soft Metal Incorporation: A Technical Contribution, *J. Therm. Spray Technol.*, 13(2), 2004, p 184-189

[93] R. Lima, J. Karthikeyan, C. Kay, J. Lindemann, C. Berndt, Microstructural characteristics of cold-sprayed nanostructured WC-Co coatings, *Thin Solid Films*, 416, 2002, p 129-135

[94] H.-J. Kim, C.-H. Lee, S.-Y. Hwang, Fabrication of WC-Co coatings by cold spray deposition, *Surf. Coat. Technol.*, 191, 2005, p 335-340

[95] R. McCune, W. Donlon, O. Popoola, E. Cartwright, Characterization of Copper Layers Produced by Cold Gas-Dynamic Spraying, *J. Therm. Spray Technol.*, 9(1), 2000, p 73-82

[96] E. Irissou, J.-G. Legoux, B. Arsenault, C. Moreau, Investigation of Al-$Al_2O_3$ Cold Spray Coating Formation and Properties, *J. Therm. Spray Technol.*, 16(5-6), 2007, p 661-668

[97] R. Maev, V. Leshchynsky, A. Papyrin, Structure Formation of Ni-based Composite Coatings during Low Pressure Gas Dynamic Spraying, *Thermal Spray 2006: Building on 100 Years Success*, B. Marple, M. Hyland, Y. Lau, R. Lima, J. Voyer (Eds.), May 15-18 (Seattle, Washington, USA), ASM International

[98] Y. Zou, W. Qin, E. Irissou, J.-G. Legoux, S. Yue, J. Szpunar, Dynamic recrystallization in the particle/particle interfacial region of cold-sprayed nickel coating: Electron backscatter diffraction characterization, *Scripta Mater.*, 61, 2009, p 899-902

[99] H. Mäkinen, J. Lagerbom, P. Vuoristo, Adhesion of cold sprayed coatings: effect of powder, substrate, and heat treatment, T*hermal Spray 2007: Global Coating Solutions*, B. Marple, M. Hyland, Y.-C. Lau, C.-J. Li, R. Lima, G. Montavon (Eds.), May 14-16 (Beijing, China), ASM International, p 31-36

[100] H. Koivuluoto, M. Kulmala, P. Vuoristo, Structural Properties of High-Pressure Cold-Sprayed and Low-Pressure Cold-Sprayed Coatings, *Surface Modification Technologies XXII*, T. Sudarshan, P Nylen (Eds.),September 22-24,2008, (Trollhättan, Sweden), p 65-72

[101] A. Bolesta, V. Fomin, M. Sharafutdinov, B. Tolochko, Investigation of interface boundary occurring during cold gas-dynamic spraying of metallic particles, *Nuclear Instrum. Methods in Phys. Research A*, 470, 2001, p 249-252

[102] S. Semiatin, Recovery, Recrystallization, and Grain-Growth Structures, Metalworking: Bulk Forming, Vol.14A, ASM Handbook, ASM International, 2005, p 552-562

[103] M. Decker, R. Neiser, D. Gilmore, H. Tran, Microstructure and Properties of Cold Spray Nickel, *Thermal Spray 2001: New Surfaces for a New Millennium*, C. Berndt, K. Khor, E. Lugscheider (Eds.), May 28-30 (Singapore), ASM International, p 433-439

[104] A. Shkodkin, A. Kashirin, O. Klyuev, T. Buzdygar, Metal Particle Deposition Stimulation by Surface Abrasive Treatment in Gas Dynamic Spraying, *J. Therm. Spray Technol.*, 15(3), 2006, p 382-386

[105] M. Kulmala, H. Koivuluoto, P. Vuoristo, Influence of laser irradiation on formation of low-pressure cold sprayed coatings, *Thermal Spray 2008: Thermal Spray Crossing Borders*, E. Lugscheider (Ed.), June 2-4 (Maastricht, The Netherlands), DVS, p 950-955

[106] E. Calla, D. McCartney, P. Shipway, Deposition of Copper by Cold Gas Dynamic Spraying: an Investigation of Dependence of Microstructure and Properties of the Deposits on the Spraying Conditions, *Thermal Spray 2004: Advances in Technology and Application*, May 10-12 (Osaka, Japan), ASM International

[107] T. Xiong, Z. Bao, T. Li, Z. Li, Study on cold-sprayed copper coating's properties and optimizing parameters for spraying process, *Thermal Spray 2005: Explore its surfacing potential!*, May 2-4 (Basel, Switzerland), ASM International, p 178-183

[108] J. Lagerbom, H. Mäkinen, P. Vuoristo, Effect of heat treatment on properties of cold sprayed coatings, *Thermal Spray 2005: Explore its surfacing potential!*, May 2-4 (Basel, Switzerland), ASM International, p 240-244

[109] H. Fukanuma, N. Ohno, Study of Adhesive Strength of Cold Spray Coatings, T*hermal Spray 2004: Advances in Technology and Application*, May 10-12 (Osaka, Japan), ASM International

[110] T. Schmidt, F. Gärtner, H. Kreye, T. Klassen, Correlation of impact conditions and coating properties in cold spraying, *Thermal Spray 2008: Thermal Spray Crossing Borders*, E. Lugscheider (Ed.), June 2-4 (Maastricht, The Netherlands), DVS, p 724-731

[111] H. Mäkinen, J. Lagerbom, P. Vuoristo, Mechanical properties and corrosion resistance of cold sprayed coatings, *Thermal Spray 2006: Building on 100 Years of Success*, B. Marple, M. Hyland, Y.-C. Lau, R. Lima, J. Voyer (Eds.), May 15-18 (Seattle, Washington, USA), ASM International

[112] D. Jones, 1996, *Principles and Prevention of Corrosion*, Prentice-Hall, Upper Saddle River, NJ, 2nd ed., 572 p

[113] D. Talbot, J. Talbot, 1998, *Corrosion Science and Technology*, CRC Press LLC, 390 p

[114] G. Frankel, Pitting corrosion, Corrosion Fundamentals, Testing, and Protection, ASM Handbook, Volume 13A, ASM International, 2003, p. 236-241

[115] P.A. Schweitzer, Ed., 1996, *Corrosion Engineering Handbook*, Marcel Dekker, 736 p

[116] U. Chatterjee, S. Bose, S. Roy, 2001, *Environmental degradation of metals*, Marcel Dekker Inc., New York, USA, 498 p

[117] R. Kelly, Crevice corrosion, Corrosion Fundamentals, Testing, and Protection, ASM Handbook, Volume 13A, ASM International, 2003, p. 242-247

[118] R. Baboian, Galvanic corrosion, Corrosion Fundamentals, Testing, and Protection, ASM Handbook, Volume 13A, ASM International, 2003, p. 210-213

[119] L. Erb, Corrosion Control - Galvanic Table, Army Missile Command Report RS-TR-67-11, Practical Galvanic Series, 1997

[120] H. Koivuluoto, J. Näkki, P. Vuoristo, Structure and Corrosion Behavior of Cold-Sprayed Tantalum Coatings, *Thermal Spray 2009: Expanding Thermal Spray Performance to New Markets and Applications,* B. Marple, M. Hyland, Y.-C. Lau, C.-J. Li, R. Lima, G. Montavon (Eds.), May 4-7 (Las Vegas, Nevada, USA), ASM International, p 314-319

[121] ASM Handbooks Online, Volume 13A, Corrosion: Fundamentals, Testing, and Protection, Passivity, General Aspects.

[122] "Standard Test Method of Salt Spray (Fog) Testing," B117-90, *Annual Book of ASTM Standards*, ASTM, p 19-25

[123] M. Vreijling, 1998, *Electrochemical characterization of metallic thermally sprayed coatings*, printed in the Netherlands, 143 p

[124] ASM Metals Handbook Online, vol. 13B, Corrosion: Materials, Corrosion of nonferrous Alloys and Speciality Products, Corrosion of Tantalum and Tantalum Alloys

[125] H.C. Starck, Amperit and Amperweld Homepage, Amperit Thermal Spray Powder Procedure, Available from http://www.amperit.info, referred 2008

[126] R. Blose, D. Vasquez, W. Kratochvil, Metal Passivation to Resist Corrosion using the Cold Spray Process, *Thermal Spray 2005: Explore its surfacing potential!*, May 2-4 (Basel, Switzerland), ASM International

[127] T. Xiong, Y. Tao, C. Sun, H. Jin, H. Du, T. Li, Study on Corrosion Behavior of Cold Sprayed Al/α-$Al_2O_3$ Deposit on AZ91D Alloy, *Thermal Spray 2009: Expanding Thermal Spray Performance to New Markets and Applications*, B. Marple, M. Hyland, Y.-C. Lau, C.-J. Li, R. Lima, G. Montavon (Eds.), May 4-7 (Las Vegas, Nevada, USA), ASM International, p 669-672

[128] J. Villafuerte, D. Dzhurinskiy, R. Ramirez, E. Maeva, V. Leshchynsky, R. Maev, Corrosion Behavior and Microstructure of the Al-$Al_2O_3$ Coatings Produced by Low Pressure Cold Spraying, *Thermal Spray 2009: Expanding Thermal Spray Performance to New Markets and Applications*, B. Marple, M. Hyland, Y.-C. Lau, C.-J. Li, R. Lima, G. Montavon (Eds.), May 4-7 (Las Vegas, Nevada, USA), ASM International, p 908-913

[129] W. Kroemmer, P. Heinrich, Cold spraying - Potential and New Application Ideas, *Thermal Spray 2006: Building on 100 Years of Success*, B. Marple, M. Hyland, Y.-C. Lau, R. Lima, J. Voyer (Eds.), May 15-18 (Seattle, Washington, USA), ASM International

[130] S. Marx, A. Paul, A. Köhler, G. Hüttl, Cold spraying - innovative layers for new applications, *Thermal Spray 2005: Explore its surfacing potential!*, May 2-4 (Basel, Switzerland), ASM International, p 209-215

[131] H. Hoell, P. Richter, KINETIKS® 4000 - new perspective with cold spraying, *Thermal Spray 2008: Thermal Spray Crossing Borders*, E. Lugscheider (Ed.), June 2-4 (Maastricht, The Netherlands), DVS, p 479-480

[132] M. Beneteau, W. Birtch, J. Villafuerte, J. Paille, M. Petrocik, R. Maev, E. Strumban, V. Leshchynsky, Gas Dynamic Spray Composite Coatings for Iron and Steel Castings, *Thermal Spray 2006: Building on 100 Years of Success*, B. Marple, M. Hyland, Y.-C. Lau, R. Lima, J. Voyer (Eds.), May 15-18 (Seattle, Washington, USA), ASM International

[133] R. Caron, J. Staley, Effects of Composition, Processing, and Structure on Properties of Nonferrous Alloys, Copper and Copper Alloys, ASM Handbooks Online, 20, Materials Selection and Design, ASM International, 1997

[134] R. Caron, J. Staley, Effects of Composition, Processing, and Structure on Properties of Nonferrous Alloys, Nickel and Nickel Alloys, ASM Handbooks Online, 20, Materials Selection and Design, ASM International, 1997

[135] ASM handbooks online, Volume 13B, Corrosion Materials, Corrosion of Nickel and Nickel-Base Alloys

[136] Cold Gas Technology GmbH, website: http://www.cgt-gmbh.com/, referred 2009.

[137] W. Krömmer, P. Heinrich, P. Richter, Cold Spraying - Equipment and Application Trends, *Thermal Spray 2003: Advancing the Science & Applying the Technology*, C. Moreau, B. Marple (Eds.), May 28-30 (Orlando, Florida, USA), ASM International, p 97-102

[138] C. Borchers, F. Gärtner, T. Stoltenhoff, H. Kreye, Microstructural bonding features of cold sprayed face centered cubic metals, *J. Appl. Phys.*, 8(96), 2004, p 4288-4292

[139] H. Koivuluoto, M. Kotilainen, P. Vuoristo, Overview of Structure and Properties of High-Pressure and Low-Pressure Cold-Sprayed Coatings, *Weld. Cutt.*, 2, 2009, p 98-104

[140] L.-M. Berger, P. Ettmayer, P. Vuoristo, T. Mäntylä, W. Kunert, Microstructure and Properties of WC-10%-4%Cr Spray Powders and Coatings: Part 1. Powder Characterization, *J. Therm. Spray Technol.*, 10(2), 2001, p 311-325

[141] W. Tait, 1994, *An Introduction to Electrochemical Corrosion Testing for Practicing Engineers and Scientists*, Pair O Docs Publications, Racine, WI, 138 p

# Publication I

Heli Koivuluoto, Juha Lagerbom and Petri Vuoristo

**Microstructural Studies of Cold Sprayed Copper, Nickel, and Nickel-30%Copper Coatings**

*Journal of Thermal Spray Technology*, 16 (4) 2007, p. 488-497

# Publication II

Heli Koivuluoto, Juha Lagerbom, Mikko Kylmälahti and Petri Vuoristo

**Microstructure and Mechanical Properties of Low-Pressure Cold-Sprayed (LPCS) Coatings**

*Journal of Thermal Spray Technology*, 17 (5-6) 2008, p. 721-727

# Publication III

Heli Koivuluoto and Petri Vuoristo

**Effect of Ceramic Particles on Properties of Cold-Sprayed Ni-20Cr+$Al_2O_3$ Coatings**

*Journal of Thermal Spray Technology*, 18 (4) 2009, p. 555-562

# Publication IV

Heli Koivuluoto, Jonne Näkki and Petri Vuoristo

**Corrosion Properties of Cold-Sprayed Tantalum Coatings**

*Journal of Thermal Spray Technology*, 18 (1) 2009, p. 75-82

# Publication V

Heli Koivuluoto, Mari Honkanen and Petri Vuoristo

**Cold-sprayed copper and tantalum coatings – Detailed FESEM and TEM analysis**

*Surface & Coatings Technology*, 204 (15) 2010, p. 2353-2361

# Publication VI

Heli Koivuluoto and Petri Vuoristo

**Structural Analysis of Cold-Sprayed Nickel-Based Metallic and Metallic-Ceramic Coatings**

J*ournal of Thermal Spray Technology*, DOI: 10.1007/s11666-010-9481-4, in press.

# Publication VII

Heli Koivuluoto and Petri Vuoristo

**Effect of Powder Type and Composition on Structure and Mechanical Properties of $Cu+Al_2O_3$ Coatings Prepared by Using Low-Pressure Cold Spray Process**

*Journal of Thermal Spray Technology*, DOI: 10.1007/s11666-010-9491-2, in press